Bulletin 679

Pacific Manganese Nodules: Characterization and Processing

By Benjamin W. Haynes, Stephen L. Law, David C. Barron
Gary W. Kramer, Riki Maeda, and Michael J. Magyar

UNITED STATES DEPARTMENT OF THE INTERIOR
Donald Paul Hodel, Secretary

BUREAU OF MINES
Robert C. Horton, Director

As the Nation's principal conservation agency, the Department of the Interior has responsibility for most of our nationally owned public lands and natural resources. This includes fostering the wisest use of our land and water resources, protecting our fish and wildlife, preserving the environment and cultural values of our national parks and historical places, and providing for the enjoyment of life through outdoor recreation. The Department assesses our energy and mineral resources and works to assure that their development is in the best interests of all our people. The Department also has a major responsibility for American Indian reservation communities and for people who live in island territories under U.S. administration.

Library of Congress Cataloging in Publication Data

Main entry under title:

Pacific manganese nodules, characterization and processing

(Bulletin / U.S. Dept. of the Interior, Bureau of Mines ; 679)

Bibliography: p. 43

Supt. of Docs. no.: I 28.3:679

1. Manganese nodules – Pacific Ocean. 2. Manganese – Metallurgy. 3. Iron-Metallurgy. I. Haynes, Benjamin W. II. Series: Bulletin (United States. Bureau of Mines) ; 679.

QE390.2.M35P3 1985 553.4'629'09164 85-600142

For sale by the Superintendent of Documents, U.S. Government Printing Office
Washington, DC 20402

CONTENTS

ILLUSTRATIONS

TABLES

UNIT OF MEASURE ABBREVIATIONS USED IN THIS REPORT

Å	angstrom	μg/g	microgram per gram
A/m²	ampere per square meter	μg/mL	microgram per milliliter
atm	atmosphere	μm	micrometer
°C	degree Celsius	min	minute
cm	centimeter	mL	milliliter
cm/s	centimeter per second	mL/min	milliliter per minute
deg	degree	mm	millimeter
dpy	day per year	mV	millivolt
g	gram	ng/g	nanogram per gram
gal	gallon	nm	nanometer
g/L	gram per liter	pct	percent
h	hour	pg/g	picogram per gram
hpd	hour per day	ppm	part per million
in	inch	psi	pound per square inch
kg	kilogram	psig	pound per square inch gage
L	liter	mtpd	metric ton per day
L/min	liter per minute	mtpy	metric ton per year
lb	pound	wt pct	weight percent
m	meter	yr	year
μg	microgram		

PACIFIC MANGANESE NODULES: CHARACTERIZATION AND PROCESSING

By Benjamin W. Haynes,[1] Stephen L. Law,[2] David C. Barron,[3]
Gary W. Kramer,[4] Riki Maeda,[5] and Michael J. Magyar[6]

ABSTRACT

The Bureau of Mines conducted research to provide technical information needed to devise waste management plans for the processing of manganese nodules. Studies included summary descriptions of Pacific manganese nodules, process options and flowsheets, methods for characterizing nodules and their tailings, and results of analyses of laboratory and pilot-plant generated tailings. This information is the result of a cooperative research effort of the Bureau of Mines and the National Oceanic and Atmospheric Administration (NOAA), with NOAA providing funding and the Bureau conducting the research.

A summary of the extensive literature review is provided for manganese nodule mineralogy, chemistry, processing techniques, and methods of analyses. Characterizations and analyses of laboratory-generated tailings and slags are given, as well as the results of the leaching studies on these waste materials. Leachability was determined by three standard leachate tests—the Environmental Protection Agency (EPA) extraction procedure (EP) toxicity test, the American Society for Testing and Materials shake extraction test, and the U.S. Army Corps of Engineers-EPA seawater elutriant test. While the wastes generated in the laboratory may not be entirely representative of those to be generated in full-scale plants, results of these studies provide a positive indication that commercial recovery of cobalt, copper, manganese, and nickel from manganese nodules would be environmentally acceptable.

[1]Supervisory research chemist.
[2]Research supervisor.
[3]Research chemist (now with city of Erie, Erie, PA).
[4]Research chemist (now with Safety Management, Bureau of Mines, Washington, DC).
[5]Chemical engineer (now with Rochester Institute of Technology, Rochester, NY).
[6]Chemical engineer.
Avondale Research Center, Bureau of Mines, Avondale, MD.

INTRODUCTION

As part of its mission, the Bureau of Mines conducts studies to provide information needed to ensure the environmental acceptability of domestic mineral processing operations. This Bureau of Mines bulletin is a compilation of a series of reports (*1–5*)[7] issued by the Bureau to document the results of a research project entitled "Analysis and Characterization of Manganese Nodule Processing Rejects." Deep seabed mining for manganese nodules, including the processing of nodules to recover value metals, raises a variety of environmental, social, and economic considerations. To address the waste management aspects of the recovery of value metals from nodules, the National Oceanic and Atmospheric Administration (NOAA) of the Department of Commerce, the Environmental Protection Agency (EPA), and the Department of Interior's Bureau of Mines and Fish and Wildlife Service, after consultation with affected and concerned interests, embarked on a multiyear cooperative research program that had as its overall objective:

> "To provide information needed by Federal and State Agencies in preparation for receipt of industry's commercial waste management plans."

Under the Deep Seabed Hard Mineral Resources Act of 1980 (Public Law 96-283), NOAA was designated as the lead agency in developing terms, conditions, and restrictions for the proposed mining of nodules and for the disposal of wastes. The NOAA-funded research conducted by the Bureau had the objective of obtaining a first-order chemical and physical characterization of rejects from the types of manganese nodule processing techniques representative of those being developed by industry. The final products of this research are six technical reports that can be used by (a) scientists in subsequent research to assess the potential effects of waste management alternatives and (b) regulatory agencies in the determination of the standards and test requirements to be met. Results reported here are expected to facilitate the development of a basic framework for assuring protection of the environment during the development of a new industry.

The five reports published during the course of this research addressed the various aspects of the objective to obtain a first-order characterization of waste materials from processing nodules. One of the reports describes the mineralogical and elemental characteristics of Pacific Ocean manganese nodules (*1*), providing important knowledge of the processing feed material. A second report (*2*) details the five most technically feasible process flowsheets for first generation plants. The flowsheet report is based on an earlier report (*6*) by Dames & Moore and EIC Corp., and contains updated and improved operating parameters for the five processes duplicated in the laboratory. A third report (*3*) uses information on nodule composition (*1*) and processing methods (*2, 6*) to predict the compositions of the tailings generated by each of the processes. The fourth report (*4*) details methods for physical and chemical analyses of nodules and tailings. The fifth report details the laboratory generation of tailings and the results obtained from the characterization of the tailings from the bench-scale processing of manganese nodules (*5*).

Of the many processes potentially available for the recovery of value metals (Co, Cu, Mn, Mo, and Ni) from manganese nodules, only five are considered at present to be technically feasible for first-generation nodule processing (*2, 6*). These processes are as follows:

1. Gas reduction and ammoniacal leach (GRAmL).
2. Cuprion ammoniacal leach (CuAmL).
3. High-temperature and high-pressure sulfuric acid leach (HTPSAL).
4. Reduction and hydrochloric acid leach (RHClAL).
5. Smelting and sulfuric acid leach (SmSAL).

The two ammoniacal leach processes and the high-temperature and high-pressure sulfuric acid process are designed to recover three metals (Co, Cu, and Ni) with some possible recovery of Mn. These are called three-metal processes although some manganese could be recovered from the tailings if required. In the laboratory processing, no attempt was made to recover manganese from the tailings of the three-metal processes. The remaining two processes, hydrochloric acid leach and smelting and sulfuric acid leach are designed to recover four metals (Co, Cu, Mn, and Ni) and are called four-metal processes. Manganese is recovered as either electrolytic manganese (RHClAL process) or as ferromanganese (SmSAL process). All five of these processes were operated on a bench-scale modeled after the flowsheets (*2, 6*) to generate sufficient tailings (rejects) for analyses.

Based on in-house expertise gained during the characterization of other waste materials (*7–11*), the tailings were characterized physically, chemically, and mineralogically using methods described previously (*4*). The tailings were also subjected to the three leachate tests: the EPA extraction procedure (EP) toxicity test (*12*); the American Society for Testing and Materials (ASTM) shake extraction test (*13*); and the EPA-U.S. Army Corps of Engineers (COE) seawater elutriant test (*14*).

ACKNOWLEDGMENTS

The authors wish to acknowledge the assistance of personnel of Kennecott Minerals Co. for manganese nodule samples, for Cuprion process pilot-plant tailings for comparative analysis, and for manuscript reviews; Ocean Minerals Co. for manganese nodule samples, standards, and manuscript reviews; Ocean Mining Associates for manganese nodule standards, samples, and manuscript reviews; Ocean Management, Inc., for manuscript reviews; and F. C. Brown, president, F. C. Brown Associates, Inc., for helpful discussions, manuscript reviews, and copies of flowsheets from reference 6.

This work was performed under interagency agreement NA80AAGO 3026 with the Department of Commerce (NOAA). The overall research direction and monitoring were the responsibilities of A. L. Lane, M. K. Jugel, R. F. Dill, and J. Padan, Office of Marine Minerals and Energy, NOAA.

[7]Italic numbers in parentheses refer to items in the list of references at the end of this report.

The authors wish to thank Professor V. M. Burns and Professor R. G. Burns, Massachusetts Institute of Technology, Cambridge, MA, for their many helpful discussions, comments, and reviews and their assistance in providing information on newly published articles and also for their assistance in providing scanning electron microscope photomicrographs of nodules. The authors thank Professor R. K. Sorem, Washington State University, Pullman, WA, for assistance in providing nodule photographs, R. H. Fewkes, consultant, Pullman, WA, for manuscript review, J. B. Frazer, consultant, Richmond, CA, for providing information and analyses from the Sediment Data Bank, and A. R. Foster, consultant, Kirkland, WA, and M. Williamson, consultant, Kirkland, WA, in providing the cross-sectional analysis.

PACIFIC MANGANESE NODULES

Ferromanganese oxides are deposited in a variety of forms in marine environments. In reporting on samples collected by the H.M.S. *Challenger* expedition (1872–76), Murray and Renard (*15*) noted hydrates of manganese as "colouring matters, or as thin or thick coatings on shells, corals, shark's teeth, bones, and fragments of rock." There is no universally accepted delineation between objects that are stained or very thinly encrusted with manganese and objects that may be called manganese nodules (*16*). However, for purposes of chemical comparison of nodules from throughout the Pacific Ocean, a "manganese nodule" will be arbitrarily defined as having a ferromanganese oxide encrustation at least four times greater in bulk than the nucleus object. Otherwise a nucleus, or multinucleated objects greater than 20 pct of the total weight, will have too significant an influence upon the observed chemistry of the specimen for valid comparisons with manganese nodules having small nuclei. For example, the Drake Passage series of nodules described by Sorem and Fewkes (*17*) contains rock fragment cores comprising 50 pct or greater of the nodule and are, therefore, not included in the study. Also, it is doubtful that thinly encrusted objects will ever be considered commercially attractive in the sense implied in the term "manganese nodule." Of course, if the nucleus of a nodule is a fragment of another nodule, it will be classified as a manganese nodule regardless of nucleus size.

Manganese micronodules are a special case of the nodule category not included in this study. Micronodules are individual grains generally less than 1 mm in diameter and usually lack a discernible nucleus. Also not included as manganese nodules are the large, slablike concretions such as the manganese pavement from the San Pablo Seamount described by Aumento (*18*).

The existence of varying populations of nodules at different localities in the Pacific Ocean can be attributed to several factors, including type of nucleation substrate available, bathymetric position, bottom current activity, sediment type, benthic organism activity, and the chemical environment (*16*). Details of nodule genesis are not completely understood, though the layering nature and chemical associations characteristic of manganese nodules have been known for many years. That nodule formation requires some special conditions is illustrated by the discontinuous distribution of nodule fields and the fact that some fields are rich in Mn, Cu, and Ni whereas others, with essentially the same underlying sediments are high in Fe and low in Mn, Cu, and Ni. Nodules apparently accrete from both sides, with Ni and Cu accreting primarily from the sediment side. Raab and Meylan (*16*, pp. 109–146) were unable to verify that chemical gradients found in nodules could be ascribed to the upward migration of trace metals owing to diffusion, and their theory on accretion only on the sediment side is no longer accepted by most researchers. Intraplate igneous activity resulting in the extraction and transport of metals from the sediment to the mud-water interface is postulated by Raab and Meylan (*16*, pp. 109–146) as the source of metals for the concentric layering of nodules. Once the warm, metal-rich brine layer is dissipated, the newly formed nodules are exposed to normal seawater leaching of metals until the next intraplate intrusive event.

The key to a more complete understanding of manganese nodule origin lies in the domain of researchers studying the microfeatures and chemical associations in nodules from many areas and was beyond the scope of this research.

MORPHOLOGY

The morphology of manganese nodules has been described in detail in recent publications (*1*, *19–20*). The term morphology is used here in its broadest sense to include not only external shape but also the internal structure of the nodule contributing to the total nodule properties. Table 1 provides an abbreviated summary of the nature and variability of the morphological characteristics of Pacific manganese nodules.

The five external shapes generally exhibited by Pacific manganese nodules and listed in table 1 are spheroidal, ellipsoidal, discoidal, botryoidal, and flat faced. The shape of a nodule, especially the smaller flat-faced nodules, may be influenced by the shape of the nucleus. Table 1 lists the various solid objects that may form the nucleus. Two general surface textures, smooth or granular, generally occur on opposite sides of the same nodule. A different surface texture for the top and bottom of a nodule is not uncommon, especially for the larger asymmetric nodules.

Nodule size is an important factor because of the relationship between mineralogy and the nodule contact with ocean floor sediments. Accretion of crystalline manganese oxides seems to be enhanced on the portion of the nodule resting in water-saturated, fine-grained silicate sediments. Small nodules (< 3-cm diam), virtually enclosed in soupy sediment, tend to accrete crystalline oxides on all sides and maintain a spheroidal or ellipsoidal shape, or maintain the shape of the nucleus.

At a size of about 3 cm or greater, nodules usually tend to develop a pronounced asymmetry of shape because of nonuniform growth rates. The most common pattern is a gradual increase in the horizontal dimensions so that a spheroidal nodule becomes ellipsoidal, and an ellipsoidal nodule approaches a discoidal shape. When the top of the larger nodule comes in contact with relatively sediment-free water, thin iron-rich amorphous oxide layers are slowly added. The bottom and sides of the large nodule, however, remain in contact with watery sediment and continue adding layers of crystalline manganese oxides in which fine silicate grains from the substrate are entrapped. The accentuated asym-

Table 1.—Morphological characteristics of Pacific manganese nodules

Characteristic	*Nature and extent of variability*
Size	Generally 0.5 to 20 cm. Concretions larger than about 20 cm in diameter generally assume the form of slabs.
External shape	Numerous terms used. Most frequent are— Spheroidal (peas to cannonballs). Ellipsoidal (potatoes). Discoidal or tabular (includes slabs). Botryoidal, polylobate, or coalespheroidal (grape cluster). Flat faced or polygonal (or irregular shape, owing to angular nucleus or fracturing).
Surface texture	Surfaces are usually mammillated, with texture occurring in two general classifications— Smooth: Smooth to the touch and to the eye, though close examination may reveal densely packed minute botryoids. Granular: Feels gritty and may leave tiny oxide particles on the hand upon handling. Close examination may show tiny, closely spaced dendritic oxide forms that may be so abundant in some nodules that the surface botryoids are almost completely obscured.
Color	Refers to nodular exterior, free of clay. Generally dark reddish brown to black, with variations of black as the most common color.
Crustal zone	The outermost layer or set of layers that appear to represent continuous accretion up to the time of collection. Varies from well-defined, uniform to asymmetric, to very thin or absent.
Nucleus	Can be any solid object. Often influences external shape of nodule. Examples— Rock: Igneous, metamorphic, sedimentary. Nodule fragment. Slab of clay. Biological fragment: Tooth, vertebra, bone, fossil, sponges, etc. Volcanic glasses—like pumice, glassy lapilli—almost always profoundly altered. No apparent foreign nucleus: May have formed around a nodule fragment with indeterminate laminations, or original nucleus was altered and replaced.
Internal fractures	Generally filled with clay and readily visible in cut nodules. Occasional clay-free fractures lined with overgrowth of ferromanganese oxides. Two types— Radial or random: An extension feature having greatest separation toward center of nodule and tapering toward edges. Often do not emerge at surfaces but some open toward the sediment side. Show characteristics of shrinkage cracks. Concentric: A fracture along nodule zoning but almost never continuous around entire nodule, frequently terminated by radial fractures.
Breaks	Breakup generally attributed to benthic organisms or bottom currents acting on a fracture-weakened nodule. Terms include— Spalling: Peeling of layers, observed occasionally only in larger nodules (7-cm diam or larger). Cross section: Transects the nodule layers more or less at right angles; a more common break. α-breaks: Fresh breaks essentially complete before physical recovery from the ocean floor, with the final break occurring during handling in a crust holding the nodule together; more common in large nodules. β-breaks: Old fracture surfaces with entire fracture covered by a crust of manganese material; more common in smaller nodules (<7-cm diam).
Interior zoning	Some zonal pattern in nodule cross section, produced by variation in mineral content of the growth layers, is generally present in all nodules. Three types— Continuous, varied bands: Thicker in one half of the nodule, tapering to a thin portion starting near the equator and becoming very thin at the side opposite the thick portion. Textures and composition of the two portions of the band usually differ. Continuous, uniform bands: Often close to the core, suggesting a uniform growth environment. Discontinuous bands: Bands that are completely terminated, usually by sudden tapering near the nodule equator.

metrical shape of many nodules is due to the more rapid deposition of manganese-rich oxides compared with the amorphous iron-oxide layer growth, and growth of the manganese-rich layers is further enhanced by the incorporation of sediment.

The upper surface and the bottom surface of a nodule are usually chemically different from each other and from the nodule interior. The top is generally higher in Fe, Co, and Pb and lower in Cu, Ni, Mo, Zn, and Mn; the bottom shows the reverse general pattern. The equatorial area of the surface shows intermediate concentrations of the metals. The core of a nodule is often deficient in Fe, Co, and Pb content relative to the crustal surface. However, the zoning within a nodule generally exhibits the same antithetic relationship between manganese content and iron content, and provides further evidence for the different growth processes for the top and bottom portions of nodules. The texture of the layer refers to the relationships of the intergrown oxides and nonoxides. The variations in texture are often accompanied by variations in thickness of layers.

With aging, only limited changes seem to occur in the older layers of a nodule. These include the development of shrinkage cracks, both radial and concentric, followed by deposition of oxide veinlets and clay fillings from solutions circulating along the cracks and through pore spaces. The nodule cracking and subsequent physical disturbance may result in breakage of the nodule. As noted in table 1, older fracture surfaces with the entire fracture covered by an oxide crust are referred to as β-breaks. Fractures that occur at the time of nodule removal from the ocean floor environment are called α-breaks.

Recrystallization and/or replacement of oxides and nonoxides may be observed to some extent in older nodules, and alteration or even complete replacement of the original nucleus may occur. Basically, however, the mineralogy and most of the textural features in nodule interiors are virtually identical to the outermost layers, indicating that most nodules change little upon aging.

MINERALOGY

Manganese nodules consist of a complex mixture of materials, including organic and colloidal matter, nucleus fragments, and crystallites of various minerals of detrital and authigenic origins. The phases in nodules are fine grained, often metastable, poorly crystallized, and so intimately intergrown that it is often quite difficult to characterize the minute mineral crystallites or to extract a homogenous, single-phase sample for study. The minerals are usually characterized by numerous structural defects, essential vacancies that may not be ordered, domain intergrowths, extensive solid solutions, and cation exchange properties that lead to nonstoichiometry and detract from long-range ordering of the crystals. Distinguishing between authigenic and detrital minerals, particularly the silica, clay, and iron oxyhydroxide phases, is also a challenge, as these phases either formed in situ or were transported to the nodule as suspensions in seawater.

The major interest in manganese nodules centers on the oxide minerals of manganese and iron. However, mention will also be made of authigenic and detrital accessory phases. For the purposes of this report, a mineral is defined as an inorganic solid with a crystalline particle size exceeding 30 to 40 Å, having a limited chemical composition range and a systematic three-dimensional atomic order. The isotropic oxides in manganese nodules are amorphous to X-ray diffraction and cannot be classified usefully by optical means. Particle sizes less than 30 to 40 Å are also amorphous even to electron microscopy. These amorphous materials in manganese nodules and other materials lacking an internal structure of atoms are not included as minerals, but are classed as mineraloids.

Prior to discussion of the manganese, iron, and accessory mineral phases, it is important to note that much of the work involving the minerals present in manganese nodules is based on laboratory studies using special sampling techniques, especially in the case of the iron phase. Standard X-ray diffraction techniques cannot generally determine more than one or two of the manganese and accessory phase minerals. The best results to date have been obtained by scanning and transmission microscope studies. Recent work by Turner (*21–23*) and Siegel (*24*) has determined the existence and structure of todorokite in manganese nodules. Chukhrov (*25–27*) performed research on the iron phases in nodules, but identification is difficult because of the need to preserve the nodule mineralogy once the nodule is removed from the ocean. The dehydration and oxidation of both the manganese and iron phase minerals occur readily.

Manganese Minerals

Manganese forms a large number of oxide minerals, but only the low-temperature oxides that can be formed in water are relevant to the mineralogy of nodules. The tetravalent manganese predominates in nodules, but the presence of Mn^{2+} and Mn^{3+} ions in some phases has been inferred from crystallographic and thermodynamic data. Table 2 lists the oxide phases of manganese relevant to nodule mineralogy. Available crystallographic data, crystal structures, and chemical composition, are provided. References to occurrence are provided elsewhere (*1, 16*). The mineral listing in table 2 follows an approximate order of increasing complexity of crystal structure.

Todorokite, birnessite, and vernadite are the predominant manganese oxide minerals, occurring as cryptocrystalline phases in manganese nodules. The todorokite and birnessite appear to contain variable linkages of edge-shared [MnO_6] octahedra and are characterized by numerous structural defects, cation vacancies in the chains or layers of linked octahedra, domain intergrowths of mixed periodicities, cation exchange properties, and extensive substitution of Ni^{2+}, Cu^{2+}, Zn^{2+}, Mg^{2+}, or other divalent ions for Mn^{2+}. The formation of vernadite, sometimes catalyzed by microorganisms, results in poorly crystalline to amorphous phases with a large specific surface area and cation adsorption properties, concentrating cobalt by substitution of Co^{3+} for Mn^{4+} (*28–29*). Postdepositional recrystallization of vernadite to todorokite may occur inside manganese nodules.

Todorokite or 10-Å Manganite

The manganese oxide mineral characterized by X-ray diffraction lines at 9.5 to 9.8 Å and 4.8 to 4.9 Å is one of the

Table 2.—Manganese minerals in Pacific manganese nodules

Mineral	Approximate formula	Crystal system and space group	Cell parameter, Å			
			a	b	c	z
Pyrolusite (β-MnO_2)	MnO_2	Tetragonal, $P4_2/mnm$	4.39	4.39	2.87	2
Ramsdellite	MnO_2	Orthorhombic, Pbnm	4.53	9.27	2.87	4
Nsutite (γ-MnO_2)	$(Mn^{2+},Mn^{3+},Mn^{4+})$ $(O,OH)_2$	Hexagonal, NA	9.65	NAp	4.43	NA
Hollandite (α-MnO_2)	$(Ba,K)_{1-2}Mn_8O_{16}\cdot xH_2O$	Tetragonal, I4/m	9.96	9.96	2.86	NA
		Monoclinic, $P2_1/n$	10.03	5.76	9.90	NA
Cryptomelane	$K_{1-2}Mn_8O_{16}\cdot xH_2O$	Tetragonal, I4/m	9.84	9.84	2.86	NA
		Monoclinic, I2/m	9.79	2.88	9.94	NA
Romanechite (psilomelane)	$(Ba,K,Mn^{2+},Co)_2$ $Mn_5O_{10}\cdot xH_2O$	Monoclinic, A2/m	9.56	2.88	13.85	2
		Orthorhombic, $P2_12_12$	8.254	13.40	2.864	NA
Todorokite	(Ca,Na,K,Ba,Ag) (Mg,Mn^{2+},Zn) $Mn_3O_{12}\cdot xH_2O$	Monoclinic, NA	9.75	2.85	9.59	NA
Buserite	NaMn oxide hydrate	Hexagonal, NA	8.41	NAp	10.01	NA
Chalcophanite	$ZnMn_6O_{14}\cdot 6H_2O$	Triclinic, $P\bar{1}$	7.54	7.54	8.22	NA
Synthetic birnessite	$Na_4Mn_{14}O_{27}\cdot 9H_2O$	Orthorhombic, NA	8.54	15.39	14.26	NA
Do.	$Mn_7O_{13}\cdot 5H_2O$	Hexagonal, NA	2.84	NAp	7.27	NA
Birnessite	(Na,Ca,K) (Mg,Mn) $Mn_6O_{14}\cdot 5H_2O$	Hexagonal, NA	2.85	NAp	7.08–7.31	NA
Vernadite[1] (δ-MnO_2)	$MnO_2\cdot m(R_2O_1,RO_1,R_2O_3)\cdot nH_2O$	Hexagonal, NA	2.86	NAp	4.7	NA
Rancieite	$(Ca,Mn)Mn_4O_9\cdot 3H_2O$	Hexagonal, NA	2.84	NAp	7.07	NA
Groutite	α-MnOOH	Orthorhombic, Pbnm	4.56	10.70	2.85	NA
Manganite	γ-MnOOH	Monoclinic, $B2_1/d$	8.88	5.25	5.71	8

NA Not available. NAp Not applicable. [1]R = Na, Ca, Co, Fe, Mn.

Figure 1.—Electron microscope observation of todorokite. (Photograph courtesy of reference 33)

most common phases observed in manganese nodules. This phase, a hydrated Mn-Mg-Ca-Na-Ni-Cu oxide often with significant concentrations of Ni and Cu, has been identified as either todorokite or 10-Å manganite. A synthetic structural analogue of todorokite also gives a ~10-Å diffraction peak, but to avoid confusion with the mineral manganite ($\gamma Mn^{III}OOH$), this synthetic 10-Å manganite phase, called buserite in honor of W. Buser (*30*), is generally considered not to occur in nodules (*31*).

The chemical formula for todorokite is $(Mn^{2+},Ca,Mg)Mn_3^{4+}O_7 \cdot H_2O$ (*32*). The marine form of todorokite found in manganese nodules as adopted by Burns (*33*) is $(Ca,Na,K)(Mg,Mn^{2+})Mn_5^{4+}O_{12} \cdot H_2O$. Most todorokites consist of fibrous aggregates of small acicular crystals. The crystals consist of narrow lathes or blades elongated along the b axis (see figure 1) and frequently show two perfect cleavages parallel to the (001) and (100) planes. These fibers are commonly twinned at 120° angles. Chukhrov (*34–36*) has indicated that as many as five todorokite polymorphs might exist, all having similar b (2.84 Å) and c (9.59 Å) unit cell parameters, but with the a parameters as multiples of 4.88 Å.

Todorokite, both terrestrial and marine, has a tunnel structure with single, double, and triple chains of edge-shared $[MnO_6]$ octahedra (*21–23, 34–35*) along the b axis. Essential Mn^{2+} and other divalent cations of comparable ionic radii (e.g., Mg^{2+}, Co^{2+}, Ni^{2+}, Cu^{2+}, Zn^{2+}) may be located in specific positions in the chains of edge-shared $[MnO_6]$ octahedra. The larger Ca^{2+}, Na^{+}, and related group I and II cations, together with water molecules, may occupy the large tunnel structure of todorokite. Some tunnel structures are disrupted by faults along the chain length with the faults going from triple to quadruple chains (*23*). Marine todorokites have been observed to contain quadruple, quintuple, and larger chains. Figure 2 shows the proposed atomic arrangement of one common structure for todorokite (*23*).

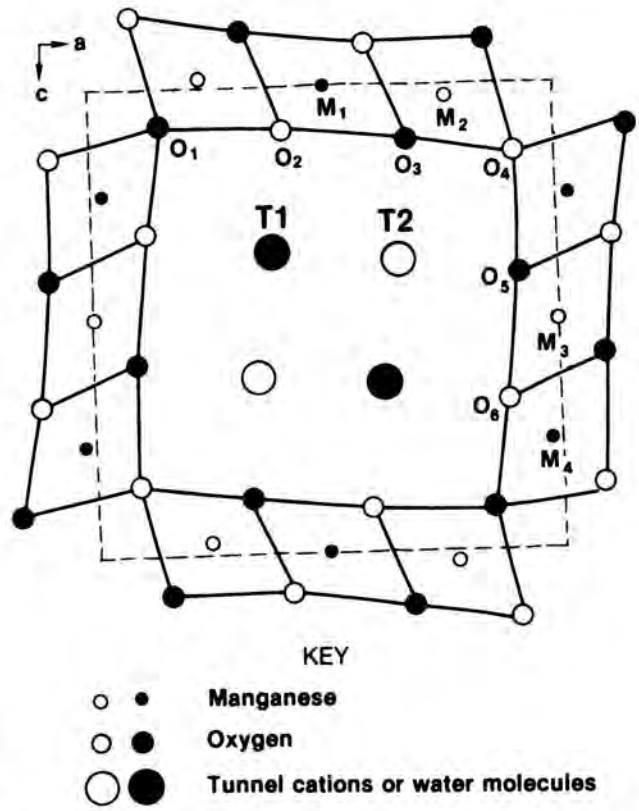

Figure 2.—Proposed atomic arrangement for one common todorokite structure. (Photograph courtesy of reference 23)

Birnessite or 7-Å Manganite

Birnessite in manganese nodules is characterized by X-ray diffraction lines at 7.0 to 7.3 Å and 3.5 to 3.6 Å. Both sets of lines must be present to establish the presence of birnessite, because hollandite-cryptomelane, zeolites such as phillipsite, and clay-mica groups also have d-spacings around 7 Å. The chemical formula for birnessite is $Na_4Mn_{14}O_{22} \cdot 9H_2O$ (*32*); however, Burns (*33*) used $(Na,Ca,K)(Mg,Mn)Mn_6O_{14} \cdot 5H_2O$ as the marine form. The platy habit of birnessite observed by scanning electron microscopy is distinctive.

The birnessite structure is postulated to contain layers of edge-shared [MnO_6] octahedra separated by about 7.2 Å along the c axis, which enclose sheets of H_2O molecules. In synthetic sodium birnessite, one out of six octahedral sites in the layer of linked [MnO_6] is unoccupied. The vacant Mn^{4+} sites are distributed according to different patterns for adjacent [MnO_6] octahedral layers, resulting in a two-layer orthorhombic cell with periodicity c = 14.26 Å. The Mn^{2+} and Mn^{3+} ions are arranged above and below the vacancies, and are bonded with oxygens in both the [MnO_6] layer and the sheet of H_2O molecules. The structure of sodium-free birnessite has disordered vacancies in the [MnO_6] layers, leading to a hexagonal cell with periodicity c = 7.27 Å. Divalent cations of Cu, Ni, Co, Zn, etc. are located directly above and below vacancies in the edge-shared [MnO_6] octahedral sheets, bound in the birnessite structure rather than randomly adsorbed on external surfaces of the microcrystallites.

Vernadite or δ-MnO_2

The phase in manganese nodules giving only two diffuse X-ray diffraction lines at 2.40 to 2.45 Å and 1.40 to 1.42 Å is designated as vernadite, a poorly crystalline δ-MnO_2 or supergene hydrated manganese (IV) oxide. The chemical composition of vernadite is variable, as reflected in its proposed formula: $MnO_2 \cdot m(R_2O, RO, R_2O_3) \cdot nH_2O$, where R = Na, Ca, Co, Fe, Mn (*33*). Fleischer (*32*) lists vernadite as $(Mn^{4+},Fe^{3+},Ca,Na)(O,OH)_2 \cdot nH_2O$. The iron observed to be present may be an intimately associated or epitaxial intergrowth of feroxyhyte, δ'-FeOOH, rather than a part of the vernadite structure.

The vernadite is distinguished from a structurally disordered birnessite by its distinctive large specific surface area and its significant concentrations of Co, Ca, and Pb. The leaflets of vernadite are tens of angstroms smaller than flakes of birnessite, and are often curved and folded to resemble fibers.

The vernadite structure is represented as a two-layer hexagonal packing of oxygen atoms and water molecules in which the octahedra are completely filled, but less than half with the tetravalent manganese. The extent of filling by Mn^{4+} is apparently determined by the contents of water and cations other than Mn^{4+}. By inclining leaflets of vernadite with respect to the electron beam, reflections with d spacing equal to 2.18 to 2.20 Å, corresponding to the (101) plane, lead to an approximate c parameter of 4.7 Å. This is the approximate width of two layers of close-packed oxygens.

The poor crystallinity and high specific surface area of vernadite result in this phase having high cation adsorption properties, particularly for cobalt. The substitution of low-spin Co^{3+} (ionic radius 0.53 Å) for Mn^{4+} (0.54 Å) in the [MnO_6] octahedra of vernadite has been confirmed by photoelectron spectroscopy (*29*).

Other Manganese Minerals

Other manganese minerals that have been reported in manganese nodules include pyrolusite or β-MnO_2, ramsdellite, nsutite or γ-MnO_2, hollandite or α-MnO_2, cryptomelane, romanechite or psilomelane, chalcophanite, rancieite, groutite, and manganite. However, they do not appear to be common, and some identifications are not fully accepted. A good discussion of these minerals and others is found in reviews by Burns (*33, 37*).

Manganese Mineral-Element Association

Several elements are associated solely with the manganese mineral phase of the nodule. Other elements have been shown to exist with the manganese mineral phase and with the iron or accessory mineral phases. Those elements associated almost entirely with the manganese mineral phase are Cu, Mo, Ni, and Zn. Other elements associated with the manganese phase, but which may be found in other phases also, are Ba, Cd, Ca, Mg, Sb, Sr, and V.

Iron Oxide Minerals

The oxide, oxide hydroxide (or oxyhydroxide), and hydrated oxide phases of iron relevant to manganese nodule mineralogy are listed in table 3. References to occurrence are published elsewhere (*1, 16*). As stated earlier, the information to date is based on limited studies, and identification of these iron phases is difficult because they are extremely fine grained. By analogy with the manganese oxides, the structures of many of the iron oxides consist of close-packed oxygens containing Fe^{3+} and/or Fe^{2+} ions in various octahedral interstices forming different assemblages of edge-shared [FeO_6] octahedra. Certain Fe(III) oxide hyroxides are isostructural with manganese (IV) oxides, with [FeO_6] and [MnO_6] octahedra edge shared in different arrangements. The larger ionic radius of Fe^{3+} compared with Mn^{4+} results in larger spacings for the $(10\bar{1}0)$ and $(11\bar{2}0)$ planes of the hexagonal close-packed systems (approximately 2.50 to 2.56 Å and 1.48 to 1.54 Å, respectively), and Fe-Fe interatomic distances across edge-shared [Fe(O, OH)$_6$] octahedra range from 2.95 to 3.05 Å. The most commonly observed iron-bearing phases in manganese nodules, to be discussed in more detail, are ferox-

Table 3.—Iron oxide minerals in Pacific manganese nodules

Mineral	Approximate formula	Crystal system and space group	Cell parameter, Å			
			a	b	c	z
Goethite (α-FeOOH)	FeOOH	Orthorhombic, Pbnm	4.65	10.02	3.04	4
Akaganeite (β-FeOOH)	$(OH,Cl,H_2O)_{1-2}$ $Fe_8(O,OH)_{16}$	Tetragonal, I4/m	10.48	10.48	3.028	1
Lepidocrocite (γ-FeOOH)	FeOOH	Orthorhombic, Amam	3.88	12.54	3.07	4
Hydrated oxyhydroxide polymer (synthetic).	$FeO_{(3-x)/2}(OH)_x$	Hexagonal, NA	5.88	NAp	9.4	NA
	$Fe_3HO_8 \cdot 4H_2O$	Hexagonal, NA	5.08	NAp	9.4	NA
Ferrihydrite	$5Fe_2O_3 \cdot 9H_2O$	Hexagonal, NA	5.08	NAp	9.4	NA
Feroxyhyte (δ'-FeOOH)	FeOOH	Hexagonal, NA	2.93	NAp	4.60	1
Hematite (α-Fe_2O_3)	Fe_2O_3	Hexagonal, R$\bar{3}$c	5.04	NAp	13.77	6
Maghemite (γ-Fe_2O_3)	Fe_2O_3	Cubic, P2$_1$3	8.32	8.32	8.32	8
		Tetragonal, P4$_1$2$_1$2	8.338	8.338	25.014	NA
Magnetitie (spinel)	Fe_3O_4	Cubic, Fd3m	8.39	8.39	8.39	8

NA Not available. NAp Not applicable.

yhyte, goethite, and lepidocrocite. Other iron oxide minerals observed include akaganeite, ferrihydrite, hematite, magnetite, and maghemite.

Feroxyhyte

Feroxyhyte is considered to be a polymorph with akaganeite, goethite, and lepidocrocite and has a formula of δ'-FeOOH (*27*). The structure is thought to be a hexagonal close packing of oxygen and differs only from δ-FeOOH by the arrangement of the iron atoms. Feroxyhyte is found as yellow-brown plates in admixtures of clay minerals and goethite. Its strongest diffraction lines are 2.54 and 2.23 Å, with other lines at 1.69 and 1.47 Å (*27*).

As a magnetically disordered form of δ-FeOOH, no reflection characterizing an ordered distribution of Fe^{3+} in the octahedral sites is observed in electron diffraction patterns from feroxyhyte. Feroxyhyte is unstable in air and transforms to goethite (*38*).

Goethite

Goethite (α-FeOOH) is the polymorph to which most other FeOOH phases revert upon aging. It is isostructural with the manganese minerals ramsdellite and groutite, consisting of double chains of $[Fe(O,OH)_6]$ octahedra linked together by sharing opposite edges. An octahedron from one chain shares an edge with two octahedra from another chain, and the double chains are further crosslinked to adjacent double chains through double sharing of oxygen, producing an orthorhombic symmetry. The goethite in this structure occurs in a habit of acicular needles, 0.1 to 1.0 μm in length. The iron atoms occupy only octahedral positions in this yellow-brown colored mineral (*38*).

Goethite is an antiferromagnetic mineral, that is, goethite remains weakly magnetized even when a magnetic field is removed. The magnetization is not reversible. High Cl^- concentrations in seawater should inhibit the formation of goethite. Thus, the widely reported occurrence of goethite in nodules may result from the fact that it is the end product of both hydrolysis and oxidation action in the other FeOOH phases (*38*).

Lepidocrocite

The abundance of reported lepidocrocite (γ-FeOOH) appears to indicate a relatively rapid oxidation of Fe(II) solutions, though it may occasionally form from Fe(III). Lepidocrocite has a cubic close-packed oxygen lattice structure with no structural analogues among the manganese oxides or hydroxide phases. The iron atoms occupy only octahedral positions in the stacking of oxygen-hydroxyl planes along the [051] direction. This orange-colored mineral forms lathe-shaped crystals ranging from 0.5 to 1.0 μm long (*38*).

Lepidocrocite is neither ferrimagnetic nor antiferromagnetic at ordinary temperatures, and so it carries no magnetic remnants. It is transformed to maghemite at 250° to 300° C.

Other Iron Oxide Minerals

Akaganeite (β-FeOOH) is the form of iron hydroxide that precipitates from Cl^- rich solutions such as seawater. The failure to identify akaganeite more frequently in nodules may be the result of rapid conversion to the more stable goethite under seawater conditions, though akaganeite has been shown to be stable for up to 2 yr at pressures up to 1,000 atm (*38*). Also the cryptocrystallinity of akaganeite may have resulted in the mineral being amorphous to X-ray diffraction, or phases identified as phillipsite may have actually been mixtures of goethite and akaganeite (*38*).

Magnetite (Fe_3O_4) and maghemite (γ-Fe_2O_3) result from relatively slow oxidation of Fe(II) solutions, and can form authigenically in the ferromanganese nodules. Hematite can crystallize from the seawater dissolution of fine-grained goethite or by dehydration of the goethite, but environmental conditions may cause the formation of both minerals by separate pathways. Hematite, once formed, does not appear to rehydrate to form goethite. Hematite is also formed by the aggregation of small ferrihydrite particles followed by nucleation and crystallization of hematite. Ferrihydrite also serves as a source of dissolved iron for the crystallization of goethite.

Iron Oxide Mineral-Element Association

Several elements are associated solely with the iron oxide phase of the nodule. Other elements have been shown to exist in iron oxide phases and with manganese or accessory phases. Those elements associated almost entirely with the iron oxide phase are Pb and Ti with Co occurring in both the iron and manganese phases depending on the oxidation-reduction potential of the seafloor (generally related to depth). Other elements associated with the iron phase, but which may also be found in other phases, are Ce, Co, Sr, V, and Zr.

Accessory Minerals

The accessory minerals found in Pacific manganese nodules can be divided into the following three general categories:

1. Sheet silicates and zeolite minerals.
2. Clastic silicates and volcanic minerals.
3. Biogenic minerals.

These minerals are poorly defined in manganese nodules because most exist as fine-grained crystallites similar to the manganese- and iron-phase minerals. Some of these accessory minerals were identified in the residue of acid leached nodules. This acid leaching tends to concentrate, and potentially recrystallize and/or flocculate these minerals together with the iron phase minerals while dissolving the manganese-phase minerals. Because of their low concentrations in nodules, the accessory minerals are often not detected by X-ray diffraction methods on bulk samples. Some minerals have been identified by selective area electron diffraction.

Although most published studies on manganese nodules do not address the accessory minerals, some of these minerals may be necessary for the nucleation and growth of the iron and manganese oxides. Quite often, the core or nucleus of nodules consists of volcanic rock fragments, glass, shark teeth, fish bones, or siliceous and calcareous remains of marine organisms. Table 4 lists the various accessory minerals, their formulas, and other parameters. References to occurrence are published elsewhere (*1, 16*).

Sheet Silicates and Zeolites

Several sheet silicates and zeolites have been reported in manganese nodules. The clays found in nodules are those associated with the sediments where the nodules were formed (*39-40*), and are fine-grained hydrous aluminum silicates probably formed by submarine alteration of the primary mineral basalts. The sheet silicates reported in nodules are chlorite, illite, kaolinite, montmorillonite, nontronite, pyrophyllite, and

Table 4.—Accessory minerals in Pacific manganese nodules

Mineral group and mineral	Formula	Crystal system and space group	Cell parameters, Å			
			a	b	c	z
SILICATES						
Tectosilicates:						
Zeolites:						
Analcite	$NaAlSi_2O_6 \cdot H_2O$	Cubic, Ia3d	13.72	13.72	13.72	16
Clinoptilolite	$(Na,K,Ca)_{2-3}Al_3(Al,Si)_2Si_{13}O_{36} \cdot 12H_2O$	Monoclinic, I2/m	15.85	17.89	7.41	4
Epistilbite	$CaAl_2Si_6O_{16} \cdot 5H_2O$	Monoclinic, NA	8.92	17.73	10.21	3
Erionite	$(Ca,Na,K,Mg)_5Al_9Si_{27}O_{72} \cdot 27H_2O$	Hexagonal, $P6_3/mmc$	13.26	NAp	15.12	NA
Mordenite	$(Ca,Na_2,K_2)_4Al_8Si_{40}O_{96} \cdot 28H_2O$	Orthorhombic, Cmcm	18.13	20.49	7.52	4
Phillipsite	$KCa(Al_3Si_5O_{16}) \cdot 6H_2O$	Orthorhombic, B2mb	9.96	14.25	14.25	4
Do.	$K_{28}Na_{16}Al_{44}Si_{116}O_{32} \cdot 10H_2O$	Monoclinic, P2, or $P2_1/m$	10.02	14.28	8.64	2
K-feldspar (orthoclase)	$KAlSi_3O_8$	Monoclinic, C2/m	8.56	12.96	7.21	4
Labradorite (feldspar)	$Ab_{50}An_{50} - Ab_{30}An_{70}$	Triclinic, NA	8.17	12.85	7.13	NA
Plagioclase (feldspar)	$(Na,Ca)Al(Si,Al)Si_2O_8$	Triclinic, NA	8.14	12.84	7.16	8
Sanidine (feldspar)	$(Na,K)AlSi_3O_8$	Monoclinic, C2/m	8.56	13.03	7.17	4
Quartz	SiO_2	Hexagonal, $P3_221$-$P3_121$	4.91	NAp	5.41	3
Phyllosilicates:						
Chlorite	$(Mg,Fe)_3(Si,Al)_4O_{10}(OH)_2 \cdot (Mg,Fe)_3(OH)_6$	Monoclinic, C2/m	5.2	9.2	28.6	4
Illite	General term for mica-like clays	NAp	NAp	NAp	NAp	NAp
Kaolinite	$Al_2Si_2O_5(OH)_4$	Triclinic, Pl.	5.14	8.93	7.37	2
Montmorillonite	$(Al,Mg)_8(Si_4O_{10})_3(OH)_{10} \cdot 12H_2O$	Monoclinic, C2/m	5.23	8.93-9.00	29.8	NA
Nontronite	$Fe_2(Al,Si)_4O_{10}(OH)_2Na_{0.3}4(H_2O)_4$	Monoclinic, NA	5.23	9.10-9.12	NA	NA
Pyrophyllite	$Al_2Si_4O_{10}(OH)_2$	Monoclinic, C2/c	5.16	8.88	18.64	2
Talc	$Mg_3Si_4O_{10}(OH)_2$	Monoclinic, C2/c	5.27	9.12	18.85	4
Biotite (mica)	$K(Mg,Fe)_3(AlSi_3O_{10})(OH)_2$	Monoclinic, C2/m	5.31	9.23	10.18	2
Prehnite	$Ca_2Al(AlSi_3O_{10})(OH)_2$	Orthorhombic, P2c/m	4.65	5.48	18.49	2
Stilpnomelane	$K(Fe,Mg,Al)_3Si_4O_{10}(OH)_2 \cdot xH_2O$	Monoclinic, NA	5.40	9.42	12.14	1
Inosilicates (double chain):						
Hornblende (amphibole)	$(Ca,Na)_{2-3}(Mg,Fe,Al)_5Si_6(SiAl)_2O_{22}(OH)_2$	Monoclinic, C2/m	9.87	18.01	5.33	2
Inosilicates (single chain):						
Augite (pyroxene)	$(Ca,Na)(Mg,Fe,Al)(Si,Al)_2O_6$	Monoclinic, C2/c	9.73	8.91	5.25	4
Nesosilicates: Olivine	$(Mg,Fe)_2SiO_4$	Orthorhombic, Pmcn	4.76-4.82	10.20-10.48	5.98-6.11	4
Other silicates:						
Opal (amorphous)	$SiO_2 \cdot nH_2O$	NAp	NAp	NAp	NAp	NAp
Titanite (sphene)	$CaTiO(SiO_5)$	Monoclinic, C2/c	6.56	8.72	7.44	4
NONSILICATES						
Volcanics:						
Anatase	TiO_2	Tetragonal, $I4_1/amd$	3.78	3.78	9.51	4
Barite	$BaSO_4$	Orthohombic, Pnma	8.87	5.45	7.14	4
Ilmenite	$FeTiO_3$	Hexagonal, $R\bar{3}$	5.09	Nap	14.06	6
Magnetite (spinel)	$(Fe,Mg)Fe_2O_4$	Cubic, Fd3m	8.40	8.40	8.40	8
Rutile	TiO_2	Tetragonal, $P4_2/mnm$	4.59	4.59	2.96	2
Biogenics:						
Apatite	$Ca_5(PO_4)_3(F,Cl,OH)$	Hexagonal, $P6_3/m$	9.39	NAp	6.89	2
Aragonite	$CaCO_3$	Orthorhombic, Pmcn	4.95	7.96	5.73	4
Calcite	$CaCO_3$	Hexagonal, $R\bar{3}c$	4.99	NAp	17.06	6

NA Not available. NAp Not applicable.

talc. The common clay present is montmorillonite. These minerals in nodules occur probably from inclusion of the sediments during nodule growth.

The zeolites found in nodules are authigenic and are found in cracks and cavities in the interior of nodules. The zeolites are hydrous silicates with a very open framework and large interconnecting spaces or channels that are filled with sodium, calcium, and variable amounts of water. The zeolites reported in nodules are analcite, clinoptilolite, epistilbite, erionite, mordenite, and phillipsite. The most commonly reported zeolite is phillipsite, whereas the remaining zeolites are rare with some question of their proper identification. Phillipsite, because of its delicate euhedral crystal habit and its occurrence in the leached interior cavities of nodules appears to have formed authigenically (fig. 3). Phillipsite crystals in some nodules appear to have grown together with some of the manganese oxide phase minerals, particularly todorokite (*39-40*).

Clastic Silicates and Volcanics

Many silicate minerals and some volcanic minerals have been observed in manganese nodules. They consist of individual grains of clastic sediments of various minerals that may form the core or become incorporated into the nodule during nodule growth. The more common minerals present are quartz and various feldspars. One mineral, opal, is believed to have formed authigenically. The volcanic minerals reportedly observed in manganese nodules are barite, magnetite (spinel), and the titanium-containing minerals, anatase, ilmenite, rutile, and sphene.

Biogenics

The biogenic minerals found in manganese nodules come from the debris of dead organisms, such as of bones and teeth of fish, sharks, and whales, and the siliceous remains of the

Figure 3.—Scanning electron photomicrograph showing crystals of the zeolite phillipsite in an oxide cavity of a manganese nodule. (Photograph courtesy of reference 17, p. 60)

zooplankton radiolaria. The larger debris such as bones and teeth are generally associated with the cores of nodules whereas the radiolaria remains are observed throughout the nodules. These radiolaria remains are probably incorporated from the sediment as the nodule grows. The debris in the interior of the nodule may undergo dissolution and may be associated with the formation of phillipsite and todorokite. The minerals of biogenic origin are apatite, primarily from bones and teeth; aragonite and calcite, from the shells of various animals; and opal, which may also be derived from radiolaria.

Sea Salt Residue

Minerals in dried nodules that are the result of seawater evaporation are sylvite, halite, and other common evaporites present in dissolved form in seawater. These residues are also the primary source of the anions—borate, bromide, chloride, fluoride, and iodide—in manganese nodules.

Accessory Mineral-Element Association

Several elements are associated solely with the accessory minerals of the nodule. Other elements have been shown to exist in accessory minerals and with the iron oxide or manganese phases. Those elements associated almost entirely with the accessory minerals are Al, Cr, K, P, and Si. Other elements associated with the accessory minerals and possibly other phases are Ba, Mg, Na, and Zr.

Moisture Content

Water comprises about 45 to 50 wt pct of the manganese nodules when removed from the sea. Drying in air removes approximately half of the water. Drying at 110° C reduces the moisture content of nodules to approximately 5 to 10 wt pct. Thermal gravimetric analysis in the temperature range of 110° to 1,200° C indicates that the 5 to 10 wt pct water is bound in the crystal structure.

ELEMENTAL COMPOSITION

The elemental characterization of Pacific manganese nodules is a topic addressed by many authors. Major element composition of these nodules is well established, whereas data on many minor and most trace elements are limited. This section summarizes available data on most of the elements, and where data are sufficient, gives ranges, means, medians, and number of samples. In the case of the major, most minor, and some trace elements, the data are divided into four distinct areas of the Pacific Ocean floor (see figure 4).

1. The Clarion-Clipperton fracture zone area (CC-Zone area).
2. The mid-Pacific seamounts area (MPS area), <3,000-m depth.
3. Other abyssal plains area >3,000-m depth, and exclusive of CC-Zone area.
4. Other seamounts, ridges, and continental margins area (<3,000-m depth).

For these elements, comparison tables are presented for the different areas to show variations of these elements by area. Where a paucity of data exist for the remaining elements, tables are presented for the composition based on the total Pacific Ocean. In some cases, data are limited (<40 sample analyses). Nodules from the Drake Passage area of the Pacific and most of the ocean area directly south of Australia have also been omitted. The Drake Passage nodules are omitted because of their tendency to contain large rock fragments as nuclei, thereby making their bulk chemical analysis atypical of the other Pacific nodules. The area south of Australia is considered the southeast portion of the Indian Ocean and not part of the Pacific Ocean.

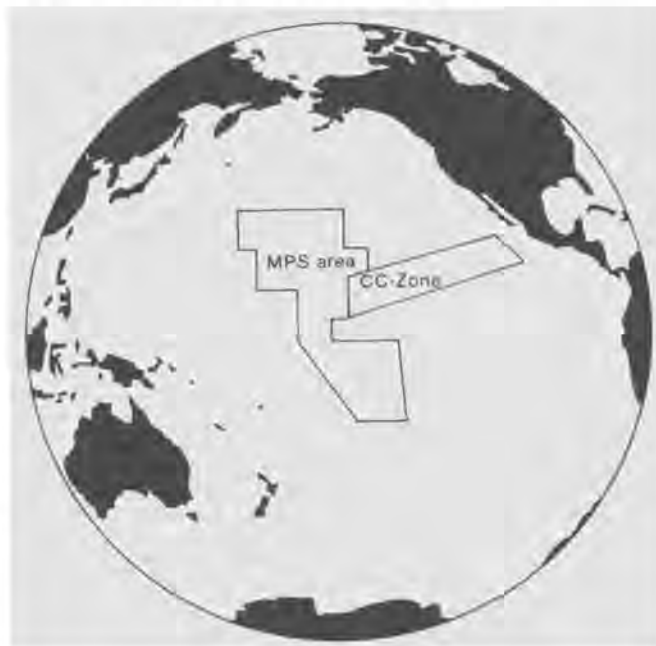

Figure 4.—Map of the Pacific Ocean showing CC Zone and MPS areas.

Table 5.—Distribution of elements of potential economic interest in Pacific manganese nodules, by area, weight percent

Area	Range	Median	Mean, $\bar{x}$	Number of samples	Range	Median	Mean, $\bar{x}$	Number of samples
	Manganese				Cobalt			
Clarion-Clipperton zone	1 -39	26 -27	25.4	2,227	<0.10 -0.90	0.20-0.30	0.24	1,925
Mid-Pacific seamounts	1 -40	20 -21	20.8	183	<.10 -2.50	70- .80	.76	182
Other abyssal plains, >3,000 m	1 -40	18 -19	18.5	2,354	<.10 -1.40	.20- .30	.24	2,219
Other seamounts, <3,000 m	1 -40	16 -17	17.8	315	<.05 -1.40	.20- .30	.31	293
	Iron				Zinc			
Clarion-Clipperton zone	1 -25	6 - 7	6.9	2,215	<0.05 -0.95	0.10-0.15	0.14	1,539
Mid-Pacific seamounts	2 -25	14.5 -15.5	14.7	185	<.05 - .25	.05-0.10	0.07	82
Other abyssal plains, >3,000 m	1 -25	12 -13	12.7	2,325	<0.05 - .95	.05- .10	.09	1,285
Other seamounts, <3,000 m	1 -25	16 -17	15.6	312	<.05 - .55	.05- .10	.07	191
	Nickel				Vanadium			
Clarion-Clipperton zone	0.10- 2.00	1.30- 1.40	1.28	2,237	<0.005-0.08	0.04-0.05	0.047	70
Mid-Pacific seamounts	.10- 1.50	.40- .50	.49	188	<.005- .30	.07- .08	.086	29
Other abyssal plains, >3,000 m	.10- 2.00	.50- .60	.63	2,334	<.010- .30	.04- .05	.048	370
Other seamounts, <3,000 m	.10- 1.30	.30- .40	.35	315	<.005- .14	.06- .07	.067	38
	Copper				Molybdenum			
Clarion-Clipperton zone	0.10- 2.00	1.00- 1.10	1.02	2,236	<0.005-0.12	0.05-0.06	0.052	265
Mid-Pacific seamounts	<.01- 1.00	<.05	.10	176	<.005- .11	.05- .06	.052	56
Other abyssal plains, >3,000 m	<.05- 2.00	.30- .40	.42	2,282	<.005- .13	.03- .04	.036	746
Other seamounts, <3,000 m	<.05- 1.20	<.05	.11	304	<.005- .15	.03- .04	.050	88

The data for the elements are broken down into seven groups based on either their chemistry or special interest. The groups of elements are presented in the following order:

1. Major and minor elements of potential economic interest (Mn, Fe, Ni, Cu, Co, Zn, V, Mo).
2. Other major and minor elements (Al, Ca, Mg, K, Si, Na, Sr, Ti, Zr).
3. Elements of environmental interest (As, Ba, Cd, Cr, Pb, Hg, Se, Ag).
4. Rare-earth elements (lanthanides) (La, Ce, Pr, Nd, Sm, Eu, Gd, Tb, Dy, Ho, Er, Tm, Yb, Lu, Hf).
5. Precious-metal-group and radioactive elements (Au, Ir, Pd, Pt, Ra, Re, Ru, Th, U).
6. Other trace elements (Sb, Be, Bi, B, Cs, Ga, Ge, Li, Nb, Rb, Sc, Ta, Te, Tl, Sn, W, Y).
7. Anion-forming elements (Br, C, Cl, F, I, N, P, S).

Within the first group, each element is discussed briefly and the chemical form of occurrence in nodules is given if known. Of the naturally occurring elements (exclusive of inert gases and hydrogen), no data were obtained for the following elements: Rh, In, Pm, Os, Po, At, Fr, Ac, and Pa. Oxygen is not discussed specifically but is the major combining form for most elements. All concentrations are reported on a dry-weight basis. The majority of the information contained in these sections comes from Frazer (*41-44*), Sorem (*45*), Fewkes (*46-47*), and Monget (*48*).

Major and Minor Elements of Potential Economic Interest

The elements in this section are those major and minor elements that are of potential economic interest. The eight elements are Mn, Fe, Ni, Cu, Co, Zn, V, and Mo. Because of the amount of data available, the concentrations of these elements are divided into the four areas of the Pacific as mentioned previously. Table 5 gives a breakdown, by element, for the four areas, and gives range, median range, arithmetic mean, and the number of samples used for the statistical base.

Table 6.—Distribution of elements of potential economic interest in Pacific manganese nodules, composite, weight percent

Element	Range	Range of medians	Weighted mean	Number of samples
Manganese ...	1 -40	16 -27	21.6	5,079
Iron	1 -25	6 -17	10.4	5,037
Nickel	.1 - 2.0	.3 - 1.4	.9	5,074
Copper	<.01 - 2.0	<.05- 1.10	.66	4,998
Cobalt	<.05 - 2.5	.2 - .8	.26	4,619
Zinc	<.05 - .95	.05- .15	.11	3,097
Vanadium	<.005- .30	.04- .08	.05	507
Molybdenum .	<.005- .15	.03- .06	.04	1,157

Table 6 gives composite data for those elements from Pacific nodules. The weighted mean in table 6 is calculated based on the number of data points for each element in each area and the respective concentrations.

Manganese

Manganese concentrations in Pacific nodules vary from 1 to 40 wt pct with a median range of 16 to 27 wt pct, and weighted mean of 21.6 wt pct based on 5,079 sample analyses. The median value for CC-Zone area nodules is the highest of all other areas at 26 to 27 wt pct with a mean of 25.4 wt pct. Nodules from the other three areas are much lower in manganese with a median range of 16 to 21 wt pct and with much higher iron values. Manganese occurs in Pacific nodules as several minerals, all oxides and hydrated oxides. These minerals are todorokite, birnessite, and vernadite (δ-MnO_2).

Manganese in the CC-Zone area is positively correlated with Cd, Cu, Mg, Mo, Ni, Sr, V, and Zn and is negatively correlated with Al, Fe, K, Si, Na, and Ti. In the MPS area, manganese shows a positive correlation with Co, Pb, Mo, Ni, Sr, Zn, and Zr, and a negative correlation with Al and Ca. In the other abyssal plains area manganese is positively correlated with Cd, Cu, Mo, Ni, and Zn and negatively correlated

with Al, Fe, K, and Si. In the other seamounts area, manganese is positively correlated with Ba, Ni, and Na and negatively correlated with Al, Cd, and Fe. Where elements are not mentioned, no correlation was obtained. A positive correlation of manganese with Cu, Ni, Mo, and Zn and a negative correlation of manganese with Al and Fe are observed in all areas. The difference in elemental composition between the lesser depths (MPS and other seamounts) and greater depths (CC-Zone and other abyssal) may reflect difference in oxidation potential as well as sediment type.

Iron

Iron concentrations in Pacific nodules vary from 1 to 25 wt pct with a median range of 6 to 17 wt pct and a weighted mean of 10.4 wt pct based on 5,037 sample analyses. The median value for for CC-Zone area nodules is lowest of all areas at 6 to 7 wt pct with a mean of 6.9 wt pct. The other three areas are much higher in iron with a median range for these areas of 12 to 17 wt pct. Iron occurs in Pacific nodules as goethite and other iron oxides and hydrated oxides.

Iron in CC-Zones area nodules is positively correlated with Co, Pb, Ti, and Zr and negatively correlated with Cd, Cu, Mg, Mn, Mo, Ni, and Zn. In the MPS area, iron is positively correlated with Ti and Zr, and negatively correlated with Ba and Ca. In the other abyssal area, iron is positively correlated with Co, Pb, Sr, Ti, V, and Zr, and negatively correlated with Cd, Cu, Mn, Ni, and K. In the other seamount area, iron is positively correlated with Cr, Ti, V, and Zr, and negatively correlated with Ba, Ca, and Mn.

Nickel

Nickel concentrations in Pacific nodules vary from 0.1 to 2.0 wt pct with a median range of 0.3 to 1.4 wt pct and a weighted mean of 0.9 wt pct based on 5,074 sample analyses. The median value for CC-Zone area nodules is 1.3 to 1.4 wt pct with a mean 1.3 wt pct. The other three areas are much lower in nickel content with a median range of 0.3 to 0.6 wt pct.

Nickel occurs in Pacific nodules as part of the manganese mineral structure probably adding stability to the minerals. The nickel is strongly correlated with manganese in all areas of the Pacific. The ionic radius of Ni^{2+} allows for direct substitution of Ni^{2+} for Mn^{2+} in the crystal structures.

Nickel in CC-Zone area nodules is positively correlated with Cd, Cu, Mg, Mn, Mo, Sr, V, and Zn and negatively correlated with Fe, Si, and Ti. In the MPS area, nickel is positively correlated with Cr, Co, Mg, Mn, Mo, Na, and Zn, and negatively correlated with Al only. In the other abyssal plains area, nickel is positively correlated with Cd, Cu, Mn, Mo, and Zn, and negatively correlated with Fe and Si. In the other seamounts area, nickel is positively correlated with Cd, Co, Cu, Mg, Mn, and Zn with no negative correlations found.

Copper

Copper concentrations in Pacific nodules varies from <0.01 to 2.0 wt pct with a median range of <0.05 to 1.1 and a weighted mean of 0.66 based on 4,998 sample analyses. The median value for CC-Zone area nodules is 1.0 to 1.1 wt pct with a mean of 1.0 wt pct. The other three areas are much lower in copper with a median range of <0.05 to 0.4 wt pct.

Copper occurs in Pacific nodules in a manner similar to that of nickel, which is part of the manganese mineral structure with no copper minerals present. The ionic radius of Cu^{2+} allows direct substitution for Mn^{2+} in the manganese minerals crystal structure.

Copper in CC-Zone area nodules is positively correlated with Al, Cd, Mg, Mn, Mo, Ni, Sr, V, and Zn, and negatively correlated with Fe, Pb, K, Si, Na, Ti, and Zr. In the MPS area, copper is positively correlated with Cr only and negatively correlated with Al and Zr. In the other abyssal plains area, copper is positively correlated with Cd, Mn, Ni, and Zn, and negatively correlated with Fe and Pb. In the other seamounts area, copper is positively correlated with Cd, Mg, Ni, V, and Zn, and shows no negative correlation with the other elements.

Cobalt

Cobalt concentrations in Pacific nodules vary from <0.05 to 2.5 wt pct with a median range of 0.2 to 0.8 wt pct and a weighted mean of 0.26 wt pct based on 4,619 sample analyses. The median value for CC-Zone area nodules is 0.2 to 0.3 wt pct with a mean of 0.24 wt pct. Cobalt values are lowest in the two deep-ocean areas (CC-Zone and other abyssal plains) and the other seamounts area with all three having similar median ranges and means. The MPS area has the highest cobalt values, with a median range of 0.7 to 0.8 wt pct and a mean of 0.76 wt pct.

Cobalt occurs in Pacific nodules in both the manganese and iron phases. Its occurrence is dependent on the oxidation of cobalt to either Co^{2+} or Co^{3+}. In the MPS area, oxidation to Co^{3+} is one probable explanation of high cobalt values, whereas in the deep ocean the oxidation potential may be insufficient to oxidize Co^{2+} to Co^{3+}. Some cobalt in nodules can also be attributed to volcanic seamounts. Cobalt in the Co^{2+} state has an ionic radius similar to Mn^{2+}, whereas Co^{3+} has an ionic radius very close to that of Mn^{4+} and substitutes for Mn^{4+} in vernadite (*28-29*).

Cobalt in CC-Zone area nodules has a slight positive correlation with Fe, Pb, and Ti and a slight negative correlation with Cd. In the MPS area, cobalt is positively correlated with Ba, Pb, Mg, Mn, Ni, Sr, Ti, and Zr, and negatively correlated with Al, Ca, K, Si, and Na. In the other abyssal plains area, cobalt has a slight positive correlation with Fe and Sr, and a slight negative correlation with Al, Cd, and Si. In the other seamounts area, cobalt is positively correlated with Pb and Ti and has a slight positive correlation with nickel. Cobalt in this area has a slight negative correlation with Cd and Si.

Zinc

Zinc concentrations in Pacific nodules vary from <0.05 to 0.95 wt pct with a median value of 0.05 to 0.15 wt pct and a weighted mean of 0.11 wt pct based on 3,097 sample analyses. The median value for CC-Zone area nodules is 0.10 to 0.15 wt pct with a mean of 0.14. Zinc values are highest in CC-Zone nodules; approximately a factor of two higher than the other three areas. The median range for the other three areas is 0.05 to 0.10 with a mean range of 0.07 to 0.09 wt pct with lower values occurring in the seamount areas.

Zinc appears to occur in Pacific nodules as a substitute in the manganese mineral structure similar to copper and nickel. No zinc minerals have been identified in Pacific nodules. The zinc ionic radius is similar to Mn^{2+} and would allow a direct substitution.

Zinc in CC-Zone area nodules is positively correlated with Cu, Mn, and Ni, and negatively correlated with Fe and Zr, with only a slight negative correlation with Pb and Ti. In the MPS area, zinc is positively correlated with Ba, Mn, Ni, Na,

and V, and negatively correlated with Mg, Ti, and Zr. In the other abyssal plains area, zinc is positively correlated with Cu, Mn, and Ni and negatively correlated with Al. In the other seamounts area, zinc is positively correlated with Cd, Cu, and Ni and negatively correlated with Na.

Vanadium

Vanadium concentrations in Pacific nodules vary from <0.005 to 0.30 wt pct with a median value of 0.04 to 0.08 wt pct and a weighted mean of 0.05 wt pct based on 507 sample analyses. The median value for CC-Zone area nodules is 0.04 to 0.05 wt pct with a mean for 0.047 wt pct. The CC-Zone and other abyssal plains area have somewhat lower median and mean values than the two seamount areas by about a factor of 1.5 to 2.0.

Vanadium appears to be another of the many elements that occur with manganese mineral structure and may possibly substitute for Mn^{4+} or fill the large tunnels in the manganese mineral structure as oxides. Correlation coefficient data indicate a tendency for vanadium to occur with Mn, Cu, and Ni, all of which have been shown to substitute for manganese in the manganese mineral structure.

Vanadium in CC-Zone area nodules correlates positively with Ca, Cu, Mn, and Ni and negatively with Al and Na. In the MPS area, vanadium correlates positively with K, Na, and Zn and negatively with Pb, Mo, and Ti. In the other abyssal plains area, vanadium correlates positively with Fe and Mo and negatively with Si. In the other seamounts area, vanadium correlates positively with Al, Cu, Fe, K, and Ti, and negatively with Ba and Ca. Vanadium data are very limited in the seamount areas so that correlations in these areas may not accurately reflect the actual correlation of vanadium to other elements.

Molybdenum

Molybdenum concentrations in Pacific nodules vary from <0.005 to 0.15 wt pct with a median value of 0.03 to 0.06 and a weighted mean of 0.04 wt pct based on 1,157 sample analyses. The median value for CC-Zone area nodules is 0.05 to 0.06 wt pct with a mean value of 0.05 wt pct. Molybdenum concentrations appear to be somewhat uniform throughout all four areas with only a slightly lower mean for the other abyssal plains area.

Molybdenum appears to occur in a manner similar to that of Cu and Ni; that is, as a substitute in the manganese structure. No molybdenum minerals have been identified in Pacific nodules. The ionic radius of molybdenum in oxidation states 4 and 6 is similar to Mn^{4+}, and therefore it may be a substitute for Mn^{4+} or it may be contained in the smaller tunnel structure of the manganese minerals.

Molybdenum in CC-Zone area nodules is positively correlated with Cd, Cu, Mn, and Ni, and negatively correlated with Fe. In the MPS area, molybdenum is positively correlated with Mn, Ni, and Na and negatively correlated with Al and V. In the other abyssal plains area, molybdenum is positively correlated with Cd, Mn, Ni, and V, and negatively correlated with Al and Si. In the other seamounts area, molybdenum is positively correlated with Pb and Na and has no negative correlation. Molybdenum data in the two seamount areas are limited; therefore, correlation coefficients may not accurately reflect the actual correlation of molybdenum to other elements.

General Observations

CC-Zone area nodules contain the highest levels of Mn, Ni, Cu, and Zn and the lowest amounts of Fe and Co. Vanadium content is slightly lower in the CC-Zone area than in other areas and molybdenum appears to be uniformly concentrated in all areas. The seamount areas contain the highest levels of Fe and Co with a slight elevation of V, and they contain the lowest levels of Ni and Cu. The different environments encountered in the seamount areas versus the abyssal areas may show the effect of oxidation and sediment types on the formation of Pacific nodules. Cobalt occurs with both the Fe and Mn phases, with higher cobalt and iron values being observed in nodules formed in the more elevated sea floor areas (MPS and other seamounts areas).

Other Major and Minor Elements

The major and minor elements discussed in this section are not of any present economic or environmental interest as applied to manganese nodule processing. The nine elements, Al, Ca, Mg, K, Si, Na, Sr, Ti, and Zr, are presented with data divided into the four geographic areas as shown in table 7. Table 8 gives composite data for these elements from Pacific nodules.

The two abyssal plains areas have the higher levels of Al, K, Si, and Na by about a factor of 2 over the two seamount areas. In contrast, the two seamount areas have higher Ca and Sr by the same factor. Magnesium, titanium, and zirconium values are relatively uniform with the CC-Zone area having the lowest zirconium values and the MPS area having the highest titanium values.

Aluminum occurs primarily as an aluminum silicate in clay inclusions in Pacific nodules in the form of alkali and plagioclase feldspars. Calcium occurs in Pacific nodules in several forms including calcite, apatite, and/or in feldspars. Calcium also is known to substitute in the manganese mineral structure to some degree.

Magnesium occurs in Pacific nodules in several forms. Some of the magnesium content of nodules is a result of dissolved seawater salts. Magnesium also occurs in the manganese mineral structures. Its ionic radius is such that it could substitute in the same sites as Cu and Ni. The occurrence of potassium in Pacific nodules is in two forms: as dissolved sea salts that crystallize when the samples dry, probably as KCl (sylvite), and as plagioclase feldspars. Silicon occurs in Pacific nodules in two forms: as silicates in the feldspars and clays and as silica (SiO_2).

Sodium occurs in Pacific nodules in several forms. It occurs as dissolved sea salts that crystallize upon drying. It can also occur in some feldspars in the plagioclase group. Sodium is also a constituent of the manganese mineral structure of todorokite but is generally replaced by other cations such as Cu^{2+} and Ni^{2+}, which are thought to stabilize the crystal structure of the todorokite. Titanium in Pacific nodules appears to be associated with the iron phases present based on positive correlations with Fe and Co and negative correlations with Mn, Cu, and Ni. The ionic radius of Ti^{4+} is similar to that of Fe^{3+} and may allow it to substitute for iron. Titanium has also been observed in nodules as ilmenite, rutile, and anatase. Zirconium appears to occur in Pacific nodules in association with the iron phases. The ionic radius of Zr^{4+} is similar to that of Fe^{3+} and may allow some substitution in the iron phases.

Table 7.—Distribution of other major and minor elements in Pacific manganese nodules, by area, weight percent

Area	Range	Median	Mean, $\bar{x}$	Number of samples	Range	Median	Mean, $\bar{x}$	Number of samples
	Aluminum				Sodium			
Clarion-Clipperton zone	<0.50- 8.00	2.50-3.00	2.90	234	0.50 -6.75	2.00-2.25	2.79	106
Mid-Pacific seamounts	<.25- 6.00	.25- .75	1.20	48	.50 -5.50	1.45-1.55	2.13	28
Other abyssal plains, >3,000 m	<.50-10.0	2.50-3.00	3.05	570	<.25 -5.75	1.75-2.00	2.07	297
Other seamounts, <3,000 m	<.50- 7.00	1.00-1.50	1.70	79	.25 -3.75	1.25-1.50	1.64	37
	Calcium				Strontium			
Clarion-Clipperton zone	<0.5 -18.0	1.5 -2.0	1.7	872	<0.005-0.16	0.04-0.05	0.045	78
Mid-Pacific seamounts	<.5 -25.0	2.0 -2.5	4.2	91	<.005- .30	.14- .15	.13	27
Other abyssal plains, >3,000 m	<.5 -13.0	1.5 -2.0	1.8	914	<.005- .18	.07- .08	.08	320
Other seamounts, <3,000 m	<.5 -25.0	2.0 -3.0	4.5	200	<.005- .28	.13- .14	.135	68
	Magnesium				Titanium			
Clarion-Clipperton zone	<0.25- 3.00	1.50-1.75	1.65	209	0.10 -2.20	0.40-0.50	0.53	265
Mid-Pacific seamounts	.50- 3.50	.75-1.25	1.41	35	.20 -2.20	1.10-1.20	1.12	102
Other abyssal plains, >3,000 m	<.25- 5.00	1.25-1.50	1.43	361	<.05 -2.50	.60- .70	.78	854
Other seamounts, <3,000 m	<.25- 4.25	1.50-1.75	1.79	64	<.05 -1.60	.40- .50	.47	89
	Potassium				Zirconium			
Clarion-Clipperton zone	0.20- 3.00	0.80- .90	1.01	123	0.010-0.09	0.03-0.04	0.035	33
Mid-Pacific seamounts	.10- .90	.30- .40	.41	35	<.005- .11	.07- .075	.06	18
Other abyssal plains, >3,000 m	.10- 3.00	.70- .80	.93	335	<.005 - .20	.05- .06	.06	226
Other seamounts, <3,000 m	.10- 1.60	.30- .40	.54	66	<.005 - .20	.04- .05	.05	27
	Silicon							
Clarion-Clipperton zone	1.0 -25.0	6.0 -6.5	7.6	339				
Mid-Pacific seamounts	<.50-15.0	2.0 -3.0	3.6	45				
Other abyssal plains, >3,000 m	<.50-25.0	7.0 -8.0	8.8	460				
Other seamounts, <3,000 m	<.50-23.0	3.0 -4.0	4.8	91				

Table 8.—Distribution of other major and minor elements in Pacific manganese nodules, composite, weight percent

Element	Range	Range of medians	Weighted mean	Number of samples
Aluminum	<0.25 -10.0	0.25-3.0	2.80	931
Calcium	<.05 -25.0	1.50-3.0	2.12	2,077
Magnesium	<.25 - 5.0	.75-1.75	1.53	669
Potassium	.10 - 3.0	.30- .90	.87	559
Silicon	<.50 -25.0	2.0 -8.0	7.72	935
Sodium	<.25 - 6.75	1.25-2.25	2.20	468
Strontium	<.005- .300	.04- .15	.083	493
Titanium	<.05 - 2.50	.40-1.20	.73	1,310
Zirconium	<.005- .20	.03- .075	.058	304

Elements of Environmental Interest

Any of the following eight elements, As, Ba, Cd, Cr, Pb, Hg, Se, and Ag, when leached from wastes under conditions specified by the U.S. Environmental Protection Agency, will result in the waste being classified as a hazardous material, if their concentrations are greater than 100 times the National Drinking Water Standard. Data for Ba, Cd, Cr, and Pb are presented in table 9, by area, as in the previous sections. Data for the remaining elements (As, Hg, Se, and Ag), along with the other four listed in table 9, are presented in table 10 as a composite for Pacific Ocean nodules. These data are taken from the Sediment Data Bank (*41-44*) as well as

Table 9.—Distribution of elements of environmental interest in Pacific manganese nodules, by area

Area	Range	Median	Mean, $\bar{x}$	Number of samples	Range	Median	Mean, $\bar{x}$	Number of samples
	Barium, wt pct				Chromium, ppm			
Clarion-Clipperton zone	<0.01 - 0.76	0.20- 0.22	0.28	213	1- 150	15- 20	27	107
Mid-Pacific seamounts	.04 - .68	.18- .20	.30	39	1- 40	10- 20	58	22
Other abyssal plains, >3,000 m	<.005- .800	.14- .16	.20	499	1- 150	15- 20	25	227
Other seamounts, <3,000 m	.06 - .80	.32- .34	.37	59	1- 130	30- 40	60	38
	Cadmium, ppm				Lead, ppm			
Clarion-Clipperton zone	1 -35	10 -15	12.3	127	50-1,800	400- 500	450	921
Mid-Pacific seamounts	1 -25	5 -10	8.3	15	100-4,700	1,700-1,800	1,860	105
Other abyssal plains, >3,000 m	1 -35	5 -10	10.7	133	50-3,000	700- 800	820	1,185
Other seamounts, <3,000 m	1 -35	5 -10	10.2	23	50-3,000	1,000-1,100	1,030	206

Table 10.—Distribution of elements of environmental interest in Pacific manganese nodules, composite

Element	Range	Range of medians	Weighted mean	Number of samples
Arsenic ..ppm..	20-540	164	159	122
Barium wt pct..	<0.005-0.800	0.140-0.340	0.24	810
Cadmium ppm..	1.0-35	5-15	11	298
Chromium ppm..	1.0-150	10-40	31	394
Lead ....ppm..	50-4,700	400-1,800	742	2,417
Mercury .ppm..	0.002-0.78	0.085	0.15	68
Selenium ppm..	30-77	53	52	56
Silver ....ppm..	0.001-0.68	0.039	0.10	56

from Toth (*49*), Harris (*50*), and from analytical studies sponsored by the Bureau (*1*).

Nodules are enriched in As, Cd, Pb, and Se relative to their concentrations in deep-sea clays. The elements Ba, Cr, Hg, and Ag occur in Pacific nodules at levels similar to or less than corresponding levels of these elements reported for deep-sea clays.

In Pacific nodules, Ba and Cd are correlated with the Mn phases, and As, Pb, and Hg are correlated with the Fe phases. Barium may also occur as barite in the gangue minerals. Chromium appears to be correlated with silicon and may occur with entrapped sediments. No correlations for selenium and silver were noted.

The CC-Zone area and other abyssal plains areas contain the lowest Cr, Pb, and Se levels and the highest levels of Ba and Cd. The highest lead values occur in the MPS area.

Data for As, Hg, Se, and Ag are very limited; most of these data were generated for this study from selected nodule samples. Data for Ba, Cd, Cr, and Pb are more prevalent, and interpretations of these data are made with greater confidence. Based on the available information, the concentrations of many of these elements are too low to warrant environmental interest.

Rare-Earth Elements

The elements examined in this section are hafnium and all of the lanthanide series elements with the exception of promethium. For Pr, Dy, and Er, only limited sample analyses were available. Data for these elements are presented for the composite of the Pacific nodules as they are too limited to be presented by area. Table 11 lists the elements by atomic number with concentration range, median, mean, and total number of data points. A majority of the data available for these elements is from analysis of nodules taken from the CC-Zone area.

Table 11.—Rare-earth elements in Pacific manganese nodules, parts per million

Element	Range	Median	Mean	Number of samples
Lanthanum	66- 979	130	157	151
Cerium	74-3,000	345	530	131
Praseodymium	26- 46	34	36	8
Neodymium	60- 700	141	158	96
Samarium	14- 141	32	35	115
Europium	1- 27	7	9	115
Gadolinium	14- 53	33	32	57
Terbium	1- 11	5	5.4	104
Dysprosium	22- 42	32	31	18
Holmium	1- 8	4	4	66
Erbium	11- 27	19	18	18
Thulium	1- 9	2	2.3	41
Ytterbium	8- 100	17	20	171
Lutetium	1- 6	2	1.8	76
Hafnium	3- 14	5	6	96

The rare-earth values for Pacific nodules are primarily based on three publications, Glasby (*51*), Piper and Williamson (*52*), and Elderfield (*40*), plus data from the Sediment Data Bank (*41*). Rare-earth element content of nodules, with the exception of cerium, exhibits a decrease in rare-earth content relative to seawater content with increasing atomic number. Cerium shows a large enrichment relative to other rare-earth elements because of its oxidation to Ce^{4+} in nodules and it is associated primarily with the iron phase. Other rare-earth elements occur as oxides in both the iron and gangue phosphate phases. It has been reported that total rare-earth element content of Pacific nodules increases with increasing distance from land and is correlated with both the iron and manganese contents of nodules (*53*). A negative correlation of rare earths to silica content has also been observed. Rare-earth elements are incorporated in nodules mainly from seawater. Most variations of rare-earth content of nodules can be explained by dilution of the iron and manganese phases by silicate minerals. The rare earths are preferentially incorporated into nodules because of hydrolysis under oxidizing conditions (*51*). The rare-earth elements (exclusive of Ce) occur in two phases, a phosphate phase composed of fish debris and/or recrystallized biogenic apatite, and the hydrous iron oxide phase with chemisorbed phosphate.

Precious-Metal-Group and Radioactive Elements

The elements in this section are those elements that are classified as precious metals and/or platinum-group metals and radioactive elements. Very limited sample analyses are available for Au, Ir, Pd, Pt, Re, and Ru (*51, 54-56*). No data are available for Os and Rh, and Ag is discussed with the elements of environmental interest. Over 250 sample analyses are available for U and Th and nine values for Ra. A summary of the elemental composition of Pacific nodules for the nine elements is given in table 12.

Gold values show a positive correlation with silica content, whereas iridium values show a negative correlation (*51*). Gold and palladium are depleted in Pacific nodules compared to deep-sea sediments, whereas iridium shows an enrichment in nodules relative to deep-sea sediments. The ability for some of these elements to form stable anionic species (gold and rhenium) in seawater may explain their depletion in nodules.

The uranium and thorium content of Pacific nodules (and other nodules) can be explained by coprecipitation from seawater with the iron phase. Uranium and thorium content of nodules is enriched over seawater and deep-sea sediments.

Table 12.—Precious-metal-group and radioactive elements in Pacific manganese nodules

Element	Range	Median	Mean	Number of samples
Precious metal, ng/g:				
Gold	0.13-3.9	1.92	1.93	10
Iridium	0.2-23.1	4.3	9.1	11
Palladium	2.9-9.2	6.3	6.2	10
Platinum	<5-145	110	97	5
Rhenium	<0.2	NAp	NAp	2
Ruthenium	18	NAp	NAp	1
Radioactive:				
Radium ...pg/g..	1.0-35.7	5.1	8.5	9
Thorium ..ppm..	5-154	21	28	283
Uranium ..ppm..	1-68	5	6.8	255

NAp Not applicable

Their concentration is highest near the top surface interface with seawater and lowest at the bottom surface interface with the sediment. The interior of nodules has a concentration intermediate of the top and bottom surfaces.

Other Trace Elements

The 17 elements in this section for which data are available are Sb, Be, Bi, B, Cs, Ga, Ge, Li, Nb, Rb, Sc, Ta, Te, Tl, Sn, W, and Y. The data in table 13 come from the Sediment Data Bank (*41-44*) and other sources.

Of the 17 elements in this section, only 8 have more than 40 data points and only 4 have more than 100 sample analyses. Antimony is thought to be primarily associated with the manganese phase. All 17 trace elements may occur with any of the three phases and/or be present as a result of seawater residue incorporation.

Thallium merits special attention as the most enriched element in nodules when compared to deep-sea sediments. An inverse correlation is observed between thallium and silica content of nodules. Thallium as Tl^{+} is stable in acid and alkaline environments whereas Tl^{3+} is stable only at low pH and forms thallic hydroxide precipitate when Tl^{3+} solutions are made basic. Thallium probably exists in nodules as thallic hydroxide, $Tl(OH)_3$. The nodule environment may oxidize the Tl^{+} in sediments and precipitate thallium as the hydroxide (*51*).

Anion-Forming Elements

The eight elements in this section occur almost exclusively as anions in the chemical structure of Pacific nodules. These elements are Br, C, Cl, F, I, N, P, and S occurring as bromide, carbonate, chloride, fluoride, iodide, nitrate, phosphate, and sulfate anions. The anions, chloride, fluoride, bromide, and iodide present in nodules are primarily the result of residues from the evaporation of seawater.

Carbon occurs as carbonate in the form of gangue minerals such as calcite and other carbonate minerals and as entrapped organic matter.

Phosphorus is present as phosphate minerals such as apatite and calcium phosphate and is associated with the iron phases. Sharks' teeth inclusions in nodules increase the phosphate level substantially. Phosphorite pellets (apatite) have been observed as nucleii and inclusions in manganese nodules.

Sulfur as sulfate occurs in nodules in the form of barite ($BaSO_4$) and other sulfate minerals. The sulfide form is rare in the oxidizing environment in which nodules are formed.

Data for nitrogen as nitrate are limited; nitrate is likely a residue from seawater. Table 14 is a summary of the data available for these elements.

Table 13.—Other trace elements in Pacific manganese nodules, parts per million

Element	Range	Median	Mean	Number of samples
Antimony	14 - 72	36	37	103
Beryllium	2 - 15	2	4	29
Bismuth	6 - 31	23	21	13
Boron	17 -1,655	221	273	94
Cesium	<.50- 2.60	.70	.75	7
Gallium	2 - 72	6	11	39
Germanium	3 - 90	37	42	4
Lithium	23 -1,055	100	160	25
Niobium	6 - 150	80	74	42
Rubidium	5 - 60	15	15	43
Scandium	1 - 29	10	10	159
Tantalum	2 - 20	11	11	4
Tellurium	172 - 272	214	216	17
Thallium	2 - 675	160	169	141
Tin	2 - 450	80	108	87
Tungsten	26 - 120	80	76	7
Yttrium	17 - 950	111	133	132

Table 14.—Anion-forming elements in Pacific manganese nodules, weight percent

Element	Form	Range	Number of samples
Bromine	Br^{-}	0.002-0.080	7
Carbon	$CO_3^{=}$	.30 -1.70	22
Chlorine	Cl^{-}	<.01 -1.10	10
Fluorine	F^{-}	<.01 - .05	6
Iodine	I^{-}	<.01 - .25	7
Nitrogen	NO_3^{-}	<.01 - .18	6
Phosphorus	P_2O_5	<.01 -2.20	158
Sulfur	$SO_4^{=}$	.07 -6.60	24

Summary Tables

This section of the report contains summary tables for the 21 major and minor elements for each of the four areas of the Pacific. Table 15 is the summary table for the CC-Zone area, the MPS area, the other abyssal plains area, and the other seamounts area. Table 16 gives the composite composition of all 74 elements discussed in this report. The mean values in table 15 for the 21 major and minor elements (including Ba, Cd, Cr, and Pb) are weighted averages based on the total number of analyses from each area. The median range for these elements is the lowest and highest median value for the four areas for each element.

Table 15.—Summary of major, minor, and some trace elements in Pacific manganese nodules, by area

Element	Range	Median	Mean	Number of samples	Range	Median	Mean	Number of samples
	Clarion-Clipperton zone				Other abyssal plains, >3,000 m			
Aluminum ..... wt pct..	0.5-8.0	2.5-3.0	2.9	234	<0.5-10.0	2.5-3.0	3.0	570
Barium ..... wt pct..	<0.01-0.76	0.20-0.22	0.28	213	<0.005-0.80	0.14-0.16	0.20	499
Cadmium ..... ppm..	1-35	10-15	12.3	127	1-35	5-10	10.7	133
Calcium ..... wt pct..	<0.5-18.0	1.5-2.0	1.7	872	<0.5-13.0	1.5-2.0	1.8	914
Chromium ..... ppm..	1-150	15-20	27	107	1-150	15-20	25	227
Cobalt .....wt pct..	<0.1-0.9	0.20-0.30	0.24	1,925	<0.1-1.4	0.2-0.3	0.24	2,219
Copper .....wt pct..	0.1-2.0	1.0-1.1	1.02	2,236	<0.05-2.00	0.30-0.40	0.42	2,282
Iron .....wt pct..	1-25	6-7	6.9	2,215	1-25	12-13	12.7	2,325
Lead .....wt pct..	0.005-0.18	0.040-0.050	0.045	921	0.005-0.30	0.07-0.08	0.082	1,185
Magnesium ....wt pct..	<0.25-3.0	1.50-1.75	1.65	209	<0.25-5.00	1.25-1.50	1.43	361
Manganese ....wt pct..	1-39	26-27	25.4	2,227	1-40	18-19	18.5	2,354
Molybdenum ...wt pct..	<0.005-0.12	0.05-0.06	0.052	265	<0.005-0.13	0.03-0.04	0.036	746
Nickel .....wt pct..	0.1-2.0	1.3-1.4	1.28	2,237	0.1-2.0	0.50-0.60	0.63	2,334
Potassium .....wt pct..	0.20-3.0	0.80-0.90	1.01	123	0.10-3.0	0.70-0.80	0.93	335
Silicon .....wt pct..	1.0-25.0	6.0-6.5	7.6	339	0.5-25.0	7.0-8.0	8.8	460
Sodium .....wt pct..	0.50-6.75	2.00-2.25	2.79	106	<0.25-5.75	1.75-2.00	2.07	297
Strontium .....wt pct..	<0.005-0.16	0.040-0.050	0.045	78	<0.005-0.18	0.07-0.08	0.07	320
Titanium .....wt pct..	0.10-2.20	0.40-0.50	0.53	265	<0.05-2.50	0.60-0.70	0.78	854
Vanadium, ...wt pct..	<.005-0.08	0.040-0.050	0.047	70	0.01-0.30	0.04-0.05	0.048	370
Zinc .....wt pct..	<0.05-0.95	0.10-0.15	0.14	1,539	<0.05-0.95	0.05-0.10	0.09	1,285
Zirconium .....wt pct..	0.010-0.09	0.030-0.040	0.035	33	<0.005-0.20	0.05-0.06	0.062	226
	Mid-Pacific seamounts				Other seamounts, <3,000 m			
Aluminum .....wt pct..	<0.25-6.00	0.25-0.75	1.20	48	<0.5-7.0	1.0-1.5	1.7	79
Barium .....wt pct..	0.04-0.68	0.18-0.20	0.30	39	0.06-0.80	0.32-0.34	0.37	59
Cadmium ..... ppm..	1-25	5-10	8.3	15	1-35	5-10	10.2	23
Calcium .....wt pct..	<0.5-25.0	2.0-2.5	4.2	91	<0.5-25.0	2.0-3.0	4.5	200
Chromium ..... ppm..	1-40	10-20	58	22	1-130	30-40	60	38
Cobalt .....wt pct..	<0.1-2.5	0.7-0.8	0.76	182	<0.05-1.40	0.20-0.30	0.31	293
Copper .....wt pct..	<0.01-1.00	<0.05	0.10	176	<0.05-1.20	<0.05	0.11	304
Iron .....wt pct..	2-25	14.5-15.5	14.7	185	1-25	16-17	15.6	312
Lead .....wt pct..	0.01-0.47	0.17-0.18	0.186	105	0.005-0.30	0.10-0.11	0.10	206
Magnesium ....wt pct..	0.50-3.50	0.75-1.25	1.41	35	<0.25-4.25	1.50-1.75	1.79	64
Manganese ....wt pct..	1-40	20-21	20.8	183	1-40	16-17	17.8	315
Molybdenum ...wt pct..	<0.005-0.11	0.05-0.06	0.05	56	<0.005-0.15	0.03-0.04	0.05	88
Nickel .....wt pct..	0.1-1.5	0.40-0.50	0.49	188	0.1-1.4	0.3-0.4	0.35	315
Potassium .....wt pct..	0.10-0.90	0.30-0.40	0.41	35	0.10-1.60	0.30-0.40	0.54	66
Silicon .....wt pct..	<0.5-15.0	2.0-3.0	3.6	45	<0.5-23.0	3.0-4.0	4.8	91
Sodium .....wt pct..	0.50-5.50	1.45-1.55	2.13	28	0.25-3.75	1.25-1.50	1.64	37
Strontium .....wt pct..	<0.005-0.30	0.14-0.15	0.13	27	<0.005-0.28	0.13-0.14	0.135	68
Titanium .....wt pct..	0.20-2.20	1.10-1.20	1.12	102	<0.05-1.60	0.40-0.50	0.47	89
Vanadium .....wt pct..	<0.005-0.30	0.07-0.08	0.086	29	<0.005-0.14	0.06-0.07	0.067	38
Zinc .....wt pct..	<0.05-0.25	0.05-0.10	0.07	82	<0.05-0.55	0.05-0.10	0.07	191
Zirconium .....wt pct..	<0.005-0.110	0.070-0.075	0.061	18	<0.005-0.20	0.04-0.05	0.054	27

Table 16.—Summary of elements in Pacific manganese nodules, composite

Element and atomic number	Range	Median	Mean	Number of samples	Element and atomic number	Range	Median	Mean	Number of samples
Aluminum 13 wt pct	<0.25-10.00	0.25- 2.00	2.80	931	Molybdenum 42 wt pct	<0.005-0.150	0.030-0.060	0.041	1,157
Antimony 51 ppm	<14-72	36	37	103	Neodymium 60 ppm	60-700	141	158	96
Arsenic 33 ppm	20-450	164	159	122	Nickel 28 wt pct	0.10-2.00	0.30-1.40	0.89	5.074
Barium 56 wt pct	<0.005-0.800	0.140-0.340	0.239	810	Niobium 41 ppm	6-150	80	74	42
Beryllium 4 ppm	2-15	2	4	29	Nitrogen[2] 7 wt pct	<0.01-0.18	0.04	0.056	6
Bismuth 83 ppm	6-31	23	21	13	Palladium 46 ng/g	2.9-9.2	6.3	6.2	10
Boron 5 ppm	17-1,655	221	273	94	Phosphorus[3] 15 wt pct	<0.01-2.2	0.21	0.23	158
Bromine 35 wt pct	0.002-0.080	0.05	0.05	7	Platinum 78 ng/g	5-145	110	97	5
Cadmium 48 ppm	1-35	5-15	11	298	Potassium 19 wt pct	0.10-3.00	0.30-0.90	0.87	559
Calcium 20 wt pct	<0.05-25.00	0.50-3.00	2.12	2,077	Praseodymium 59 ppm	26-46	34	36	8
Carbon[1] 6 wt pct	0.30-1.70	0.19	0.18	22	Radium 88 pg/g	1.0-35.7	5.1	8.5	9
Cerium 58 ppm	74-3,000	345	530	131	Rhenium 75 ng/g	<0.2	NAp	NAp	2
Cesium 55 ppm	<0.5-2.6	<0.7	0.75	7	Rubidium 37 ppm	5-60	15	15	43
Chlorine 17 wt pct	<0.01-1.10	.78	.53	10	Ruthenium 44 ng/g	18	NAp	NAp	1
Chromium 24 ppm	1-150	10-40	31	394	Samarium 62 ppm	14-141	32	35	115
Cobalt 27 wt pct	<0.05-2.50	0.20-0.80	0.44	4,619	Scandium 21 ppm	1-29	10	10	159
Copper 29 wt pct	<0.01-2.00	<0.05-1.10	0.66	4,998	Selenium 34 ppm	30-77	53	52	56
Dysprosium 66 ppm	22-42	32	31	18	Silicon 14 wt pct	<0.5-25.0	2.0-8.0	7.8	935
Erbium 68 ppm	11-27	19	18	8	Silver 47 ng/g	2-680	39	101	56
Europium 63 ppm	1-27	7	9	115	Sodium 11 wt pct	<0.25-6.75	1.25-2.25	2.20	468
Fluorine 9 wt pct	<0.01-0.05	<0.01	0.013	6	Strontium 38 wt pct	<0.005-0.300	0.040-0.150	0.083	493
Gadolinium 64 ppm	14-53	33	32	57	Sulfur[4] 16 wt pct	0.07-6.6	0.4	1.84	24
Gallium 31 ppm	2-72	6	11	39	Tantalum 73 ppm	2-20	11	11	4
Germanium 32 ppm	3-90	37	42	4	Tellurium 52 ppm	172-272	214	216	17
Gold 79 ng/g	0.13-3.90	1.92	1.93	10	Terbium 65 ppm	1-11	5	5.4	104
Hafnium 72 ppm	3-14	5	6	96	Thallium 81 ppm	2-675	160	169	141
Holmium 67 ppm	1-8	4	4	66	Thorium 90 ppm	5-154	21	28	283
Iodine 53 wt pct	0.01-0.25	0.023	0.051	7	Thulium 69 ppm	1-9	2	2.3	41
Iridium 77 ng/g	0.2-23.1	4.3	9.1	11	Tin 50 ppm	2-450	80	108	87
Iron 26 wt pct	1-25	6-17	10.4	5,037	Titanium 22 wt pct	<0.05-2.20	0.40-1.20	0.73	1,310
Lanthanum 57 ppm	66-979	130	157	151	Tungsten 74 ppm	26-120	80	76	7
Lead 82 wt pct	0.005-0.470	0.040-0.180	0.072	2,417	Uranium 92 ppm	1-68	5	6.8	255
Lithium 3 ppm	23-1,055	100	160	25	Vanadium 23 wt pct	<0.005-0.300	0.040-0.080	0.051	507
Lutetium 71 ppm	1-6	2	1.8	76	Ytterbium 70 ppm	8-100	17	20	171
Magnesium 12 wt pct	<0.25-5.00	0.75-1.75	1.53	669	Yttrium 39 ppm	17-950	111	133	132
Manganese 25 wt pct	1-40	16-27	21.6	5,079	Zinc 30 wt pct	<0.05-1.00	0.05-0.15	0.11	3,097
Mercury 80 ng/g	2-775	85	152	68	Zirconium 40 wt pct	<0.005-0.200	0.040-0.075	0.058	304

NAp Not applicable. [1]As $CO_3^=$. [2]As NO_3^-. [3]As P_2O_5. [4]As $SO_4^=$

METHODS OF ANALYSES

The ability to assess any potential environmental impact of the disposal of manganese nodule tailings is essential in the development of this emerging industry. Precise and accurate analytical procedures to determine the composition and characteristics of the tailings are necessary to evaluate this impact.

This section outlines methods that Bureau experience has indicated are applicable to the characterization of nodule feed materials and the reject waste materials from all five potential processes. The section is divided into four parts: methods for determining physical properties, methods for compound identification, methods for determining chemical characteristics, and leachate tests for hazardous waste and ocean disposal assessment.

The chemical characteristics entail the determination of elements of potential economic and/or environmental interest and anion or cation combining species. The primary elements of interest are those elements on the Toxic Substance Control Act list of priority pollutants, the Resource Conservation and Recovery Act list of leachable metals for EP toxicity, and/or major and minor elements of economic importance. These elements are As, Ba, Be, Cd, Cr, Co, Cu, Fe, Mn, Mo, Ni, Pb, Sb, Se, Tl, and Zn (*2*). Silver and mercury were not specifically addressed as their level in nodules is so low as to not warrant environmental concern (*2-3*). Ions of interest include ammonium, carbonate, chloride, fluoride, nitrate, phosphate, and sulfate.

The various methodologies for testing physical properties incorporate standard ASTM and soil mechanics procedures. Analysis of liquid and solid phase components for chemical characteristics involves the use of atomic absorption spectrophotometry, inductively coupled plasma spectroscopy, ion chromatography, X-ray fluorescence, X-ray diffraction, and/or wet chemical procedures. Parameters such as pH, reduction-oxidation potential, and chemical oxygen demand may also need to be determined.

PHYSICAL METHODS

Physical characteristics are determined by the application of ASTM methods outlined for soils and rock testing (*10*).

Table 17.—Physical property testing for manganese nodule tailings

Property	Procedure (10)
Grain size distributions:	
Plus 200 mesh	ASTM D422-63
Minus 200 mesh	Allen (58)
Specific gravity	ASTM D854-58
Triaxial shear	ASTM D2850-70
Permeability[1]	ASTM D2434-68
Density:	
Maximum	ASTM D698-78
Minimum	ASTM D2049-69
Atterberg limits:	
Liquid	ASTM D423-66
Plastic	ASTM D424-59
Soil class	ASTM D2487-69
Slurry density	ASTM D2216-71

[1] Using Bureau of Reclamation Earth Manual Procedure E13.

The test procedures listed in table 17 have been successfully applied to coal refuse by the Bureau (*57*). The same test procedures were used to determine the physical characteristics of tailings generated in pilot-plant and laboratory operations (*4-5*).

COMPOUND IDENTIFICATION METHODS

Identification of the various compounds present in nodule tailings and waste materials allows a preliminary evaluation of the environmental impact of the waste. An element present in one chemical form may be environmentally inert, whereas a more chemically active form of the element may pose problems if disposed of improperly. However, this identification is inherently difficult because of the poorly crystalline, fine-grained, or amorphous nature of the compounds in manganese nodules and their subsequent tailings. Methods, such as X-ray diffraction (XRD), optical microscopy, infrared spectroscopy, thermal analysis, and scanning and transmission electron microscopy, are available to identify major and minor compounds. Table 18 includes a brief sketch of each of these methods along with the methods primarily used for elemental and anion determinations.

XRD is the conventional technique used to identify and sometimes quantify major and minor crystalline compounds. However, in the iron and manganese matrix of manganese nodules, compounds that are present at less than 5 wt pct and/or are extremely fined grained, generally cannot be identified by this method. Many of the minerals present in nodules (*1*) are very poorly crystalline, and often amorphous, giving only a diffuse XRD pattern. The reject waste materials from manganese nodule processing are also relatively fine grained but do show better crystallinity and thus better diffraction patterns than nodules. The major and minor components such as manganese carbonate, manganese oxides, silica, clays, and feldspars can be determined. Positive association of trace elements with specific compounds is virtually impossible by the XRD method. Identification of compounds in single grains requires the use of the transmission electron microscope using selective area electron diffraction (*23*).

Infrared spectroscopy (IR) is useful for the mineralogical analyses of manganese nodules, which cannot be performed by XRD (*59-60*). For example, it eliminates the ambiguity frequently caused in XRD by silicate components, such as the confusion of kaolinite and birnessite (*60*). Being sensitive to short-range order, IR provides mineralogical information on the disordered and fine-particulate phases that cannot be studied by XRD (*59*). However, because IR is not a primary structural technique like XRD, it is necessary to calibrate it against well-crystallized materials where mineralogy has been previously determined by XRD. Similar to XRD, direct IR is limited to compounds present at 2 to 5 pct or more in the sample. Other methods of compound identification such as optical microscopy, visual inspection, reflectivity, and other chemical and physical methods have definite applications. A combination of procedures is usually required to obtain reliable compound identification on the macrocrystalline and microcrystalline scales. A detailed description of over 50 minerals identified in manganese nodules is given in reference 1.

CHEMICAL CHARACTERISTICS

Elemental determination in manganese nodule processing reject waste material is amenable to several standard analytical methods. Interferences for 16 elements of interest in manganese nodule materials are listed in table 19 for four major instrumental methods. The methods presented in table 19, atomic absorption spectrophotometry (*61-66*), inductivity coupled plasma atomic emission spectroscopy, neutron activation analysis (*67-69*), X-ray fluorescence spectrography (*44, 47, 55, 70*), ion chromatography (*8, 11, 62, 71-73*), and various wet chemical methods (*62*), are discussed in detail elsewhere (*4*). Comparison analyses of nodules and most materials are published in earlier reports (*3-5, 55*).

LEACHATE TESTS

EP Toxicity Test

According to EPA regulations under the Resource Conservation and Recovery Act (RCRA) (*74*), a solid waste must be listed as a hazardous waste if it exhibits any of the following characteristics as defined in RCRA: ignitability, corrosivity, reactivity, and/or extraction procedure (EP) toxicity (*12*).

Reject waste materials from manganese nodule processing will not exhibit any properties of ignitability or reactivity. Corrosivity applies primarily to liquid wastes and should not be a problem if adequate waste management practices are used in the washing of the tailings.

The only applicable hazardous waste criterion is the EP toxicity test. Briefly, the EP toxicity test consists of agitating, for 24 h, a minimum sample weight of 100 g of filtered material in 1,600 mL of distilled water (maintain a 16:1 water-to-solids ratio for larger sample weights) to which a maximum of 400 mL of 0.5*N* acetic acid (4 mL of acid per gram of material) may be added to maintain a pH of 5.0 ± 0.2. If all 400 mL of the acid is not required to achieve the desired pH, the remaining volume to make 2,000 mL (20:1 liquid-to-solid ratio) is added as distilled water. The solution is filtered on a 0.45-μm filter. The resulting extract (liquid portion) in the EP toxicity test is not to exceed 100 times the National Drinking Water Standard for concentrations of eight metals: Ag, As, Ba, Cd, Cr, Hg, Pb, and Se. The EP toxicity limits, in micrograms per milliliter, are as follows: Ag, 5; As, 5; Ba, 100; Cd, 1; Cr, 5; Hg, 0.2; Pb, 5; and Se, 1.

ASTM Shake Extraction Test

A second leachate test, the American Society for Testing and Materials (ASTM) shake extraction test (*13*), has been proposed by ASTM as an alternate method for evaluating

Table 18.—Compound identification and elemental analysis methods for manganese nodule materials

Atomic absorption spectroscopy:

Application—Quantitative determination of a specific element, especially minor and trace concentrations.
Principle—Absorption of atomic resonance line proportional to the concentration of the specific element.
Limitations—Usually not applicable to nonmetals. Metals are determined individually and not simultaneously.

Atomic emission spectroscopy:

Application—General qualitative and semiquantitative survey of all metallic elements.
Principle—Light emission from excited electronic states of atoms proportional to concentration.
Limitation—Poor for detecting volatile elements. Quantitative determinations are difficult.

Chemical reaction methods (classical analysis):

Application—Variety of specialized quantitative applications.
Principle—Stoichiometry of chemical reactions.
Limitations—Time consuming, interferences often a problem.

Electron microscopy and microanalysis (SEM, TEM, and probe):

Application—Morphological information and elemental composition of fine particles.
Principle—A focused beam of electrons gives rise to secondary, back-scattered, reflected, or transmitted electrons for morphological information, and X-rays for elemental information.
Limitations—Sample must be small enough to fit in the sample chamber. Less than about 6-mm-square maximum area is viewed by SEM, less than 1.5-mm-square area for TEM, and about 50-mm-square area for an electron probe.

Inductively coupled plasma:

Application—Minor, trace and ultratrace quantitative and semiquantitative element analysis including B, P, and S, with linearity often over 4 orders of magnitude.
Principle—Characteristic emissions from elements excited by an inductively coupled argon plasma have intensities proportional to concentrations.
Limitations—Some spectral and scattered light interferences may come from the high concentrations of Fe and Mn in nodules.

Ion chromatography:

Application—Rapid quantitative determination of anions. Rapid cation determination for alkali and alkaline earth metals, NH_4^+ and 1st row transition elements.
Principle—Ions separated by ion exchange techniques followed by ion electrical conductance proportional to the concentration of the specific ion.
Limitations—Usually not applicable to anions with pKa > 7. Most 2d and 3d row cations are determined with difficulty.

Infrared spectroscopy:

Application—Identification of compounds, amorphous and crystalline.
Principle—Excitation of molecular vibrations by light absorption.

Infrared spectroscopy—Continued

Limitations—Medium sensitivity down to 1 to 2 pct. Broad absorption bands of OH group may overlap other spectral features in application to nodules.

Neutron activation:

Application—Trace and ultratrace elemental analysis of most elements including N, O, and F.
Principle—Counting of radioactive species produced by neutron reactions.
Limitations—The multielement nature of nodules present problems in spectral overlaps, which require chemical separation for some elements.

Optical microscopy:

Application—Mineral or phase identification.
Principle—Properties such as color, cleavage, refractive index, and characteristic crystal shapes using plane and polarized, transmitted, and reflected light systems.
Limitations—Resolution limit is about 0.2 μm but identification of particles <5 μm is not practical, limiting the use of this technique for fine-grained nodule materials.

Thermal analysis (TGA and DTA):

Application—Qualitative and quantitative studies of materials including phase transitions, dehydration, reduction decomposition, crystallization, oxidation, and other heat-related properties.
Principle—Changes in weight are measured as a function of increased temperature over time.
Limitations—Information is often empirical, and complementary analytical methods are needed to properly interpret data.

Ultraviolet-visible spectrophotometry:

Application—Quantitative analysis usually for final determination in chemical analysis schemes.
Principle—Excitation of loosely bonded electrons with absorption of characteristic wavelength being proportional to the concentration of the compound.
Limitations—Low specificity requiring chemical separation procedures prior to final determination.

X-ray diffraction:

Application—Identification of crystalline substances.
Principle—Diffraction of X-rays from crystal planes providing "fingerprint" identification of crystalline materials.
Limitations—Many nodule minerals are too fine grained or amorphous, making X-ray diffraction inapplicable. Generally not useful in the atomic number matrix of nodules for concentrations <5 wt pct.

X-ray fluorescence spectrography:

Application—Quantitative analysis of elements and semiquantitative survey of all elements of atomic number 11 or greater.
Principle—X-ray excitation of characteristic X-rays.
Limitations—Nonsensitive to elements of atomic numbers <11 (Na). Best sensitivity for heavier atomic number elements.

wastes, especially those of low organic content such as mining waste. This test consists of contacting a minimum of 350 g of dried material with distilled deionized water; the weight of water to be four times the sample weight. The slurry is agitated in a closed container for 48 h and the liquid portion filtered on 0.45-μm filter paper. The extract is then analyzed for the desired components including those outlined in the RCRA criterion.

EPA-U.S. Army Corps of Engineers (COE) Seawater Elutriant Test

In the possible case of ocean disposal of nodule tailings and waste materials, either by ocean dumping or by ocean outfalls, a seawater leachate test may provide more appropriate data than the previous two leach tests. The EPA-COE dredge material elutriant test can be used to evaluate the extent of seawater-leachable metals in the waste materials (*14*). The procedure consists of mixing a weighed volume of material with four times the volume of seawater, agitating for 1 h, filtering and analyzing the seawater solution. Concentrations are compared with those in the seawater prior to leaching. Based on this analysis, concentrations of the elements at proposed mixing levels found in ocean outfalls or in ocean dumping can be extrapolated. Depending on final regulations in regard to ocean disposal, the degree of mixing required can be regulated by either dumping large amounts at once for minimal mixing rates or by trickling to provide for high mixing rates.

Table 19.—Source of interference in elemental determination by quantitative instrumental methods

Arsenic:
- AAS .....High Fe, Mn, and other metals will depress the sensitivity in hydride generation. Flame method gives poor sensitivity.
- ICP .....2d-order spectral overlap from Ar.
- NAA .....Interference from Se, Ge, and Br
- XRF .....Pb spectral interference at more sensitive Kα peak. Kβ peak lacks sensitivity for quantities below 0.02 pct.

Barium:
- AAS .....Ionization controlled by adding KCl. CaOH bands interfere.
- ICP .....None reported.
- NAA .....Interference from Ce and La.
- XRF .....None reported for quantities above 0.05 pct.

Beryllium:
- AAS .....High Al, Mg, and Si will depress sensitivity.
- ICP .....2d-order spectral overlap from Ar and OH band interference.
- NAA .....Not recommended.
- XRF .....Atomic number too low for XRF.

Cadmium:
- AAS .....High Si interferes.
- ICP .....None reported.
- NAA .....Interference from Sn and from shielding.
- XRF .....None reported for quantities above 0.02 pct.

Cobalt:
- AAS .....Some heavy metals and transition metals depress signal.
- ICP .....2d-order spectral overlap from Ar.
- NAA .....Ni, Cu, and Fe cause enhancements.
- XRF .....Fe spectral interference below 0.01 pct.

Chromium:
- AAS .....Fe, Ni, and PO_4^{3-} depress the signal.
- ICP .....OH band interference.
- NAA .....Interference from Fe.
- XRF .....Enhanced by high iron.

Copper:
- AAS .....None reported.
- ICP .....2d-order spectral overlap from Ar.
- NAA .....Interference from Ni and Zn.
- XRF .....None reported for quantities above 0.005 pct.

Iron:
- AAS .....Co, Cu, Ni, Si, and organic acids depress signal.
- ICP .....None reported.
- NAA .....Poor detectability from Co, Cr, Mn, and Ni.
- XRF .....None reported for quantities above 0.005 pct.

Manganese:
- AAS .....Si depresses signal. High concentration of Fe enhances signal.
- ICP .....2d-order spectral overlap from Ar and OH band interference.
- NAA .....Interference from Fe, Co, and Cr.
- XRF .....None reported for quantities above 0.005 pct.

Molybdenum:
- AAS .....Cu, Fe, Sr, and SO_4^{2-} depress the signal.
- ICP .....OH band interference.
- NAA .....Interference from Ru.
- XRF .....None reported for quantities above 0.02 pct.

Nickel:
- AAS .....High Fe or Cr will enhance signal.
- ICP .....1st order spectral overlap from Si.
- NAA .....Interference from Cu and Zn for Ni-64. No apparent interference for Ni-58.
- XRF .....None reported for quantities above 0.005 pct.

Lead:
- AAS .....High Fe or other metals will enhance the signal.
- ICP .....2d-order spectral overlap from H.
- NAA .....Interference from Bi.
- XRF .....None reported for quantities above 0.01 pct.

Antimony:
- AAS .....Spectral interference from Cu and Pb. Depressed signal in high activity.
- ICP .....1st order spectral overlap from Si and 2d-order overlap from Ar.
- NAA .....Interference from Te and from self-shielding.
- XRF .....None reported for quantities above 0.02 pct.

Selenium:
- AAS .....Some metals will depress the hydride generation signal Flame absorbs signal.
- ICP .....None reported.
- NAA .....Interference from Ge and Br.
- XRF .....None reported for quantities above 0.01 pct.

Thallium:
- AAS .....None reported.
- ICP .....1st order spectral overlap from Ar.
- NAA .....Interference from Pb and Hg.
- XRF .....None reported for quantities above 0.02 pct.

Zinc:
- AAS .....High Cu, Fe, and Ni depress signal.
- ICP .....None reported.
- NAA .....Interference from Cu and Ni.
- XRF .....None reported for quantities above 0.005 pct.

AAS Atomic absorption spectrophotometry
ICP Inductively coupled plasma
NAA Neutron activation analysis.
XRF X-ray diffraction.

MANGANESE NODULE PROCESSING

PROCESS TYPES

In the work performed by Dames and Moore in 1977 (*6*), a literature search revealed several methods for recovering the valued metals (Mn, Ni, Co, Cu) from manganese nodules using either pyrometallurgical or hydrometallurgical processes, or combinations of the two. The extraction techniques were classified by the type of leaching agent used to solubilize the metals of interest. These are ammonia-, chloride-, and sulfate-based. Using this format, Dames and Moore outlined the following 12 potential routes to metals recovery:

Ammoniacal systems:
1. Gas reduction and ammoniacal leach.
2. Cuprion ammoniacal leach.
3. High-temperature ammonia leach.

Chloride systems:
1. Reduction and HCl leach.
2. HCl reduction roast and acid leach.
3. Segregation roast.
4. Molten salt chlorination.

Sulfate systems:
1. High-temperature and high-pressure H_2SO_4 leach.
2. Smelting and H_2SO_4 leach.
3. H_2SO_4 reduction leach.
4. Reduction roast and H_2SO_4 leach.
5. Sulfate roast.

Ammoniacal systems are used to process land-based nickeliferous laterites which are, in some respects, similar to manganese nodules. Copper, nickel, and cobalt are soluble in ammonia-ammonium carbonate (Caron process) and ammonia-ammonium sulfate solutions. These processing routes involve selective reduction of the metals from their oxide states and disruption of the manganese nodule matrix to permit rapid, complete dissolution of the valuable metal (*75-83*).

Acid chloride solutions are also capable of solubilizing the metal values of interest including manganese, and a substantial body of literature exists describing process conditions for nodule reduction and metal separation and purification.

Copper, nickel, and cobalt are also soluble in strong acid sulfate systems and serve as the initial step for various possible process routes. The high-temperature H_2SO_4 leach process technology is used in recovering nickel from laterites, where the high temperature increases the rates of the dissolution of Cu, Ni, and Co, and limits the solubility of undesirable compounds such as Fe and Mn (*84-86*). Alternative routes involving the acid sulfate system include the selective high-temperature reduction of the nodules, separation of manganese-rich slags from the metallic phases, sulfidation of metallic phases, and subsequent selective leaching of the sulfide materials. A ferromanganese product could also be recovered by further selective reduction of the manganese-rich slag phases (*87-91*).

Of the 12 generic process types presented previously, seven have sufficient technical problems to preclude the likelihood of commercial development. Flowsheets have been developed for the five process options that are considered as first-generation choices, both from the published literature and by analogy to the processing of land-based ores (*2, 6*). These five process options are as follows:

1. Gas reduction and ammoniacal leach.
2. Cuprion ammoniacal leach.
3. High-temperature and high-pressure H_2SO_4 acid leach.
4. Reduction and HCl leach.
5. Smelting and H_2SO_4 leach.

The five processes may be broken down into three- and four-metal recovery systems with the three-metal systems having an option to recover Mn from the tailings. The first three processes listed above are three-metal processes; the remaining two are considered four-metal processes.

The recovery of manganese from the tailings of the three-metal systems involves two types of treatment. For the ammoniacal leach tailings, manganese can be recovered to a limited extent by the flotation of $MnCO_3$. The $MnCO_3$ could then be further processed to produce a manganese oxide product and sold as such or further processed to produce ferromanganese or other manganese alloys.

The residue from the H_2SO_4 system would require dissolution of the tailings and subsequent chemical manipulation to recover the manganese as MnO_2 or another form. The oxide product could be separated and sold or further processed to make ferromanganese or other manganese alloys. The possible direct use of the tailings from either the ammonia-based systems or the H_2SO_4 system as a feed for ferromanganese production would require some purification of the tailings. Trace metal levels as well as sulfur and possibly phosphorus levels may be too high for direct processing of the tailings by conventional methods.

MAJOR ASSUMPTIONS

Certain assumptions used in the original Dames and Moore report were also used in updating the process flowsheets (*2*). The three three-metal processes and the smelting process are assumed to operate on a 3-million-mtpy feed rate (dry basis). The four-metal HCl process is assumed to operate at a 1 million mtpy dry basis. The final products are assumed to be Cu and Ni cathodes, some Ni powder, Co powder, small amounts of Cu and Zn sulfides, Mn metal, and/or ferromanganese.

Several significant changes from the Dames and Moore report are detailed here. In the 1977 Dames and Moore study (*6*), a moisture content of 37.5 pct was used as the water value of nodules fed to the processing plant. This value represents essentially the water content of as-mined nodules. Considering the porosity of nodules (~60 pct), it is likely that a substantial amount of water will be removed during transport from the minesite. Ships currently in use equipped with Marconoflo-type[a] dewatering systems could be able to dewater the nodules.

A more reasonable value for moisture content of nodules received at the port facilities may be 15 to 20 pct. This decreases the size of several components of the materials handling section and lowers the energy cost for drying the nodules. A moisture content of 20 pct is used for nodules fed to the plant. This lowers the 3-million-mtpy dry-basis plant feed rate from 12,500 to 10,900 mtpd, and the 1-million-mtpy dry-basis plant feed rate from 3,750 to 3,640 mtpd.

A second major change from the 1977 study (*6*) is the increase in size of the smelting plant from 1 million mtpy dry basis to 3 million mtpy dry basis to allow use of conventionally sized furnaces. Also, particle size of the nodule feed increased to minus 65 mesh instead of minus 200 or minus 325 mesh as previously used (*6*).

SUMMARY PROCESS DESCRIPTIONS

A brief description of each of the five technically feasible potential first-generation processes is presented along with block diagrams for each process. Detailed process descriptions and flowsheets for each process are presented elsewhere (*2, 6*).

Gas Reduction and Ammoniacal Leach Process

This process is an adaptation of the Caron process used on nickeliferous laterites (*75-80*). The primary differences between Caron process practice and the proposed manganese nodule process are in the separation and purification steps. The reduction and leaching steps are direct applications of the Caron process.

Copper, nickel, and cobalt can be recovered from nodules by a process involving carbon monoxide gas reduction followed by an ammoniacal leach. A simplified block diagram for the process is shown in figure 5. Table 20 gives the proposed operating parameters for the process.

The first step in this process is a high-temperature (625° C) reduction of manganese dioxide (MnO_2) to manganese oxide (MnO) by a carbon-monoxide-rich producer gas. This reduction disrupts the mineral structure and releases the contained metals. The metal values are solubilized from the reduced nodules with a strong aqueous solution of 10 pct ammonia and 5 pct carbon dioxide at 40° C and atmospheric pressure.

[a]Reference to specific products does not imply endorsement by the Bureau of Mines.

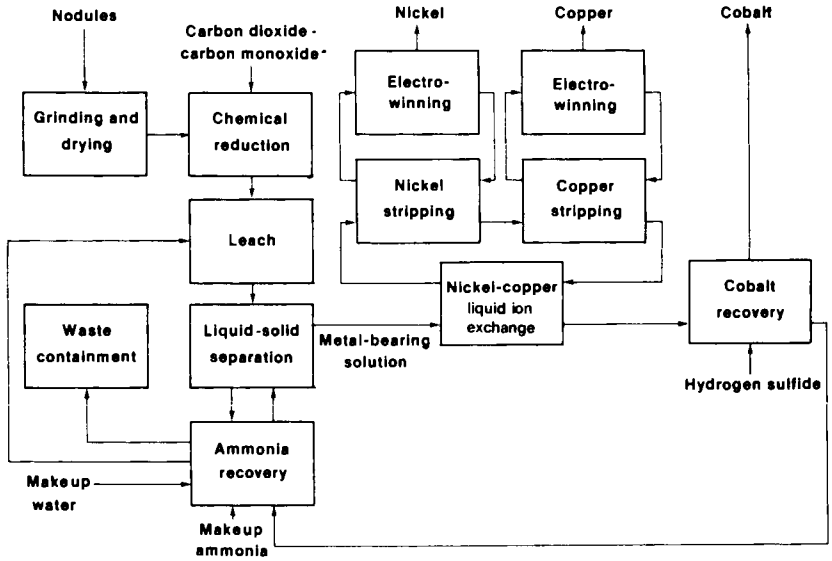

Figure 5.—Gas reduction and ammoniacal leach process.

The metal-bearing solution is decanted from the nodules and treated with a series of organic extraction steps that selectively remove the copper and nickel from the aqueous solution. The metal values are selectively stripped from the organic extract with acidified aqueous solutions. The metal products, cathode copper and nickel, are produced from these acidic solutions by electrowinning.

Cobalt is then recovered from the aqueous ammonia-carbon dioxide solution by contacting it with hydrogen sulfide, which precipitates the insoluble sulfides of Co as well as small amounts of residual Cu, Ni, Zn, and other metals not removed in previous steps. The solids are removed from the aqueous ammonia-carbon dioxide solution and contacted with air and 100° C H_2SO_4 to selectively redissolve the Co and the small amount of Ni present. The undissolved sulfides are sold as minor products, and the cobalt and nickel are recovered from solution in powder form by selective reduction with hydrogen at 34 atm and 185° C.

The nodule residue, from which the major portion (98 pct) of the soluble metals has been removed, is contacted with steam at 120° C and 2 atm to remove residual ammonia and carbon dioxide. The ammonia-carbon dioxide-steam mixture is condensed and, together with the aqueous ammonia-carbon dioxide-steam mixture from which cobalt was removed, is recycled to extract more metal values from freshly reduced nodules. The steam-stripped nodule residues may be combined with smaller amounts of other process solid and liquid wastes and sent to containment.

Cuprion Ammoniacal Leach Process

The Cuprion process is similar to the Caron process (*75*) except that an excess of cuprous ion in an aqueous ammoniacal solution at near ambient temperature is used to effect the manganese dioxide reduction, and the metals separation and purification steps are different (*81-83*). Copper, nickel, and cobalt can be recovered from nodules by the Cuprion process employing a reducing ammoniacal leach. A simplified block diagram of this process is shown in figure 6. Table 21 gives the proposed operating parameters for this process.

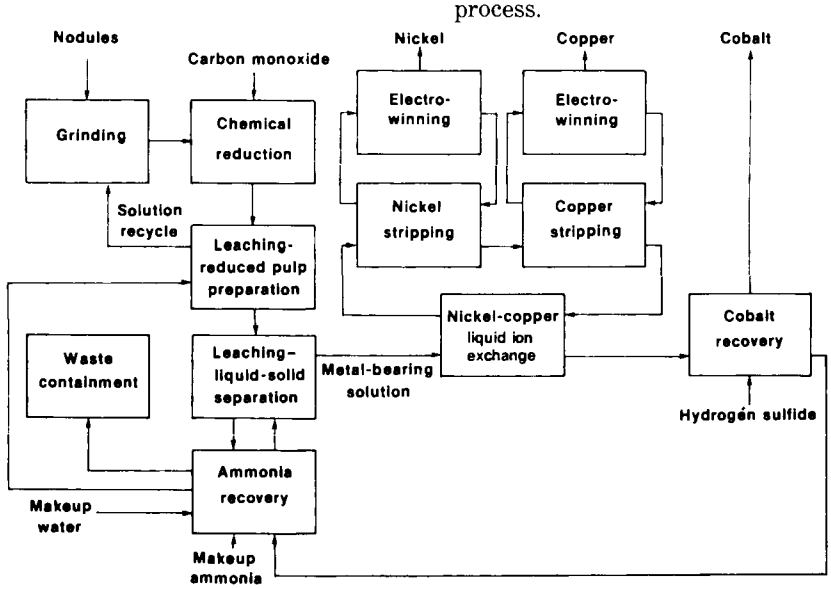

Figure 6.—Cuprion ammoniacal leach process.

Table 20.—Operating parameters for gas reduction and ammoniacal leach process

Parameter and unit	Value
ORE PROCESSING AND DRYING	
Feed rate, wet basis (330 dpy; 24 hpd) ..... mtpd ..	10,900
Feed size to reduction ..... mesh ..	−65
Drying temperature ..... °C ..	150
REDUCTION	
Reductant gas composition, pct:	
CO	18.2
CO_2	7.8
H_2	10.9
N_2	49
H_2O	10.1
CH_4	3.6
Gas temperature ..... ° C ..	825
Reduction temperature ..... ° C ..	625
Mn carbonation ..... pct ..	95
Cooling temperature ..... ° C ..	125
Conversion, pct:	
Co	100
Cu	100
Fe	98
Mn	98
Ni	100
LEACHING-AERATION	
Number of stages	3
Temperature ..... ° C ..	40
Time per stage ..... h ..	1
Leach solution composition, gpl:	
NH_3	100
CO_2	50
Pressure ..... atm ..	1
Solubilization of metals, pct:	
Co	70
Cu	90
Fe	≈1
Mn	≈1
Mo	80
Ni	90
Zn	40
SOLID-LIQUID SEPARATION	
Underflow density ..... pct solids ..	35–40
Wash ratio ..... kg/kg liquor ..	2
Wash recovery ..... pct ..	98
Wash liquor composition, g/L:	
NH_3	100
CO_2	50
LIQUID ION EXCHANGE-EXTRACTION	
Extraction:	
Extractant	[1]LIX 64N
Number of stages	3
Organic-aqueous ratio	2:1
Metals extraction, pct:	
Co	1
Cu	99.9
Ni	99.9
Zn	10
Washing (primary):	
Washing agent ..... pct NH_3 ..	1
Number of stages	2
Organic-aqueous ratio	3:1
Residual NH_3 in organic ..... g/L ..	0.1
LIQUID ION EXCHANGE-STRIPPING	
Washing (secondary):	
Wash composition, g/L:	
$(NH_4)_2SO_4$	200
H_2SO_4	1
Number of stages	2
Organic-aqueous ratio	1:1
Residual NH_3 in organic ..... g/L ..	0.01
Ni stripping:	
Strip solution composition, g/L:	
Cu	<0.001
H_2SO_4	40
Ni	50
Zn	≈0
Number of stages	3
Organic-aqueous ratio	5:1
Stripping, pct:	
Co	0.3
Cu	<0.004
Ni	98.8
Zn	≈0
Cu stripping:	
Strip solution composition, g/L:	
Cu	40
H_2SO_4	160
Ni (max)	10
Zn	5
Number of stages	2
Organic-aqueous ratio	3:1
Stripping, pct:	
Co	0.2
Cu	87
Ni	≈0
Zn	100
Temperature ..... ° C ..	40
COPPER ELECTROWINNING—COMMERCIAL	
Current density ..... A/m^2 ..	180
Current efficiency ..... pct ..	94
Temperature ..... ° C ..	50
Cu in-out ..... g/L ..	53-40
H_2SO_4 in-out ..... g/L ..	160-180
NICKEL ELECTROWINNING—COMMERCIAL	
Current density ..... A/m^2 ..	180
Current efficiency ..... pct ..	93
Temperature ..... ° C ..	60
Ni in-out ..... g/L ..	75-50
H_2SO_4 in-out ..... g/L ..	0.016-40
Na_2SO_4 ..... g/L ..	100
H_3BO_3 ..... g/L ..	15
COBALT RECOVERY	
Preciptating agent ..... pct NH_4HS ..	30
Precipitation, pct:	
Co	98
Cu	99.9
Ni	99
Zn	99.9
Temperature ..... ° C ..	80
Clarifier density ..... pct solids ..	5
Wash ratio	2:1
Co leaching: slurry ..... pct ..	40
Leaching agent ..... pct H_2SO_4 ..	70
Evaporation-crystallization water removal ..... pct ..	70
Co oxidation:	
Temperature ..... ° C ..	100
Pressure ..... psig ..	150
Co reduction:	
Temperature ..... ° C ..	175
Pressure ..... psig ..	500
Reductant	H_2
AMMONIA RECOVERY	
CO_2 absorber:	
Temperature ..... ° C ..	40
Pressure ..... atm ..	1.2
Efficiency for CO_2 ..... pct ..	99
Number of stages	1
NH_3 absorber:	
Temperature ..... ° C ..	35
Pressure ..... atm ..	1.2
Number of stages	1
NH_3 stripper:	
Pressure ..... atm ..	1.5
Recovery of NH_3 ..... pct ..	99
Number of stages	2

[1]Reference to specific products does not imply endorsement by the Bureau of Mines.

Table 21.—Operating parameters for Cuprion ammoniacal leach process

Parameter and unit	Value
ORE PREPARATION	
Feed rate, wet basis (330 dpy; 24 hpd) ..... mtpd	10,900
Feed size to reduction ..... mesh	−65
Pulp density, solids	35
REDUCTION LEACH	
Reductant gas composition, pct:	
CO	40-60
H_2	30-45
H_2O	6-12
N_2	1
Temperature ..... ° C	50
Pressure ..... atm	1
Leachate composition, g/L:	
NH_3	100
CO_2	25
Cu	3-5
Number of stages	6
Reduction, pct:	
Co	50
Cu	80
Mn	97
Mo	80
Ni	90
Zn	40
Slurry density ..... pct solids	20-30
OXIDATION-LEACH	
Pregnant liquor composition, g/L:	
NH_3	100
CO_2	25
Cu	4-8
Ni	5-10
Temperature ..... ° C	50
Pressure ..... atm	1
Recovery, pct:	
Co	50
Cu	90
Ni	90
SOLID-LIQUID SEPARATION	
Underflow density ..... pct solids	35-40
Wash ratio ..... kg/kg liquor	2
Wash recovery ..... pct	98
Number of stages	6
Wash liquor composition, g/L:	
NH_3	100
CO_2	50
LIQUID ION EXCHANGE-EXTRACTION	
Extraction:	
Extractant	[1]LIX 64N
Number of stages	3
Organic-aqueous ratio	2:1
Metals extraction, pct:	
Co	1
Cu	99.9
Ni	99.9
Zn	10
Washing (primary):	
Washing agent ..... pct NH_3	1
Number of stages	2
Organic-aqueous ratio	3:1
Residual NH_3 in organic ..... g/L	0.1
LIQUID ION EXCHANGE-STRIPPING	
Washing (secondary):	
Wash composition, g/L:	
$(NH_4)_2SO_4$	200
H_2SO_4	1
Number of stages	2
Organic-aqueous ratio	1:1
Residual NH_3 in organic ..... g/L	0.01
Ni stripping:	
Strip solution composition, g/L:	
Cu	<0.001
H_2SO_4	40
Ni	50
Zn	≈0
Number of stages	3
Organic-aqueous ratio	5:1
Stripping, pct:	
Co	0.3
Cu	<0.004
Ni	98.8
Zn	≈0
Cu stripping:	
Strip solution composition, g/L:	
Cu	40
H_2SO_4	160
Ni (max)	10
Zn	5
Number of stages	2
Organic-aqueous ratio	3:1
Stripping, pct:	
Co	0.2
Cu	87
Ni	≈0
Zn	100
Temperature ..... ° C	40
COPPER ELECTROWINNING—COMMERCIAL	
Current density ..... A/m^2	180
Current efficiency ..... pct	94
Temperature ..... ° C	50
Cu in-out ..... g/L	53-40
H_2SO_4 in-out ..... g/L	160-180
NICKEL ELECTROWINNING—COMMERCIAL	
Current density ..... A/m^2	180
Current efficiency ..... pct	93
Temperature ..... ° C	60
Ni in-out ..... g/L	75-50
H_2SO_4 in-out ..... g/L	0.016-40
Na_2SO_4 ..... g/L	100
H_3BO_3 ..... g/L	15
COBALT RECOVERY	
Preciptating agent ..... pct NH_4HS	30
Precipitation, pct:	
Co	98
Cu	99.9
Ni	99
Zn	99.9
Temperature ..... ° C	80
Clarifier density ..... pct solids	5
Wash ratio	2:1
Co leaching: slurry ..... pct	40
Leaching agent ..... pct H_2SO_4	70
Evaporation-crystallization water removal ..... pct	70
Co oxidation:	
Temperature ..... ° C	100
Pressure ..... psig	150
Co reduction:	
Temperature ..... ° C	175
Pressure ..... psig	500
Reductant	H_2
AMMONIA RECOVERY	
CO_2 absorber:	
Temperature ..... ° C	40
Pressure ..... atm	1.2
Efficiency for CO_2 ..... pct	99
Number of stages	1
NH_3 absorber:	
Temperature ..... ° C	35
Pressure ..... atm	1.2
Number of stages	1
NH_3 stripper:	
Pressure ..... atm	1.5
Recovery of NH_3 ..... pct	99
Number of stages	2

[1]Reference to specific products does not imply endorsement by the Bureau of Mines.

The first step in this process is a low-temperature (50° C) hydrometallurgical reduction of manganese dioxide (MnO_2) to manganese oxide (MnO) by an aqueous ammonia solution containing an excess of cuprous ions (Cu^+). The metal values are solubilized from the reduced nodules with a strong aqueous solution of ammonia and carbon dioxide at low temperature and atmospheric pressure.

The remainder of the metals separation and purification steps are identical to those of the previous process.

High-Temperature and High-Pressure Sulfuric Acid Leach Process

The high-temperature and high-pressure sulfuric acid leach process is analogous to the process used at Moa Bay, Cuba, on nickeliferous laterites. However, the metal separation and purification steps in the nodule process are different and complicated by the chemical similarity of copper, nickel, and cobalt (*84-86*). A simplified block diagram for the recovery of cobalt, copper, and nickel using this process is shown in figure 7. Table 22 gives the proposed operating parameters for this process.

The first step in the process is a high-temperature (245° C) and high-pressure (35 atm) treatment of the ground nodules. The major metals of value, except manganese, are dissolved in the 30 pct sulfuric acid solution. Iron is not solubilized to any appreciable extent. After cooling, the nodule residue and acid solution are separated by decantation. The water used to wash the residue free of acid and soluble metals is combined with the acid solution; the residue is sent to a containment area.

The metal-bearing acid solution is pH-adjusted prior to copper and nickel extraction. Copper and nickel are removed from the solution with an organic extractant. The extracted nickel and copper are separately and selectively stripped from their respective organic extracts and transferred to acidified aqueous solutions, which accumulate nickel and copper sulfate, respectively. The metal products, cathode nickel and copper, are produced from these acidic solutions by electrowinning.

Cobalt is recovered by precipitation with hydrogen sulfide, which also precipitates small amounts of residual Cu, Ni, Zn, and other metals not removed in the previous steps. The solid residue is removed from solution and contacted with air and 100° C H_2SO_4 to selectively redissolve the cobalt and the small amount of nickel present. The undissolved sulfides are sold as minor products, and the cobalt and nickel are recovered from solution in powder form by selective metal reduction through the use of hydrogen gas at 34 atm and 185° C.

The solution, depleted of Cu, Ni, and Co, is chemically treated to recover the ammonia introduced during the neutralization step. The recovered ammonia is recycled for use in the process, and the ammonia-free solution is returned to wash freshly leached nodules.

Reduction and Hydrochloric Acid Leach Process

The reduction and HCl leach process for extracting Cu, Ni, Co, and Mn has no known analogy in present extractive metallurgy technology. A simplified block diagram is shown in figure 8. Table 23 gives the proposed operating parameters for this process.

The chemical basis of the HCl process is the reduction of the manganese dioxide nodule matrix with hydrogen chloride to yield soluble manganese chloride, thereby releasing the Ni, Cu, and Co for dissolution. A portion of the hydrogen chloride is oxidized to chlorine, and the unreacted hydrogen chloride is separated from the accompanying chlorine and water vapor for recycling. Separation is accomplished by absorption of gaseous HCl in concentrated HCl, in which chlorine has very limited solubility. The remaining chlorine gas is dried by passage through concentrated sulfuric acid.

Extensive solubilization of the iron content of the nodules during the initial high-temperature (500° C) reaction with gaseous hydrogen chloride is prevented by injection of steam. This results in the hydrolysis of the iron chloride produced in the initial step to insoluble iron (ferric) hydroxide, simplifying subsequent metals separation and minimizing HCl regeneration requirements. In the next step, the soluble metal

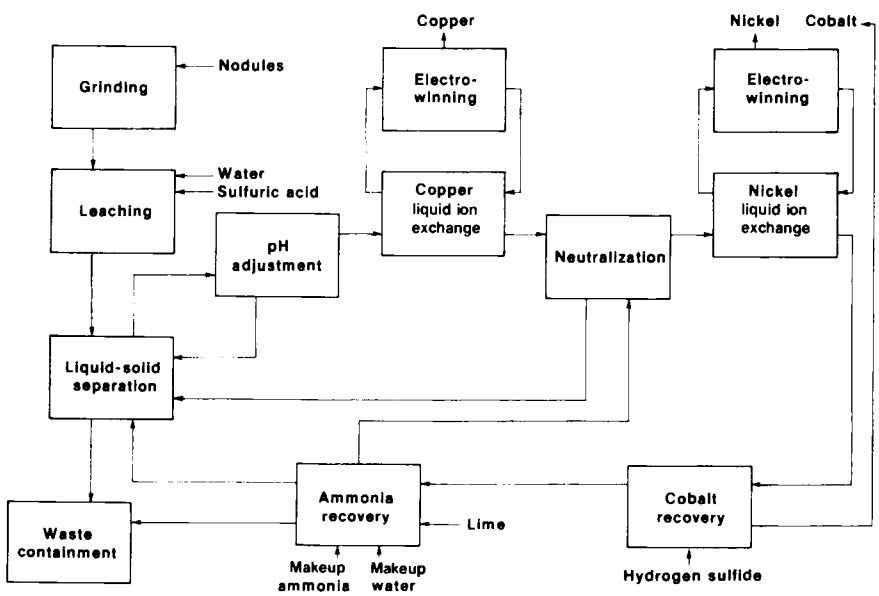

Figure 7.—High-temperature and high-pressure sulfuric acid leach process.

Table 22.—Operating parameters for high-temperature and high-pressure sulfuric acid leach process

Parameter and unit	Value
ORE PROCESSING	
Feed rate, wet basis (330 dpy; 24 hpd) ..... mtpd	10,900
Feed size to leaching ..... mesh	−65
Pulp density, solids ..... pct	35-40
LEACHING	
Temperature ..... ° C	245
Pressure ..... atm	35
Acid feed ..... pct H_2SO_4	93
Recovery, pct:	
CO	90
Cu	95
Fe	1
Mn	5
Ni	95
Zn	90
Contact time ..... h	4
H_2SO_4 consumption ..... lb/lb nodules	0.4
SOLID-LIQUID SEPARATION	
Number of stages	6
Efficiency ..... pct	98
Underflow density ..... pct solids	35-40
Wash ratio ..... kg/kg liquor	2
PREGNANT LIQUOR pH ADJUSTMENT	
Adjustment agent	$CaCO_3$
H_2SO_4 concentration, final ..... g/L	0.5
Entrained solids ..... ppm	≈100
COPPER LIQUID ION EXCHANGE	
Extraction:	
Extractant	[1]LIX 64N
Number of stages	3
Organic-aqueous ratio	1:1
Metals extraction, pct:	
Co	0.1
Cu	99.5
Fe	0.1
Mn	0.1
Ni	0.1
Zn	0.1
Ammonia wash ..... pct NH_3	25
Residual NH_3 in organic ..... g/L	1
Stripping:	
Strip solution concentration, g/L:	
H_2SO_4	160
Ni (max)	10
Cu	40
Zn	5
Number of stages	2
Organic-aqueous ratio	3:1
Temperature ..... °C	40
Stripping, pct:	
Co	0.2
Cu	87
Ni	0.9
Zn	100
COPPER ELECTROWINNING—COMMERCIAL	
Current density ..... A/m^2	180
Current efficiency ..... pct	94
Temperature ..... ° C	50
Cu in-out ..... g/L	53-40
H_2SO_4 in-out ..... g/L	160-180
COPPER RAFFINATE pH ADJUSTMENT	
Number of stages	4
Precipitation agent	NH_3
Final pH	≈4.0
NICKEL LIQUID ION EXCHANGE-EXTRACTION	
Extraction:	
Extractant	[1]LIX 64N
Number of stages	3
NICKEL LIQUID ION EXCHANGE-EXTRACTION—Continued	
Extraction—Continued	
Organic-aqueous ratio	5:1
Temperature ..... ° C	40
Metals extraction, pct:	
Co	1
Cu	1
Ni	99.5
Washing (primary):	
Washing agent ..... pct NH_3	1
Number of stages	3
Organic-aqueous ratio	3.3:1
Residual NH_3 in organic ..... g/L	0.1
NICKEL LIQUID ION EXCHANGE-STRIPPING	
Ammonia scrub (secondary):	
Wash composition, gpl:	
$(NH_4)_2SO_4$	200
H_2SO_4	1
Number of stages	2
Organic-aqueous ratio	1:1
Residual NH_3 in organic ..... g/L	0.01
Temperature ..... ° C	40
Nickel stripping:	
Strip solution composition, g/L:	
Cu	<0.001
H_2SO_4	40
Ni	50
Number of stages	3
Organic-aqueous ratio	5:1
Stripping, pct:	
Co	0.3
Cu	<0.004
Ni	98.8
NICKEL ELECTROWINNING—COMMERCIAL	
Current density ..... A/m^2	180
Current efficiency ..... pct	93
Temperature ..... ° C	60
Ni in-out ..... g/L	75-50
H_2SO_4 in-out ..... g/L	0.016-40
Na_2SO_4 ..... g/L	100
H_3BO_3 ..... g/L	15
COBALT RECOVERY	
Preciptating agent ..... pct NH_4HS	30
Precipitation, pct:	
Co	98
Cu	99.9
Ni	99
Zn	99.9
Temperature ..... ° C	80
Clarifier density ..... pct solids	5
Wash ratio	2:1
Co leaching: slurry ..... pct	40
Leaching agent ..... pct H_2SO_4	70
Evaporation-crystallization water removal ..... pct	70
Co oxidation:	
Temperature ..... ° C	100
Pressure ..... psig	150
Co reduction:	
Temperature ..... ° C	175
Pressure ..... psig	500
Reductant	H_2
AMMONIA RECOVERY	
NH_3 absorber:	
Temperature ..... ° C	35
Pressure ..... atm	1.2
Number of stages	1
NH_3 stripper:	
Pressure ..... atm	1.5
Recovery of NH_3 ..... pct	99
Number of stages	2

[1]Reference to specific products does not imply endorsement by the Bureau of Mines.

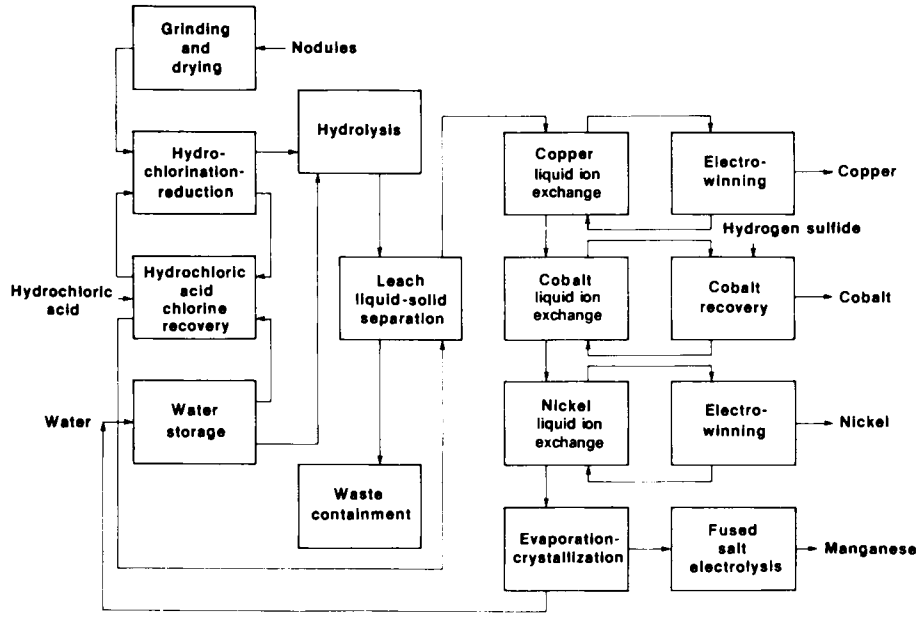

Figure 8.—Reduction and hydrochloric acid leach process.

chlorides, particularly those of Mn, Ni, Cu, and Co, are brought into solution with water and aqueous HCl. In this process, as distinct from the other nodule treatment processes, the major metals separation steps are carried out from the chloride solution.

Copper may be selectively extracted from the pregnant leach liquor by contact with an organic liquid ion exchange reagent. After separation of the copper-loaded organic phase from the copper-depleted aqueous chloride solution, the copper is stripped into a strong H_2SO_4 solution. The resulting copper sulfate solution is sent to electrowinning, producing cathode copper and a partially copper-depleted, strong H_2SO_4 "spent" electrolyte that is returned to the liquid ion exchange circuit to strip more copper.

The chloride leach solution from which the copper has been removed is neutralized and passed to a solvent extraction step, where a different organic liquid ion exchange reagent selectively removes the cobalt from solution. The cobalt is recovered in a sequence of steps that includes stripping from the organic solvent, hydrogen sulfide precipitation as cobalt sulfide, selective leaching, and hydrogen reduction to cobalt powder.

The copper and cobalt-depleted solution is next sent to a liquid ion exchange circuit where nickel is selectively separated from the solution and stripped into an acidic sulfate solution for nickel electrowinning. The nickel separation has many features in common with copper separation, except that much lower acid concentrations are appropriate in the case of nickel.

One option for manganese recovery from nodules involves drying of the final aqueous chloride solution to produce a dry, impure manganese chloride. The manganese chloride is charged to a high-temperature electrolysis furnace, where it dissolves in a molten alkali chloride bath. Electrolysis of the bath liberates molten manganese, which is tapped from the furnace, cast into molds, and sold as manganese metal. Fused salt impurities are skimmed off, solidified, and sent to waste disposal.

The second major product of the electrolysis is chlorine gas, which would be recovered along with the chlorine produced in the initial hydrochlorination step. The recovered chlorine needs to be reconverted to hydrogen chloride or otherwise utilized offsite in a large-scale chemical process.

Smelting and Sulfuric Acid Leach Process

The smelting and sulfuric acid leach process has similarities with several nonferrous smelting processes and has been referenced for manganese nodules (*87-91*). Cobalt, copper, nickel, and a ferromanganese alloy, if desired, can be recovered from nodules by a smelting and H_2SO_4 process. A simplified block diagram of this process is shown in figure 9. Table 24 gives the proposed operating parameters for the process.

The nodules are first dried by direct contact with combustion gases to remove water not chemically bound to the minerals. The manganese dioxide and ferric oxide are then reduced to manganous and ferrous oxides by contact, in the presence of coal, with a carbon monoxide-rich producer gas at high temperature (625° to 1,000° C). The hot, reduced nodules are then charged to an electric furnace, along with coke and silica. In this step most of the Cu, Ni, Co, and Fe and some of the Mn are reduced at 1,425° C and form a molten alloy phase, which separates by gravity from the unreduced manganese slag.

The hot alloy is transferred to converter vessels where, with additional silica, the manganese and most of the iron are reoxidized with air, separated as a slag, and returned to the electric furnace. Gypsum and coke or possibly sulfur are then added to the alloy, producing a metal sulfide "matte" phase that contains the Cu, Ni, and Co. A second liquid-liquid separation is made in the converter, with the slag returned to the electric furnace and the matte granulated by quenching it in cold water.

The electric furnace manganese slag, with recycled iron-rich slags, may be further reduced at 1,480° C with additional coke in an electric furnace to produce a molten ferromanganese alloy, which separates by gravity from the silicate slag. The ferromanganese is cast for sale, and the waste slag is granulated for disposal.

The metals are recovered from the granulated matte by dissolution into 5 pct, 110° C H_2SO_4 solution in the presence

Table 23.—Operating parameters for reduction and hydrochloric acid leach process

Parameter and unit	Value
ORE PROCESSING AND DRYING	
Feed rate, wet basis (330 dpy; 24 hpd) ..... mtpd..	3,640
Feed size to reduction ..... mesh..	−65
Drying temperature ..... °C..	150
HYDROCHLORINATION	
Temperature ..... ° C..	500
Pressure ..... atm..	1
Reagent	HCl
Hydrolysis:	
Temperature ..... ° C..	200
Pressure ..... atm..	1
Hydrochlorination, pct:	
Co	100
Cu	96
Fe	27
Mn	94
Mo	96
Ni	100
LEACHING AND WASHING	
Final pH	2
Underflow density ..... pct solids..	15
Wash ratio	2:1
Number of stages	6
Soluble metals removed ..... pct..	98
COPPER LIQUID ION EXCHANGE	
Extraction:	
Extractant	[1]Kelex 100
Cu feed ..... g/L..	≈8
Number of stages	3
Organic-aqueous ratio	2:1
Cu extraction ..... pct..	99.5
Washing:	
Wash composition	H_2O
Number of stages	2
Organic-aqueous ratio	3:1
Temperature ..... ° C..	40
Metals extraction, pct:	
Co	99.5
Cu	99.5
Ni	99.5
pH (with NaOH)	4
Stripping:	
Strip solution composition, g/L:	
H_2SO_4	160
Cu	40
Number of stages	2
Organic-aqueous ratio	4:1
Cu stripping ..... pct..	95
Temperature ..... ° C..	40
COPPER ELECTROWINNING—COMMERCIAL	
Current density ..... A/m^2..	180
Current efficiency ..... pct..	94
Temperature ..... ° C..	50
Cu in-out ..... g/L..	53-40
H_2SO_4 in-out ..... g/L..	160-180
pH ADJUSTMENT AND COBALT EXTRACTION	
Cu raffinate pH adjustment:	
pH adjustment agent	NaOH
Number of stages	1
Final pH	4
Co liquid ion exchange extraction:	
Extractant	TIOA
Number of stages	3
Organic-aqueous ratio	2:1
Metals extraction, pct:	
Co	99
Cu	100
Mn	10
Ni	0
Zn	99.5

Parameter and unit	Value
pH ADJUSTMENT AND COBALT EXTRACTION—Continued	
Co stripping:	
Stripping solution pH	4
Number of stages	2
Organic-aqueous ratio	5:1
Stripping, pct:	
Co	99
Mn	99
Co recovery:	
Precipitating agent	H_2S
Precipitation ..... pct..	100
Temperature ..... ° C..	80
Pressure ..... atm..	1
NICKEL LIQUID ION EXCHANGE	
Extraction:	
Extractant	[1]Kelex 100
Number of stages	2
Organic-aqueous ratio	2:1
Temperature ..... ° C..	40
Metals extraction, pct:	
Co	99.5
Cu	99.5
Ni	99.5
pH (with NaOH)	4
Washing:	
Washing agent	H_2O
Number of stages	2
Stripping:	
Strip solution composition, g/L:	
H_2SO_4	40
Ni	50
Number of stages	2
Organic-aqueous ratio	6:1
Ni stripping ..... pct..	99
NICKEL ELECTROWINNING—COMMERCIAL	
Current density ..... A/m^2..	180
Current efficiency ..... pct..	93
Temperature ..... ° C..	60
Ni in-out ..... g/L..	75-50
H_2SO_4 in-out ..... g/L..	0.016-40
Na_2SO_4 ..... g/L..	100
H_3BO_3 ..... g/L..	15
MANGANESE RECOVERY	
Trace elements removal agent	H_2S
Evaporation-crystallization water removal ..... pct..	99.9
Fused salt electrolysis:	
Mn recovery ..... pct..	90
Temperature, metal ..... ° C..	1,300
Temperature, salt ..... ° C..	800
Current density ..... A/m^2..	46
COBALT RECOVERY	
Slurry feed, solids ..... pct..	40
Evaporation-crystallization water removal ..... pct..	70
Co oxidation:	
Temperature ..... ° C..	100
Pressure ..... psig..	150
Co reduction:	
Temperature ..... ° C..	175
Pressure ..... psig..	500
Reductant	H_2
Leaching agent ..... pct H_2SO_4..	70
HCl RECOVERY	
HCl absorbing agent	H_2O
Gas drying agent	H_2SO_4
WASTE RECOVERY	
Recovery agent	Slaked lime
NH_3 recovery ..... pct..	99

[1]Reference to specific products does not imply endorsement by the Bureau of Mines.

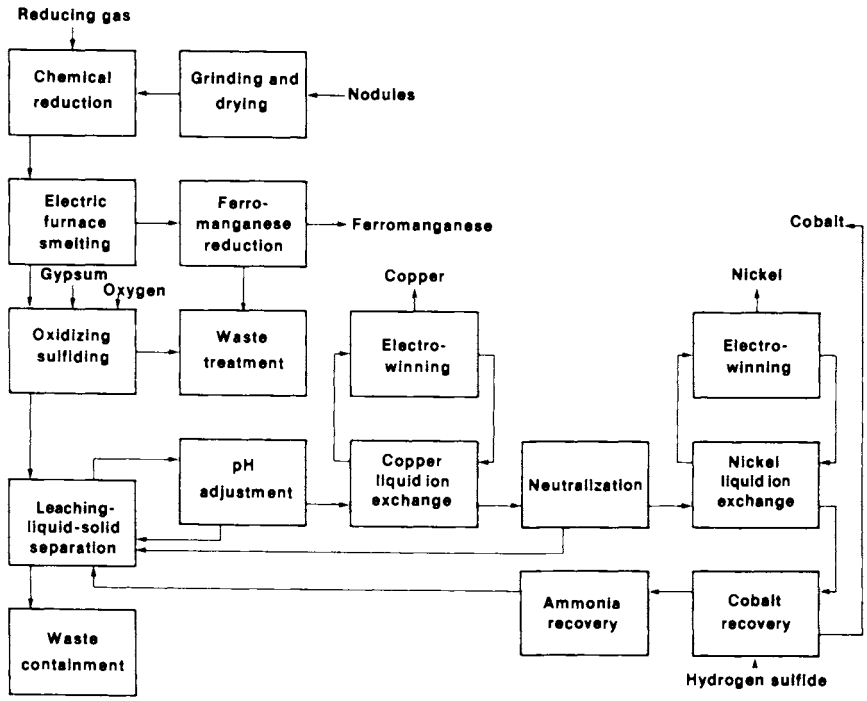

Figure 9.—Smelting and sulfuric acid leach process.

Table 24.—Operating parameters for smelting and sulfuric acid leach process

Parameter and unit	Value
ORE PREPARATION AND DRYING	
Feed rate, wet basis (330 dpy; 24 hpd) ..... mtpd ..	10,900
Feed size ..... in ..	−7/8
Drying temperature ..... °C ..	150
REDUCTION	
Reduction gas:	
Producer gas ..... pct CO ..	≈20
Other reductant ..... pct coke ..	≈4.5
Metals reduction, pct:	
Co	90
Cu	90
Fe	100
Mn	100
Mo	20
Ni	90
Temperature, ° C:	
Solids	725
Gas	925
SMELTING	
Temperature ..... ° C ..	≈1,325
Retention time ..... h ..	2
Flux	Silica
Reductant	Coke,electrodes
Alloy recovery, pct:	
Co	90
Cu	90
Fe	70
Mn	2
Mo	85
Ni	95
Slag recovery, pct:	
Co	<10
Cu	<10
Fe	20
Mn	98
Mo	15
Ni	<10

Parameter and unit	Value
CONVERTING	
Slagging:	
Flux	Silica
Oxidant	O_2-air
Removal, pct:	
Fe	12
Mn	93
Final Mn ..... pct ..	0.1
Converting and blowing:	
Flux	Silica
Fe removal ..... pct ..	83
Final alloy (matte):	
Recovery, pct:	
Co	90
Cu	90
Fe	5
Mn	<0.1
Ni	90
Slag discharge temperature ..... ° C ..	1,400
FERROMANGANESE REDUCTION	
Furnace type	Electric arc
Reductants	Coke, producer gas, electrodes
Alloy composition, pct:	
C	7
Fe	14
Mn	78
Si	1
Slag composition, pct:	
SiO_2	47
Al_2O_3	15
CaO	22
MnO	8
Na_2O	4
MgO	3

Table 24.—Operating parameters for smelting and sulfuric acid leach process—Continued

Parameter and unit	Value
MATTE LEACHING	
Matte temperature, ° C	1,325
Granulation temperature, initial, ° C	95
Grinding method	Ball mill
Output particle size, mesh	−325
Pulp density, pct	9.5
Leaching:	
Temperature, ° C	110
Pressure, psig	150
Time, h	2
Leachate	H_2SO_4
Recovery, pct:	
Co	99
Cu	99
Fe	99
Mn	80
Ni	99
Washing efficiency, pct	98
Filtration stages	2
pH ADJUSTMENT	
Agent	$CaCO_3$
H_2SO_4 in-out	5-0.5
Solids removal method	Clarifier
COPPER LIQUID ION EXCHANGE	
Extraction:	
Extractant	[1]LIX 64N
Number of stages	3
Organic-aqueous ratio	6:1
Metals extraction, pct:	
Co	0
Cu	100
Ni	0
pH (controlled by NH_3)	2.5
Temperature, ° C	40
Stripping:	
Strip solution composition, g/L:	
H_2SO_4	160
Cu	40
Number of stages	2
Organic-aqueous ratio	2:1
Stripping, pct:	
Co	0.2
Cu	87
Ni	0.9
Zn	100
COPPER ELECTROWINNING—COMMERCIAL	
Current density, A/m^2	180
Current efficiency, pct	94
Temperature, ° C	50
Cu in-out, g/L	53-40
H_2SO_4 in-out, g/L	160-180
COPPER RAFFINATE NEUTRALIZATION	
Agent	NH_3 with air
Final pH	4
Solid removal method	Filtration with filter aid
NICKEL LIQUID ION EXCHANGE-EXTRACTION	
Extraction:	
Extractant	[1]LIX 64N
Number of stages	3
Organic-aqueous ratio	7:1
Co	1
Cu	1
Ni	99.5
Temperature, ° C	40
NICKEL LIQUID ION EXCHANGE—Continued	
Ammonia wash (primary):	
Washing agent, pct NH_3	1
Number of stages	2
Organic-aqueous ratio	3:1
NICKEL LIQUID ION EXCHANGE-STRIPPING	
Ammonia wash (secondary):	
Scrub solution, g/L:	
H_2SO_4	1
$(NH_4)_2SO_4$	200
Number of stages	2
Organic-aqueous ratio	1:1
Stripping:	
Number of stages	3
Organic-aqueous ratio	6:1
Stripping, pct:	
Co	0.3
Cu	<0.004
Ni	98.8
NICKEL ELECTROWINNING—COMMERCIAL	
Current density, A/m^2	180
Current efficiency, pct	93
Temperature, ° C	60
Ni in-out, g/L	75-50
H_2SO_4 in-out, g/L	0.016-40
Na_2SP_4, g/L	100
H_3BO_3, g/L	15
COBAT RECOVERY	
Precipitating agent, pct NH_4HS	30
Metals precipitated, pct:	
Co	98
Cu	99.9
Ni	99
Zn	99.9
Temperature, ° C	80
Clarifier underflow:	
Density, pct solids	5
Wash ratio	2:1
Leaching:	
Slurry density, pct solids	40
Agent, pct H_2SO_4	70
Evaporation-crystallization water removal, pct	70
Co oxidation:	
Temperature, ° C	100
Pressure, psig	150
Co reduction:	
Temperature, ° C	175
Pressure, psig	500
Reductant	H_2
AMMONIA RECOVERY	
NH_3 recovery, pct	99
Temperature, ° C	110
Underflow density, pct solids	60
NH_3 stripping:	
Pressure, atm	1.5
Recovery, pct	99
Number of stages	2
Direct condensation:	
Temperature, ° C	40
Pressure, atm	1.3
Number of stages	1
NH_3 absorber:	
Temperature, ° C	35
Pressure, atm	1.2
Number of stages	1

[1]Reference to specific products does not imply endorsement by the Bureau of Mines.

of oxygen at 10 atm pressure. The metal-bearing solution is treated by a series of purification steps in which it is contacted with an organic extractant that selectively removes the copper and nickel from the aqueous solution. Ammonia is added to the solution to control the pH during the separations. The metal values are, in turn, selectively removed from the organic extract and transferred to acidified aqueous solutions, which accumulate copper and nickel sulfate. The metal products, cathode copper and nickel, are produced from these acidic solutions by electrowinning.

Cobalt and small amounts of copper, nickel, and other metals not removed in previous steps are recovered from the aqueous ammonium sulfate solutions by hydrogen sulfide precipitation. The solids are removed from the aqueous ammonium sulfate solution and contacted with air and 100° C H_2SO_4 to selectively redissolve the cobalt and the small amount of Ni present. The undissolved sulfides are sold as minor products, and the cobalt and nickel are recovered from solution in powder form by selective reduction with hydrogen at 34 atm and 185° C.

Lime is then added to the metal-free ammonium sulfate solution, and the mixture is contacted with steam at 120° C and 2 atm to recover ammonia for reuse in the process. The gypsum formed in this step is combined with other process solid and liquid wastes and sent to containment.

LABORATORY TAILINGS GENERATION AND ANALYSES

After completion of the studies on manganese nodules, processing, and methods of analyses, ground nodules were subjected to the five previously described processes on a laboratory scale of operations. In all cases, the processes were carried only as far as the tailings generation and solid-liquid separations. The resultant leach liquors were not processed further to recover the value metals. After washing and separation, the tailings were subjected to physical property testing, mineralogical analyses, chemical analyses, and leachate testing as described previously (*4*). A detailed report on the laboratory processing and tailings characterization has been published. (*5*).

Approximately 1 mt of Pacific manganese nodules and fragments recovered from the area of prime commercial interest, the Clarion-Clipperton fracture zone area (CC-Zone area) as shown in figure 4, was used as the bulk feed material for all five processes. The wet nodules were received in four 55-gal drums. The contents of the four drums were spread on heavy Kraft paper and allowed to air dry for approximately 3 days. The air-dried manganese nodules were crushed to minus 0.25 in. in a jaw crusher and then oven dried at 90° C for approximately 18 h. The cooled oven-dried minus 0.25-in material was further reduced to minus 80 mesh in a Braun pulverizer. The resulting minus 80-mesh material was blended for 4 h in a P-K twin shell V-blender in 200-lb lots. Three samples of each of six blends were taken, analyzed for elemental content, and the blended batches were compared to test homogeneity. Typical results of the elemental analysis for the batches are given in table 25. However, to ensure within-process feed homogeneity, small 20- to 30-lb batches were reblended in a small twin-shell V-blender and analyzed prior to use in the laboratory process systems. The elemental analysis obtained on these small reblended batches was used in determining the effectiveness of the laboratory process.

LABORATORY TAILINGS GENERATION

A summary description of each process has been published (*2, 5*) and given previously in this report. The actual laboratory conditions are given for each process in this section. The analytical results are presented together for all four processes in the next section to enable comparison of the process tailings.

The objective of the laboratory processing was to generate sufficient tailings for chemical and physical characterization. The pregnant liquor was sampled for analysis on each run to ensure adequate leaching and washing efficiencies and the remainder stored. Comparisons between laboratory operating parameters and those suggested for the five proposed commercial processes (*2, 6*) are given in tables 26 through 30 for those unit operations performed in the laboratory.

Gas Reduction and Ammoniacal Leach Process

Reduction and Quenching

The objective of the reduction and quenching operation is to disrupt the manganese nodule crystal structure of MnO_2 by reducing Mn^{4+} to Mn^{2+} and to release the lattice-bound Co, Cu, and Ni for reduction and solubilization. By reducing the Mn^{4+} to Mn^{2+}, the structures of the primary manganese

Table 25.—Homogeneity of blended manganese nodule feed material, weight percent

Element	Batch 1	Batch 2	Batch 3	Batch 4	Batch 5	Batch 6	Average	Element	Batch 1	Batch 2	Batch 3	Batch 4	Batch 5	Batch 6	Average
Al	2.52	2.61	2.50	2.42	2.50	2.59	2.52	Mg	1.86	1.84	1.87	1.90	1.93	1.88	1.88
As	.0055	.0073	.0054	.0076	.0067	.0079	.0067	Mn	29.6	28.7	29.5	30.3	29.8	30.1	29.7
Ba	.22	.17	.20	.31	.24	.22	.23	Mo	.12	.11	.11	.12	.12	.11	.12
Be	<.0002	<.0002	<.0002	<.0002	<.0002	<.0002	<.0002	Ni	1.34	1.30	1.33	1.35	1.34	1.31	1.33
Ca	1.21	1.21	1.27	1.35	1.27	1.40	1.28	Pb	.043	.041	.042	.039	.044	.043	.042
Cd	.0017	.0017	.0017	.0018	.0018	.0018	.0018	Sb	.0047	.0048	.0044	.0052	.0050	.0069	.0052
Co	.23	.22	.23	.23	.23	.24	.23	Ti	.16	.17	.16	.20	.16	.22	.18
Cr	.002	.002	.002	.002	.002	.002	.002	Tl	.020	.020	.020	.020	.020	.020	.020
Cu	1.21	1.16	1.19	1.23	1.21	1.18	1.20	V	.044	.043	.049	.045	.041	.045	.044
Fe	5.56	5.37	5.43	5.38	5.44	5.55	5.46	Zn	.15	.14	.15	.15	.16	.15	.15
K	1.00	.97	.93	.93	.91	.90	.94								

Table 26.—Comparison of operating parameters for the gas reduction and ammoniacal leach process

Parameter and unit	Proposed commercial	Actual laboratory
REDUCTION		
Reduction temperature, ° C	625	625
Cooling temperature, ° C	125	100
Mn reduction, pct	98	96.2 ± 3.4
LEACHING-AERATION		
Leachate composition, g/L:		
NH_3	100	100
CO_2	50	50
Temperature, ° C	40	40-50
Pressure, atm	1	1
Solubilization, pct:		
Co	70	51
Cu	90	87
Fe	~1	<1
Mn	~1	<2
Ni	90	65
Time per stage, h	1	1
Number of stages	3	4
SOLID-LIQUID SEPARATION		
Slurry density, wt pct	35-40	29.4
Wash ratio, kg/kg liquid	2	2
Wash liquid composition, g/L:		
NH_3	100	100
CO_2	50	50
Number of stages	4	4

Table 27.—Comparison of operating parameters for the Cuprion ammoniacal leach process

Parameter and unit	Proposed commercial	Actual laboratory
REDUCTION-LEACHING		
Temperature, ° C	50	55 ± 5
Pressure, atm	1	1
Leachate composition, g/L:		
NH_3	100	100
CO_2	50	50
Cu	3-5	3.5
Number of stages	6	1
Mn reduction, pct	97	96 ± 4
Slurry density, pct solids	20-30	20
OXIDATION-LEACHING		
Leachate composition, g/L:		
NH_3	100	100
CO_2	25	50
Temperature, ° C	50	55
Pressure, atm	1	1
Solubilization, pct:		
Co	50	32
Cu	90	89.5
Fe	~1	<1
Mn	~1	<1
Ni	90	63
Time per stage, h	1	1
Number of stages	3	4
SOLID-LIQUID SEPARATION		
Slurry density, wt pct	35-40	31.1
Wash ratio, kg/kg liquid	2	2
Wash liquid composition, g/L:		
NH_3	100	100
CO_2	50	50
Number of stages	6	6

Table 28.—Comparison of operating parameters for the high-temperature and high-pressure sulfuric acid leach process

Parameter and unit	Proposed commercial	Actual laboratory
LEACHING		
Temperature, ° C	245	245 ± 3
Pressure, psig	515	530 ± 5
Contact time, h	4	1.5
H_2SO_4 consumption lb/lb nodules	0.4	0.4
Solubilization, pct:		
Co	90	92
Cu	95	95
Fe	1	12
Mn	5	5
Ni	95	98
SOLID-LIQUID SEPARATION		
Number of stages	6	8
Slurry density, pct solids	35-40	30.5
Wash ratio, kg/kg liquor	2	2

Table 29.—Comparison of operating parameters for the reduction and hydrochloric acid leach process

Parameter and unit	Proposed commercial	Actual laboratory
HYDROCHLORINATION		
Temperature, ° C	500	500
Pressure, atm	1	1
Reagent	HCl gas	HCl gas
Percent excess HCl	100	100
Hydrolysis temperature, ° C	200	100
Hydrochlorination, pct:		
Co	100	94
Cu	96	94
Fe	27	20
Mn	94	97
Ni	100	98
LEACHING AND WASHING		
Final pH	2.0	2.3
Slurry density, pct solid	20-25	32
Wash ratio, kg/kg liquids	2:1	2:1
Number of stages	6	6
Soluble metals removed, pct	98	98

Table 30.—Comparison of operating parameters for the smelting and sulfuric acid leach process

Parameter and unit	Proposed commercial	Actual laboratory
REDUCTION-SMELTING		
Reductants	Coke CO	Coke CO
Temperature, ° C:		
Reduction	725	725
Smelting	1,325	1,400
Reduction time, h	2	1.5
Flux	Silica	Silica
Alloy recovery, pct:		
Co	90	97
Cu	90	98
Fe	70	94
Mn	2	2
Ni	95	99
Slag recovery, pct:		
Co	<10	3
Cu	<10	2
Fe	20	6
Mn	98	98
Ni	<10	1
FERROMANGANESE REDUCTION		
Reductant	Coke	Coke
Flux	Lime	Lime
Alloy composition, pct:		
Mn	78	75
Fe	14	6
C	7	7.6
SiO_2	1	3.8

minerals of todorokite, birnessite, and/or vernadite (*1*) are altered and the desired leaching agent is able to solubilize the value metals. Quenching prevents reoxidation of Mn^{2+} and facilitates the carbonation of the reduced manganese to form $MnCO_3$. The principal chemical reactions that occur during reduction follow:

$$MnO_2 + CO \rightarrow MnO + CO_2 \text{ (reduction).} \quad (1)$$

$$MnO + CO_2 \rightarrow MnCO_3 \downarrow \text{ (carbonation).} \quad (2)$$

$$Fe_2O_3 + CO \rightarrow 2FeO + CO_2. \quad (3)$$

$$FeO + CO \rightarrow Fe^0 + CO_2. \quad (4)$$

$$NiO + CO \rightarrow Ni^0 + CO_2. \quad (5)$$

$$CuO + CO \rightarrow Cu^0 + CO_2. \quad (6)$$

$$Co_2O_3 + 3CO \rightarrow 2Co^0 + 3CO_2. \quad (7)$$

$$CoO + CO \rightarrow Co^0 + CO_2. \quad (8)$$

Reaction 1 is the disruption of the MnO_2 structure allowing subsequent reduction of Ni, Cu, and Co (reactions 5 through 8) and the carbonation of reduced manganese (reaction 2). Iron is also reduced to either the Fe^{2+} state and/or possibly to Fe^0 (reactions 3 and 4). It is desirable to reduce iron only to the Fe^{2+} state because Fe^0 may alloy with nickel metal. Formation of FeNi alloy retards and often prevents solubilization of the nickel values associated with the alloy formation.

The laboratory reduction of manganese by CO-CO_2 was performed in an Applied Test Systems model 1379 rotating the tube furnace. The furnace tube was made of Inconel 601 with a 5-in internal diameter. The furnace heating zone was 30-in long. Temperature control was provided by a Chromel-Alumel thermocouple connected to the furnace controller. Reduction temperature was maintained at a minimum ~625° C with the maximum of ~650° C. The ends of the tube were plugged with firebrick and sealed with Fiberfrax moldable refractory. The reduction gas was introduced into the furnace through a small hole in the center of the firebrick and consisted of a mixture of carbon monoxide (CO) and carbon dioxide (CO_2) in a ratio of 3:2 by weight and 2.33:1.0 by volume. Total flow rate was 1 L/min. The CO and CO_2 gases were of technical grade (98 pct) and chemically pure grade (99.8 pct), respectively. The reaction time was 4 h for 1,500 g of ground nodule feed. In a total of 11 reduction runs at these conditions, the average percent reduction of Mn^{4+} to Mn^{2+} was 96.2 ± 3.4 pct.

At the completion of 4 h, the ground reduced nodules were quenched in 1 L of distilled boiled water and were sparged with CO_2 gas for 3 h to facilitate carbonation of the manganese to manganese carbonate ($MnCO_3$). After the CO_2 sparge, the reduced, carbonated nodules were divided into 150-g (dry basis) aliquots for use in the leaching step.

Leaching-Aeration

The leaching-aeration operation oxidizes and solubilizes the value metals of Cu, Co, and Ni in an ammonia-ammonium carbonate leaching agent while rejecting most of the Fe and Mn. The principal chemical reactions occurring in this operation follow:

$$Cu + \tfrac{1}{2}O_2 + 6NH_3 + 2CO_2 + H_2O \rightarrow Cu(NH_3)_4^{2+} + 2NH_4^+ + 2CO_3^{2-}. \quad (9)$$

$$Co + \tfrac{1}{2}O_2 + 8NH_3 + 2CO_2 + H_2O \rightarrow Co(NH_3)_6^{2+} + 2NH_4^+ + 2CO_3^{2-}. \quad (10)$$

$$2Co(NH_3)_6^{2+} + \tfrac{1}{2}O_2 + CO_2 \rightarrow 2Co(NH_3)_5^{3+} + CO_3^{2-}. \quad (11)$$

$$Ni + \tfrac{1}{2}O_2 + 8NH_3 + 2CO_2 + H_2O \rightarrow Ni(NH_3)_6^{2+} + 2NH_4^+ + 2CO_3^{2-}. \quad (12)$$

$$FeNi + O_2 + 12NH_3 + 3CO_2 + H_2O \rightarrow Ni(NH_3)_6^{2+} + Fe(NH_3)_4^{2+} + 2NH_4^+ + 3CO_3^{2-}. \quad (13)$$

$$Fe + \tfrac{1}{2}O_2 + 6NH_3 + 2CO_2 + H_2O \rightarrow Fe(NH_3)_4^{2+} + 2NH_4^+ + 2CO_3^{2-}. \quad (14)$$

$$4Fe(NH_3)_4^{2+} + O_2 + 2H_2O + 8(OH)^- \rightarrow 4Fe(OH)_3 \downarrow + 16NH_3. \quad (15)$$

$$MnO + CO_2 \rightarrow MnCO_3 \downarrow. \quad (16)$$

$$Mn^{2+} + 6NH_3 \rightarrow Mn(NH_3)_6^{2+}. \quad (17)$$

Reactions 9 through 13 are the solubilization of value metals including some iron (reaction 13). Reactions 13 through 15 show iron solubilization with the subsequent precipitation of iron as $Fe(OH)_3$ (reaction 15). In oxidizing conditions, the iron amine complex decomposes rapidly forming insoluble ferric hydroxide $Fe(OH)_3$, reaction 15 (*78*). Uncarbonated manganese may undergo either reactions 16 or 17. If $MnCO_3$ is formed, the manganese is no longer available to be complexed and solubilized. Reaction 17 shows the formation of the hexamine manganese complex. This complex is also relatively unstable under oxidizing conditions and will decomplex.

The laboratory leaching-aeration operation was performed in glass 4-L stirred reaction vessels with compressed air sparged into the reaction vessel by fritted glass spargers located near the bottom. The leaching agent was 100 g/L NH_3 and 50 g/L CO_2 solution prepared from NH_4OH, $(NH_4)_2CO_3$, and Na_2CO_3. Total volume was 3 L and pulp density was 5 pct (150 g in 3 L). The reaction temperature was maintained at 55° ± 5° C for 1 h per stage in the four-stage countercurrent leach. Reaction vessels were covered to prevent excess NH_3 vapor from escaping, and the operation was performed in a fume hood. The pH was maintained between 9.5 and 11.0 by addition of NH_4OH and Na_2CO_3. After equilibrium conditions were obtained in the four-stage countercurrent leaching aeration operation, 37 complete cycles were run and solids collected for tailings washing. The operation consisted of leaching with the ammonia-ammonium carbonate solution with air sparged into the solution near the bottom of the vessel for 1 h, settling for 1 h, decanting the liquids to the next appropriate stage, and continuing the leaching as before. The depleted unwashed solids were collected and divided into six batches for tailings washing and solid-liquid separation.

Tailings Washing and Solid-Liquid Separation

The tailings washing and solid-liquid separation operations solubilize the remaining value metals and remove the liquid phase from the tailings for a 30 to 50 pct solids content. Retention time per washing stage is on the order of 16 to 24 h for proposed commercial operations (*2, 6*). The washed solids are steam stripped to recover ammonia.

The laboratory operation consisted of contacting the solids from leaching-aeration operation with wash liquid of 100 g/L NH_3 and 50 g/L CO_2 [prepared from $(NH_4)_2CO_3$, NH_4OH, and Na_2CO_3)], at a solid-to-liquid ratio of 2 kg solids per kilogram liquid. The tailings were agitated for 8 h and allowed to settle overnight. The settled solids were separated by decanting the liquid phase and recontacted with fresh wash solution for a total of four complete stages. After separation of the fourth stage wash liquid, the solids were rinsed twice with distilled water at 2 kg solid-per-kilogram liquid ratio to remove ammonia. This was done in lieu of steam stripping the relatively small amount of tailings. The final rinsed tailings were combined, blended, and separated into 1-gal plastic containers prior to analysis. Because of the primary interest in physical as well as chemical properties of the laboratory tailings, no flocculants were used to enhance settling characteristics.

Cuprion Ammoniacal Leach Process

Reduction-Leaching

In the Cuprion reduction leaching operation, the manganese nodule crystal structure (MnO_2) is disrupted by reducing the Mn^{4+} to Mn^{2+}, which releases the lattice bound Co, Cu, and Ni for reduction and solubilization. In the Cuprion process, the reduction is performed by Cu^+ ion. The Cu^+ is regenerated with carbon monoxide. The primary reactions that occur in this portion of the process involving CO, Cu^+, and Mn, Fe, Cu, Ni, and Co are reactions 2 through 8 as previously given and the following reactions:

$$MnO_2 + 2Cu(NH_3)_2^+ + 2NH_3 + (NH_4)_2CO_3 \rightarrow MnCO_3 + 2Cu(NH_3)_4^{2+} + 2(OH)^- \text{ (reduction).} \quad (18)$$

$$2Cu(NH_3)_4^{2+} + CO + 2(OH)^- \rightarrow 2Cu(NH_3)_2^+ + 2NH_3 + (NH_4)_2CO_3. \quad (19)$$

Reactions 18 and 19 show the reduction of Mn^{4+} to Mn^{2+} with the regeneration of the Cu^+ complex. Reactions 2 through 8 are the overall reduction-carbonation reactions producing $MnCO_3$ and the reduction of iron and value metals of Cu, Ni, and Co to the elemental state. Once reduction is completed, the leach solution is aerated and oxidation leached as in the previous process.

The laboratory reduction-leaching operation was performed in 4-L stirred glass reactors with 1 L/min CO (technical grade–98 pct) sparged into the vessel by fritted glass spargers located near the bottom. The initial cuprous ion was added as CuCl at a concentration of 3.5 g/L. The volume was 3 L of 100 g/L NH_3 and 50 g/L CO_2 solution prepared from reagent grade $(NH_4)_2CO_3$, NH_4OH, and Na_2CO_3. The reaction temperature was maintained at 55° ±5° C during the operation. After addition of CuCl, CO was sparged into the blue-colored solution until it became nearly colorless. Ground nodules were then added in 2-g increments and the pH and electromotive force (emf) monitored. The pH was maintained between 10.0 and 11.0 by NH_4OH and Na_2CO_3; and the emf ranged from approximately −350 to −230 mV with an average range of 90 mV per each 2-g increment of nodule addition. More nodule feed was added when the emf returned to near the initial reading. Nodules were added every few minutes until the emf cycle showed rapid return to the initial readings. This indicated that copper from the nodule was being solubilized, reduced to $Cu(NH_3)_2^+$, and reacting with the manganese as shown in reactions 18 and 19. At this point, the nodule feed increments were increased gradually to 5, 10, and finally 25 g. The reaction was terminated when the pulp density reached ~20 pct or when 600 g of nodules had been added, and a new reduction-leaching operation started. The reduced carbonated nodules from the reactor were sampled and analyzed for manganese as Mn^{2+}. In a total of 21 runs, the average manganese reduction was 95.8±4.1 pct. These reduced nodules were used as feed to a four-stage countercurrent oxidation leach to solubilize the remaining value metals.

Oxidation-Leaching

The value metals of Cu, Co, and Ni are solubilized in an oxidation-leaching operation using an ammonia-ammonium carbonate solution, which rejects most of the Fe and Mn. The chemical reactions occurring in this operation are reactions 9 through 12 and 14 through 17. These reactions are the same as for leaching aeration of the previous process. The laboratory operation was performed in the same manner as the previous process and its description is not repeated here. The depleted unwashed solids were collected and divided into nine batches for tailings washing and solid-liquid separation.

Tailings Washing and Solid-Liquid Separation

The tailings washing and solid-liquid separation operation solubilizes the remaining value metals and removes the liquid phase from the tailings for a 30 to 50 pct solids content. Retention time per washing stage is on the order of 16 to 24 h for proposed commercial operation (*2, 6*), and the washed solids are steam stripped to recover ammonia. The tailings were treated in the same manner as the previous process. The rinsed tailings were combined, blended, and placed into 1-gal plastic containers prior to analysis. No flocculants were used to enhance settling characteristics so that physical as well as chemical properties of the laboratory tailings could be studied.

The Cuprion process is the only process for which the industry supplied pilot-plant generated tailings. These tailings were also tested, and results of the laboratory and pilot-plant generated tailings analyses are compared in the "Laboratory Tailings Analyses" section.

High-Temperature and High-Pressure Sulfuric Acid Leach Process

Leaching

In this process, the reduction of Mn^{4+} to Mn^{2+} to disrupt the manganese nodule crystal structure, and the solubilization of Co, Cu, and Ni occur in the same reactor. As sulfuric acid is depleted, Mn^{2+} is reoxidized to Mn^{4+} and remains in the tailings as MnO_2. This acid depletion also permits iron to precipitate as the hydroxide $Fe(OH)_3$. The primary chemical reactions that occur during the leaching operation follow, for the major and minor metals of interest.

$$MnO_2 + H_2SO_4 \rightarrow MnSO_4 + H_2O + \tfrac{1}{2}O_2. \quad (20)$$

$$Mn^{2+} + \tfrac{1}{2}O_2 + 2(OH)^- \rightarrow MnO_2 \downarrow + H_2O. \quad (21)$$

$$Fe_2O_3 + 3H_2SO_4 \rightarrow Fe_2(SO_4)_3 + 3H_2O. \quad (22)$$

$$Fe^{3+} + 3(OH)^- \rightarrow Fe(OH)_3 \downarrow. \quad (23)$$

$$NiO + H_2SO_4 \rightarrow NiSO_4 + H_2O. \quad (24)$$

$$CuO + H_2SO_4 \rightarrow CuSO_4 + H_2O. \quad (25)$$

$$CoO + H_2SO_4 \rightarrow CoSO_4 + H_2O. \quad (26)$$

$$Co_2O_3 + 2H_2SO_4 \rightarrow 2CoSO_4 + 2H_2O + \tfrac{1}{2}O_2. \quad (27)$$

Reactions 20 and 21 are the disruption of the manganese MnO_2 structure and the subsequent reoxidation at low acid strengths to MnO_2. Reactions 22 and 23 show the solubilization of iron and its subsequent reprecipitation at low acid strengths. Another possible iron product is jarosite $KFe_3(SO_4)_2(OH)_6$, but no reaction is given because it should only be a minor product. Reactions 24 through 27 show the solubilization of the value metals Co, Cu, and Ni. Molybdenum probably is not solubilized in the process and remains with the tailings. If molybdenum is solubilized during leaching, it is subsequently precipitated at the low acid strengths, possibly with the iron hydroxides.

The laboratory leaching operation was performed in a Parr Instruments model 4522, 2-L stirred pressure reactor. The reactor bomb was made of titanium and a glass liner was used to reduce potential attack. Temperature control was provided by a Chromel-Alumel thermocouple connected to the

controller. Temperature was maintained at 245° ± 3° C. Each run was made with 400 g of minus 80-mesh nodules and 111 mL of H_2SO_4 combined with 750 mL of H_2O. This gave a reagent-to-nodule ratio of 0.4 lb H_2SO_4/lb nodule. Pressure inside the bomb was maintained at 530 ± 5 psig. The nodules and acid mixture were combined just prior to startup, and the bomb sealed and brought to temperature in 60 min. Reaction time at 245° ± 3° C and 530 ± 5 psig was 90 min, and cooling required an additional 60 min. Generally two runs were made each day and a total of 55 runs were made to collect tailings. After completion of the cooldown period, the nodule residue and pregnant liquor were separated by filtration, and samples of the liquid and solid portions were taken and analyzed for Mn, Fe, Cu, Ni, Co, and Zn. After completion of the runs, the unwashed tailings were combined into eight batches and subjected to solid-liquid separation and tailings washing.

Solid-Liquid Separation

The solid-liquid separation operation removes entrained leach liquor and recovers the remaining value metals. Final tailings slurry density should be between 30 to 50 pct solids content.

The laboratory operation consisted of contacting the solids from the leaching operations with a 2.0-pH wash liquid made with H_2SO_4 at a solid-to-liquid ratio of 2 kg solids/kg liquid. The tailings were agitated for 6 h and allowed to settle. The liquid portion was decanted and the solids were contacted with fresh wash solution for a total of eight complete stages. After separation of the eighth stage wash liquid, the solids were combined, blended, and separated into 1-gal plastic containers prior to analysis. As in the previous two processes discussed, physical as well as chemical characteristics of the laboratory tailings were important so no flocculants were used to enhance settling characteristics.

Reduction and Hydrochloric Acid Leach Process

Hydrochlorination

The principle of the hydrochlorination operation is to reduce and chlorinate manganese and to chlorinate the value metals of cobalt, copper, and nickel. In this step, Mn^{4+} is reduced to Mn^{2+} and chlorine is released. This reduction allows subsequent release of the value metals and their chlorination. As the reaction is completed, water is sprayed into the furnace to hydrolyze iron to Fe^{3+} hydroxide and the iron is precipitated as $Fe(OH)_3$. The principle chemical reactions that occur during hydrochlorination follow, for the major and minor metals of interest.

$$MnO_2 + 2HCl \rightarrow MnO + H_2O + Cl_2. \quad (28)$$

$$MnO + 2HCl \rightarrow MnCl_2 + H_2O. \quad (29)$$

$$MnO_2 + 4HCl \rightarrow MnCl_2 + 2H_2O + Cl_2. \quad (30)$$

$$Fe_2O_3 + 6HCl \rightarrow 2FeCl_3 + 3H_2O. \quad (31)$$

$$FeCl_3 + 3H_2O \rightarrow Fe(OH)_3 \downarrow + 3HCl. \quad (32)$$

$$NiO + 2HCl \rightarrow NiCl_2 + H_2O. \quad (33)$$

$$CuO + 2HCl \rightarrow CuCl_2 + H_2O. \quad (34)$$

$$CoO + 2HCl \rightarrow CoCl_2 + H_2O. \quad (35)$$

$$Co_2O_3 + 4HCl \rightarrow 2CoCl_2 + 2H_2O + \tfrac{1}{2}O_2. \quad (36)$$

Reactions 28 and 29 are the stepwise reduction and hydrochlorination of MnO_2 with reaction 30 being the overall net reaction. Reaction 31 is the chlorination of iron to form $FeCl_3$. As shown, this reaction forms water that can react with iron during hydrolysis to form $Fe(OH)_3$ (reaction 32). Reactions 33 through 36 show the chlorination of the value metals Co, Cu, and Ni. Many other components of nodules are solubilized including Mo, V, Zn, and alkali and alkaline earth elements. Elements such as Al, Pb, Ti, and Tl are also solubilized by the high chloride media.

The laboratory hydrochlorination operation was performed in an Applied Test Systems model 1379 rotating tube furnace with a 5-in-ID Inconel 601 tube. The temperature in the 30-in heating zone was controlled by a Chromel-Alumel thermocouple connected to the furnace controller. The temperature was maintained at 510° ± 10° C for the 8 h of each run. Technical grade HCl gas (99.0 pct) was added at a rate of 1.5 L/min to provide the 100 pct excess HCl for the 625 g of nodule feed. At the end of the 8 h, the gas was shut off and the furnace allowed to bake off the excess HCl. The furnace was tilted to allow the chlorinated nodules to tumble into 1.5 L of boiling distilled water for quenching and hydrolysis.

Because of the corrosivity of HCl gas at temperatures over 450° C, corrosion of the Inconel 601 tube added chromium and additional nickel and iron to the solid phase. The amount of nickel and chromium added was calculated based on the chromium content as nodules contained very little chromium (< 50 μg/g). The concentration of nickel associated with chromium in Inconel 601 was taken into account when determining nickel efficiencies.

A total of 61 hydrochlorination runs were performed. The chlorinated nodules were collected and treated with aqueous HCl to complete the dissolution and solubilization of the value metals.

Leaching and Tailings Washing

The leaching and tailings washing operation is designed to solubilize the value metals of Co, Cu, Mn, and Ni, reject most of the iron to the tailings, and wash the tailings prior to disposal. Final solids content should be 30 to 50 pct by weight.

The laboratory operation consisted of leaching the chlorinated nodules with aqueous HCl at mild temperatures of approximately 80° C to complete dissolution of the value metals. The final pH of the leach solution was between 2.0 and 2.3. The solution pH was adjusted to 3.2 to precipitate the remaining iron; then the solids and liquids were separated. The tailings were washed six times to simulate the proposed commercial operation and filtered. The final pH was 6.5 and final solids content was 32 wt pct. The 26.3 lb of tailings (dry weight) was blended and divided among six 1-gal plastic containers prior to analysis. Again, no flocculants were used to enhance settling properties so that the physical as well as the chemical properties of the tailings could be studied.

Smelting and Sulfuric Acid Leach Process

Reduction-Smelting

In this process, the elements Co, Cu, and Ni are reduced to the metallic state, Co^0, Cu^0, Ni^0, along with most of the iron present. Under controlled conditions, the manganese is not reduced to Mn^0 but remains as Mn^{2+} in the slag. The Co, Cu, Fe, and Ni form a metal alloy that settles to the bottom

of the reaction vessel. The reduction is performed by using coke and CO-rich gas and slagged by using silica. The primary reactions that occur in this portion of the process involving C, CO, SiO_2, Mn, Fe, Cu, Ni, and Co are reactions 2, 5, 6, 8, and the following:

$$MnO_2 + C \rightarrow MnO + CO. \quad (37)$$

$$MnO + CO \rightarrow Mn^0 + CO_2. \quad (38)$$

$$MnO + SiO_2 \rightarrow MnSiO_3. \quad (39)$$

$$2MnO + SiO_2 \rightarrow Mn_2SiO_4. \quad (40)$$

$$2Mn^0 + O_2 \rightarrow 2MnO\ . \quad (41)$$

$$Fe_2O_3 + C \rightarrow 2FeO + CO. \quad (42)$$

$$FeO + CO \rightarrow Fe^0 + CO_2. \quad (43)$$

$$NiO + C \rightarrow Ni^0 + CO. \quad (44)$$

$$CuO + C \rightarrow Cu^0 + CO. \quad (45)$$

$$Co_2O_3 + C \rightarrow 2CoO + CO. \quad (46)$$

$$CoO + C \rightarrow Co^0 + CO. \quad (47)$$

Reactions 2, 37, and 38 show the various steps for the reduction of Mn^{4+} to Mn^{2+} and to Mn^0. Reactions 39 and 40 are slag formations, and reaction 41 shows the reoxidation of Mn^0 to Mn^{2+} by controlled blowing operations. Reactions 5, 6, 8, and 42 through 47 show the various steps for Fe, Cu, Ni, and Co reduction to the metallic state. Once the reduction is complete, the metal alloy separates from the oxide-silicate slag by gravity.

The laboratory reduction-smelting operation was performed as a single operation in a Lindberg electric resistance furnace type 56953 with temperature control of ±1° C from 500° to 1,500° C. A type R (Pt vs Pt-13 pct Rh) thermocouple was connected to a phase angle fired temperature controller (Lindberg type 59645). A mixture of 1,900 g of nodules, 100 g of coke, and 350 g of silica was blended for 2 h and placed in a size 16 SiC graphite bonded crucible. The crucible was then placed in a drying oven at 160° C overnight. The amount of coke added had the carbon equivalent to reduce all the Mn^{4+} to Mn^{2+}, and all the Fe, Cu, Co, and Ni to the metallic state. The silica was added to complex the Mn^{2+} as $MnSiO_3$ or Mn_2SiO_4 to keep the manganese in the slag phase. After drying overnight, the crucible was placed in the high-temperature furnace (500° C) and a refractory brick lid placed on top. The furnace was closed and the controller set for 1,400° C. Heat-up time to 1,400° C was approximately 6 h and allowed the initial reduction step to occur. The temperature was maintained at 1,400 ±1° C for 1.5 h and the furnace controller reset to 500° C (minimum temperature). The charge was allowed to cool overnight and then removed to cool to near room temperature. The slag and metal were then removed with an impact drill. A total of 35 runs were made with an average metal weight of 173 ± 9 g and slag weight of 1,600 ± 84 g. A total of 56 kg of slag and 6 kg of metal were produced. Approximately 98 pct of the manganese reported in the slag phase and 94 pct of the iron to the alloy. Value metal recoveries were all greater than 97 pct.

To prove process feasibility, several metal buttons were remelted, combined with silica, and blown with air to remove the remaining Mn and some Fe. The commercial operation requires low Mn levels in the metal alloy so that sulfur consumption during sulfidizing and matte formation is kept to a low level. The several tests run in the laboratory yielded manganese levels less than the maximum of 0.1 pct Mn. The slag produced in this step would be recycled back to the smelting step to recover any value metals lost during the blowing operation.

Ferromanganese Reduction

The ferromanganese reduction operation converts the slags generated in the smelting furnace to ferromanganese and a calcium and aluminum silicate slag. The slags from the smelting operation are fluxed with CaO (lime) and additional silica, and coke is added as a reductant. This allows the Ca to react with the silicates in the slag along with Al and other slag-forming elements to form Ca_2SiO_4, $Ca_2Al_2SiO_7$, and other silicates. The coke reacts with the Mn and Fe to form the metals in a ferromanganese alloy, which separates by gravity from the slags. The primary reactions that take place in this operation are reaction 39 and the following:

$$Mn_2SiO_4 + 2CaO \rightarrow 2MnO + Ca_2SiO_4. \quad (48)$$

$$MnSiO_3 + CaO \rightarrow MnO + CaSiO_3. \quad (49)$$

$$MnO + C \rightarrow Mn^0 + CO. \quad (50)$$

$$Ca_2SiO_4 + Al_2O_3 \rightarrow Ca_2Al_2SiO_7. \quad (51)$$

$$SiO_2 + 2CaO \rightarrow Ca_2SiO_4. \quad (52)$$

Reactions 39 and 48 through 50 show the reactions of lime with the manganese silicates and the subsequent reduction of Mn^{2+} to Mn^0. Reactions 48, 51, and 52 show formation of gehlenite ($Ca_2Al_2SiO_7$) and larnite (β-Ca_2SiO_4).

The laboratory generation consisted of mixing 1,000 g of slag from the reduction-smelting operation with 100 g coke and 840 g lime. The coke is the amount required to reduce the MnO to Mn^0 and the lime is twice the amount needed to react with Mn_2SiO_4 to convert it to Ca_2SiO_4. The sample mixture was placed in a size 16 SiC crucible and the crucible placed in the Lindberg furnace. The temperature controller was set for 1,450° C and required 7 h to reach temperature. The mix was held at 1,450° C for 1 h and allowed to cool to 500° C overnight. The next morning the crucible was removed, cooled to near room temperature, and the product removed. The slag contained β-Ca_2SiO_4 (larnite), $Ca_2Al_2SiO_7$ (gehlenite), and excess SiO_2 (silica) as the primary minerals. The metal was very friable and contained 75 pct Mn and about 6 pct Fe.

LABORATORY TAILINGS ANALYSES

After completion of the laboratory processing, the blended tailings were characterized by a variety of tests and analyses. The results of these tests and analyses are reported in the following order: physical property testing, mineralogical analyses, chemical analyses, and leachate testing. The acronym SmSAL-1 is used to denote the smelting slag and SmSAL-2 is used to denote the ferromanganese slag. CuAmL-Lb is used to identify the tailings generated in the laboratory by the Cuprion ammoniacal leach process, and CuAML-Pp identifies those provided by industry from pilot plant operation. The other acronyms used are the same as listed in the "Introduction" section. The analyses and testing of the tailings were done immediately after completing the laboratory operation so that tailings did not age significantly before characterization.

Physical Property Testing

The tests performed on the tailings for physical properties are listed in table 17. In the case of the GRAmL process, triaxial shear, permeability, and maximum density were not tested because of insufficient sample volume for these tests. The slags from the SmSAL process were not tested for physical properties as they are glassy and massive. The particle size is dependent on the amount of granulation or crushing that takes place for slags and many other parameters do not apply and/or are dependent on the particle size distribution.

The results shown in table 31 from the GRAmL, CuAmL-Lb, and CuAmL-Pp are very similar as predicted (*3*). The tailings from the HTPSAL process are similar to the three ammoniacal leach processes. The RHClAL process tailings are substantially different from the other four process tailings, with a lower specific gravity and maximum density, but they do have a similar particle size distribution. The lower specific gravity for the RHClAL process is because of the absence of manganese (that is extracted), making the composition primarily iron oxides and hydroxides, silica, and feldspar.

Table 31.—Physical properties of tailings from laboratory and pilot-plant leach processes

Parameter	GRAmL	CuAmL-Lb	CuAmL-Pp	HTPSAL	RHClAL
Grain size distribution, μm:					
100 pct pass	600	600	74	600	425
50 pct pass	29	13	6	15	14
0 pct pass	0.6	1	1	1	1.2
Specific gravity, dry solids	3.47	3.10	3.19	3.49	2.85
Triaxial shear[1]					
Friction angle	ND	38.5°	38.0°	5.2°	38.5°
Cohesion, psi		4.0	5.0	8.6	0.0
Permeability[1] 10^{-5} cm/s	ND	0.67	0.85	70	1.23
Maximum density, pct	ND	92.5	90.1	87.7	57.0
Atterberg limits:					
Liquid, pct	43.8	42.1	45.0	43.3	70.0
Plastic, pct	39.4	34.4	41.2	43.7	60.0
Soil class	ML	ML	ML	ML	MH
Percent solids, wt pct	29.4	31.1	41.8	30.5	32.0

MH Diatomaceous silt. ML Lean silt. ND Not determined.
[1]At 98 pct of maximum density.

Mineralogical Analyses

Air-dried samples of the tailings and slags were examined by X-ray diffraction (XRD) to determine the major and minor minerals present. With the exception of the slags from the SmSAL process, a second set of tailings samples was acid leached with aqueous HCl and the washed air-dried residue was also examined using XRD.

The results of the XRD analysis are given in table 32. The primary constituents of the three ammoniacal processes—GRAmL, CuAmL-Lb, and CuAmL-Pp—were rhodochrosite ($MnCO_3$) and hausmannite (Mn_3O_4) with minor amounts of quartz and feldspar. The Mn_3O_4 was primarily observed in the GRAmL process tailings because of incomplete carbonation. The acid insoluble fraction of all process tailings contained quartz and feldspar. The HTPSAL tailings contained poorly crystalline Mn_3O_4, MnO_2, and iron oxide compounds plus low concentrations of quartz and feldspar. The RHClAL tailings contained Fe_2O_3, quartz, and feldspar. The slags from the SmSAL process were Mn_2SiO_4 and $MnSiO_3$ for the slag produced from smelting the nodules and Ca_2SiO_4 and $Ca_2Al_2SiO_7$ for the ferromanganese reduction slags.

Chemical Analyses

The blended tailings from the tailings washing solid-liquid separation operations were sampled. The solid and liquid phases were analyzed from the GRAmL, CuAmL-Lb, CuAmL-Pp, HTPSAL, and RHClAL processes and the solid phase slags from the SmSAL process as no liquids are produced in this process. The liquid phase samples were analyzed directly by atomic absorption spectrophotometry (AAS) and ion chromotography (IC) for elemental and ion content, respectively. The solid phase samples were dried, dissolved by procedures outlined previously (*4, 11*), and the solutions analyzed by AAS and IC. A total of 25 elements and 7 anions were determined in each phase. In addition, pH, CO_2 as carbonate, and ammonium ion (NH_4^+) were determined in the liquid phase; and divalent manganese (Mn^{2+}) and NH_4^+ were determined in the solid phase. Solid phase CO_3^{2-} was determined from Leco carbon analysis, and liquid phase CO_3^{2-} was determined by IC. The elements As, Sb, and Se were determined by electrothermal atomization AAS. Mercury was not determined because of extremely low levels in nodules (*1*). Tables 33 and 34 contain results of solid phase analyses. Table 34 lists values for NH_4^+, Br^-, Cl^-, CO_3^{2-}, F^-, NO_3^-, PO_4^{3-}, and

Table 32.—Mineralogical analyses of tailings and slags from laboratory and pilot-plant leach processes

Mineral	Chemical formula	Concentration,[1] qualitative values						
		GRAmL	CuAmL-Lb	CuAmL-Pp	HTPSAL	RHClAL	SmSAL-1	SmSAL-2
Feldspars	$NaAlSi_3O_8$, $KAlSi_3O_8$, $CaAl_2Si_2O_8$.	Low	Low	Low	Very low	Minor	ND	ND.
Gehlenite	$Ca_2Al_2SiO_7$	ND	ND	ND	ND	ND	ND	Major.
Hausmannite	Mn_3O_4	Minor	ND	ND	Minor	ND	ND	ND.
Hematite	Fe_2O_3	ND	ND	ND	ND	Low	ND	ND.
Iron oxides and hydroxides.	FeO, Fe_3O_4, Fe_2O_3, $Fe(OH)_3$.	ND	ND	ND	Minor	Low	ND	ND.
Larnite	β-Ca_2SiO_4	ND	ND	ND	ND	ND	ND	Major.
Pyrolusite	MnO_2	ND	ND	ND	Minor	ND	ND	ND.
Quartz	SiO_2	Very low	Very low	Very low	Very low	Low	ND	ND.
Rhodochrosite	$MnCO_3$	Major	Major	Major	ND	ND	ND	ND.
Rhodonite	$MnSiO_3$	ND	ND	ND	ND	ND	Low	Very low.
Tephroite	Mn_2SiO_4	ND	ND	ND	ND	ND	Major	ND.

ND Not detected.
[1]Major, >25 wt pct; minor, 10-25 wt pct; low, 5-10 wt pct; very low, <5 wt pct.

Table 33.—Elemental analytical results for tailings solids and slags from laboratory and pilot-plant leach processes

Element	Analysis working limits[1]	Process and number of replicates						
		GRAmL (5)	CuAmL-Lb (6)	CuAmL-Pp (5)	HTPSAL (6)	RHCIAL (6)	SmSAL-1 (5)	SmSAL-2 (4)
		WEIGHT PERCENT						
Al	0.0075	2.53	2.28	2.37	2.0	4.3	2.8	3.16
Ba	.004	.20	.16	.24	.35	.47	.10	.15
Ca	.00025	1.58	1.42	1.60	1.5	.40	.46	24.8
Co	.001	.24	.22	.18	.04	.037	.005	<.001
Cu	.00025	.29	.31	.14	.12	.19	.06	.016
Fe	.0005	5.88	5.67	5.80	8.63	9.6	.95	.32
K	.0002	.38	.23	.59	.98	.25	.06	.06
Mg	.00002	2.20	2.11	2.03	.05	.29	1.64	2.07
Mn	.00025	33.7	27.0	27.0	32.8	1.93	31.5	6.40
Mn^{2+}	.00025	26.4	20.5	27.0	1.13	.54	25.4	5.3
Mo	.002	<.002	<.002	.0068	.13	.079	<.002	<.002
Na	.00003	1.57	1.10	.98	.095	.87	1.95	.23
Ni	.001	.86	.56	.22	.048	[2]1.15	.02	<.001
Pb	.001	.045	.042	.041	.033	.017	<.001	<.001
Si (SiO_2)	.5	13.5	13.1	12.6	16.8	58.5	41.7	33.9
Ti	.02	.53	.42	.32	.71	1.43	.54	.24
V	.01	.10	.09	.07	.10	.11	.04	<.01
Zn	.00005	.13	.11	.13	.018	.007	.003	.034
		MICROGRAMS PER GRAM						
Ag	1.5	<1.5	<1.5	<1.5	<1.5	<1.5	<1.5	<1.5
As	.5	58	52	49	60	208	<.5	.7
Be	1.5	<1.5	<1.5	<1.5	<1.5	<1.5	<1.5	<1.5
Cd	.5	14	20	20	4	<.5	.9	<.5
Cr	10	<10	<10	<10	30	[2]16,000	400	150
Li	1.5	72	68	115	<1.5	<1.5	30	51
Sb	.6	68	49	40	40	123	<.6	<.6
Se	.6	<.5	2.0	1.2	2.0	1.0	.7	<.5
Tl	30	78	73	83	95	<30	<30	<30

[1] Results below these limits are reported as less than (<) the limits. Limits are based on 2 g in 100 mL.
[2] Contaminated by inconel 601 tube.

Table 34.—Ion analyses results for tailings solids, and slags, and liquids from laboratory and pilot-plant leach processes

Ion	Analysis working limits[1]	Process and number of replicates						
		GRAmL (5)	CuAmL-Lb (6)	CuAmL-Pp (5)	HTPSAL (6)	RHCIAL (6)	SmSAL-1 (5)	SmSAL-2 (4)
		SOLIDS CONCENTRATION, wt pct						
NH_4^+	0.01	0.08	0.12	0.29	<0.01	0.11	<0.01	<0.01
Br^-	.01	<.01	<.01	<.01	<.01	<.01	<.01	<.01
Cl^-	.005	.26	.27	.36	.15	1.32	.44	.87
CO_3^{2-}	.01	13.1	23.6	8.10	<.01	<.01	<.01	<.01
F^-	.001	.09	.06	.14	.08	.05	.007	.16
NO_3^-	.01	<.01	<.01	<.01	<.01	<.01	<.01	<.01
PO_4^{3-}	.002	.10	.108	.15	.26	.25	.008	<.002
SO_4^{2-}	.002	.23	.26	.33	7.03	.09	.011	.004
		LIQUIDS CONCENTRATION, μg/mL						
NH_4^+	0.2	850	1,500	590	<0.2	19	NAp	NAp
Br^-	1.5	<1.5	<1.5	<1.5	<1.5	<1.5	NAp	NAp
Cl^-	.1	6.6	13	1,200	76	1,300	NAp	NAp
CO_3^{2-}	100	<100	<100	<100	<100	<100	NAp	NAp
F^-	.05	<.05	<.05	1.75	<.05	20	NAp	NAp
NO_3^-	.5	1.4	2.5	<.5	<.5	7.2	NAp	NAp
PO_4^{3-}	.5	<.5	<.5	<.5	<.5	<.5	NAp	NAp
SO_4^{2-}	1.0	8.7	21	430	3.4	<1.0	NAp	NAp
pH	NAp	9.5	9.6	9.0	6.5	6.5	NAp	NAp

NAp Not applicable.
[1] Results below these limits are reported as less than (<) the limits. Limits are based on 0.2 g in 100 mL for solids.

Table 35.—Elemental analytical results for tailings liquids from laboratory and pilot-plant leach processes, micrograms per milliliter

Element	Analysis working limits[1]	Process and number of replicates					Element	Analysis working limits[1]	Process and number of replicates				
		GRAmL (5)	CuAmL-Lb (6)	CuAmL-Pp (5)	HTPSAL (6)	RHCIAL (6)			GRAmL (5)	CuAmL (6)	CuAmL-Pp (5)	HTPSAL (6)	RHCIAL (6)
Ag	0.03	<0.03	<0.03	<0.03	<0.03	<0.03	Mg	0.003	3.7	4.6	3.2	6.5	14.8
Al	1.5	<1.5	<1.5	<1.5	<1.5	<1.5	Mn	.03	.06	.08	<.03	145	39.9
As	.003	.046	.005	.018	<.003	<.003	Mo	1.0	2.3	<1.0	30	<1.0	<1.0
Ba	.6	<.6	<.6	<.6	<.6	27.6	Na	.006	26	34	1,250	135	15.7
Be	.04	<.04	<.04	<.04	<.04	<.04	Ni	.05	<.05	<.05	<.05	56	9.56
Ca	.05	.24	.16	2.7	525	6.66	Pb	.2	<.2	<.2	<.2	<.2	<.2
Cd	.05	<.05	<.05	<.05	.14	<.05	Sb	.003	.004	<.003	.007	<.003	<.003
Co	.1	<.5	<.5	<.5	5.8	.24	Se	.003	<.003	<.004	.02	<.003	<.003
Cr	.3	<.3	<.3	<.3	<.2	<.2	Si	4.0	9.4	<4.0	22.4	<4.0	<4.0
Cu	.03	.37	1.2	<.03	1.2	.16	Ti	5.0	<5.0	<5.0	<5.0	<5.0	<5.0
Fe	.08	<.08	<.08	<.08	<.08	.21	Tl	.3	<.3	<.3	<.3	<.3	<.3
K	.03	83	2.1	182	<.03	8.80	V	1.3	<1.3	<1.3	<1.3	<1.3	<1.3
Li	.03	.10	.15	.23	1.05	<.03	Zn	.02	<.02	<.02	<.02	<.02	.15

[1]Results below these limits are reported as less than (<) the limits.

Table 36.—Semiquantitative optical emission spectrograph results for tailings solids and slags from laboratory and pilot-plant leach processes, weight percent

Element	Detection limit[1]	GRAmL	CuAmL-Lb	CuAmL-Pp	HTPSAL	RHCIAL	SmSAL-1	SmSAL-2
B	0.002	<0.002	<0.002	<0.002	<0.002	0.002-0.01	0.01-0.1	0.01-0.1
Bi	.002	<.002	<.002	<.002	<.002	<.002	<.002	<.002
Ga	.001	0.001- .003	0.001- .003	0.001- .003	0.001- .003	.001- .01	<.001	<.001
Nb	.005	<.005	<.005	<.005	<.005	<.005	<.005	<.005
Rb	.005	.005- .030	.005- .030	.005- .030	.01-.10	<.005	<.005	<.005
Sn	.006	<.006	<.006	<.006	<.006	<.006	<.006	<.006
Sr	.01	.01 - .10	.01 - .10	<.01	.01 - .10	.10 - .03	<.01	.03- .3
Zr	.01	<.01	<.01	.01 - .03	.01 - .03	<.01	<.01	.01- .1

[1]Results below these limits are reported as less than (<) the limits.

$SO_4^{=}$ for solid and liquid phase samples. Table 35 contains the elemental analyses results of the liquid phase samples.

Eight additional elements were determined semiquantitatively by optical emission spectroscopy. These elements, concentration ranges, and detection limits are given in table 36.

Leachate Testing

The tailings and slags from the laboratory and pilot plant leach processes were evaluated using three independent leachate tests, each run in duplicate. The three tests are the EPA extraction procedure (EP) toxicity test (*12*), the ASTM shake extraction test (*13*), and the EPA-COE seawater elutriant test (*14*). These tests are described in the "Methods of Analyses" section.

EP Toxicity Test

Table 37 lists the allowed maximum concentrations and the results of duplicate tests on the tailings and slags from each process. As shown in table 37, no elements were near the maximum allowable concentration, making these waste materials nonhazardous.

ASTM Shake Extraction Test

A second test, the American Society for Testing and Materials (ASTM) shake extraction test (*13*), has been proposed by ASTM as an alternate method for evaluating wastes. In this test, the 17 elements listed in the "Methods of Analyses" section were determined. Levels shown in table 38 for these elements are all extremely low, even lower than the values in table 37 from the EP toxicity test.

Table 37.—EP toxicity test results for tailings and slags from laboratory and pilot-plant leach processes, micrograms per milliliter

Element	Maximum allowed	GRAmL	CuAmL-Lb	CuAmL-Pp	HTPSAL	RHCIAL	SmSAL-1	SmSAL-2
Ag	5.0	<0.03	<0.03	<0.03	<0.03	<0.03	<0.03	0.03
As	5.0	.04	<.001	.004	.003	<.001	.002	<.001
Ba	100.0	6.0	<1.0	<1.0	<1.0	20	<1.0	2.5
Cd	1.0	<.05	<.05	.06	<.05	<.05	<.05	<.05
Cr	5.0	<.2	<.2	<.2	<.2	<.2	<.2	<.2
Hg	.2	ND	ND	ND	ND	ND	ND	ND
Pb	5.0	<.2	<.2	<.2	<.2	<.2	<.2	<.2
Se	1.0	<.003	<.003	<.003	<.003	<.003	<.003	<.003

ND Not determined. As reported in references 1 and 3, Hg levels in nodules are extremely low.

Table 38.—ASTM shake extraction test results for tailings and slags from laboratory and pilot-plant leach processes, micrograms per milliliter

Element[1]	GRAmL	CuAmL-Lb	CuAmL-Pp	HTPSAL	RHCIAL	SmSAL-1	SmSAL-2
Ag	<0.03	<0.03	<0.03	<0.03	<0.03	<0.03	<0.03
As	.016	<.003	<.003	<.003	<.003	<.003	<.003
Ba	<.6	<.6	<.6	<.6	19.6	<.6	<.6
Be	<.04	<.04	<.04	<.04	<.04	<.04	<.04
Cd	<.02	<.02	<.02	<02	<.02	<.02	<.02
Co	<.1	<.1	<.1	3.2	.24	<.1	<.1
Cr	<.2	<.2	<.2	<.2	<.2	<.2	<.2
Cu	.53	.16	<.05	.4	.58	<.05	<.05
Fe	<.08	<.08	<.08	.52	<.08	<.08	<.08
Mn	2.25	.94	<.03	20	1.7	1.4	<.03
Mo	<1.0	<1.0	3.8	<1.0	<1.0	<1.0	<1.0
Ni	<.05	<.05	<.05	7.0	9.5	<.05	<.05
Pb	<.2	<.2	<.2	<.2	<.2	<.2	<.2
Sb	<.003	<.003	<.003	<.003	<.003	<.003	<.003
Se	<.003	<.003	<.003	<.003	<.003	<.003	<.003
Tl	<.3	<.3	<.3	<.3	<.3	<.3	<.3
Zn	<.02	.10	<.02	.10	.13	<.02	<.02
Final pH	8.1	8.8	8.4	6.7	5.0	8.8	10.2

[1] Hg not included because of its extremely low levels of occurrence in nodules.

Table 39.—EPA-COE seawater elutriant test results for tailings and slags from laboratory and pilot-plant leach processes, micrograms per milliliter

Element[1]	Seawater	GRAmL	CuAmL-Lb	CuAmL-Pp	HTPSAL	RHCIAL	SmSAL-1	SmSAL-2
Ag	<0.03	<0.03	<0.03	<0.03	<0.03	<0.03	<0.03	<0.03
As	<.003	<.003	<.003	<.003	<.003	<.003	<.003	<.003
Ba	<1.0	<1.0	<1.0	<1.0	<1.0	<1.0	<1.0	<1.0
Be	<.07	<.07	<.07	<.07	<.07	<.07	<.07	<.07
Cd	<.02	<.02	<.02	<.02	<.02	<.02	<.02	<.02
Co	<.1	.2	.26	<.1	<.1	.14	<.1	<.1
Cr	<.2	<.2	<.2	<.2	<.2	<.2	<.2	<.2
Cu	<.05	.15	.22	<.05	.15	<.05	.12	<.05
Fe	<.08	.20	<.08	<.08	<.08	<.08	<.08	<.08
Mn	<.05	1.46	.22	.3	1.28	18.4	12.1	.22
Mo	<1.0	<1.0	<1.0	<1.0	<1.0	<1.0	<1.0	<1.0
Ni	<.05	.27	.13	<.05	.48	6.2	<.05	<.05
Pb	<.2	<.2	<.2	<.2	<.2	<.2	<.2	<.2
Sb	<.003	<.003	<.003	<.003	<.003	<.003	<.003	<.003
Se	<.003	<.003	<.003	<.003	<.003	<.003	<.003	<.003
Tl	<.3	<.3	<.3	<.3	<.3	<.3	<.3	<.3
Zn	<.02	<.02	<.02	<.02	<.02	.13	<.02	<.02
Final pH	8.5	8.0	8.2	7.9	6.5	5.8	8.5	10.0

[1] Hg not included because of its extremely low levels of occurrence in nodules.

EPA-COE Seawater Elutriant Test

In the possible case of ocean disposal of nodule tailings by ocean dumping or ocean outfall, the tailings may be subjected to a seawater leachate test. The EPA-COE dredge material elutriant test was used to evaluate the seawater leachable metals in the tailings (*14*). Table 39 gives the levels found in the extract and in the seawater prior to leaching for 17 elements.

SUMMARY AND CONCLUSIONS

This bulletin is the final requirement of the NOAA funded project conducted by the Bureau of Mines on "Analysis and Characterization of Potential Manganese Nodule Processing Rejects." The project entailed the determination of Pacific manganese nodule mineralogy, chemistry, processing, and laboratory generation and characterization of the tailings. The processing results serve only as a first order approximation of the physical and chemical characteristics of manganese nodule tailings produced from the potential first-generation processes.

The mineralogy of manganese nodules is complex but can be divided into three broad classes: manganese minerals, consisting primarily of todorokite, birnessite, and vernadite; iron oxide minerals, including feroxyhyte, goethite, and lepidocrocite; and accessory minerals, which include quartz, clays, zeolites, and other silicates and nonsilicates. The fine-grained or amorphous nature of manganese nodules and nodule tailings generally limit the identification of minerals to the major and minor constituents.

The elemental composition of Pacific manganese nodules consists primarily of manganese, iron, and silicon. Data are presented in this bulletin on 74 elements that occur in manganese nodules, and summary data tables and mineral-element associations are given.

Five managanese nodule processing options are outlined: the gas reduction and ammoniacal leach process, the Cuprion ammoniacal leach process, the high-temperature and high-pressure sulfuric acid leach process, the reduction and hydrochloric acid leach process, and the smelting and sulfuric acid leach process. These five processes are based on a 1977 Dames and Moore study (*6*), but differ from that study by using a larger mesh size of minus 65 for the feed material for all processes except smelting (where minimal size reduction is required); a moisture content of 20 pct rather than 37.5 pct for the feed nodules; an upgrade of the smelting process to a 3-million-mtpy nodule feed rate (dry basis) to allow for more conventionally sized furnaces; and the use of dewatering of the nodules during ship transport, coupled with conveyors instead of slurry pipeline transport of nodules from the port to the plant.

The five processes were operated in the laborary, but were designed to generate tailings and slags and not to produce final products. All processes except the RHClAL process are adaptations of currently practiced technology for nickeliferous laterites (*75-82, 84-85*). Approximately 30 to 40 lb of tailings was produced in the laboratory for each process, and about 125 lb of slags. Overall extraction of the value metals of Co, Cu, Ni, and/or Mn were generally greater than 90 pct for Cu, Ni, and Co with lower values for the ammonia based processes (GRAmL, CuAmL-Lb, and CuAmL-Pp) for Co and Cu.

All tailings and slags were analyzed for physical properties (except SmSAL), mineral content, elemental and ion content, and leachability using the EP toxicity test (*12*), the ASTM shake extraction test (*13*), and the EPA-COE seawater elutriant test (*14*).

For the ammonia-based processes, the physical properties, mineral content, and elemental and ion content were very similar with no significant variation in composition and physical properties. The HTPSAL process tailings physical properties were similar to the ammonia-based processes. The primary minerals were Mn_3O_4 and MnO_2. Chemical analyses were not significantly different from the ammonia-based processes. All of these processes—ammonia-based and HTPSAL—are three-metal recovery schemes and do not recover manganese. With manganese and iron as the major constituents of nodules, the tailings consist mainly of iron oxide and hydroxides, manganese oxides, and for the ammonia-based processes, $MnCO_3$.

The RHClAL process tailings were different than the other tailings, being less dense, having a finer particle size, and devoid of manganese. The primary constituents were iron oxides and hydroxides, quartz, and feldspars. Chemically the tailings were predominately iron, silicon, and aluminum.

The slags from the SmSAL process were of two types: the smelting slags and the ferromanganese slags. Each slag was analyzed mineralogically and chemically. The smelting slags were predominately Mn_2SiO_4 and were used to produce ferromanganese. The slags from the ferromanganese tests were predominately Ca_2SiO_4 and $Ca_2Al_2SiO_7$.

The final testing for all the tailings and slags involved three leachate tests. The EP toxicity test is used to identify a hazardous waste under the Resource Conservation and Recovery Act (RCRA). The ASTM shake extraction test is an alternative to the EP toxicity test prepared by ASTM and was performed for comparison purposes. The EPA-COE seawater elutriant test was used to determine which elements seawater leach in a seawater environment in the case of ocean disposal of nodule tailings.

Test results show that the tailings and slags produced in the laboratory and the pilot-plant are nonhazardous as defined in the EP toxicity test. None of the tailings and slags exceeded the maximum allowable limit for the eight regulated metals. Results of the ASTM and EPA-COE tests gave values lower than that of the EP test for the elements in common for the two tests. Overall leachability for the 17 elements was near or below detection limits.

The key findings of this project, then, are that both pilot-plant and laboratory generated tailings did not exceed the toxicity limit (*12*) under RCRA (*74*) and are classified as nonhazardous waste; and that the laboratory generated tailings were very similar to that pilot-plant tailings supplied industrially from the Cuprion process.

The laboratory generated tailings in this study cannot be considered representative of tailings that may be generated in a full-scale plant. However, it is encouraging that this first order approximation of physical and chemical characterizations of manganese nodule tailings has indicated that tailings from commercial operation may be environmentally acceptable.

REFERENCES

1. Haynes, B. W., S. L. Law, and D. C. Barron. Mineralogical and Elemental Description of Pacific Manganese Nodules. BuMines IC 8906, 1982, 60 pp.

2. Haynes, B. W., S. L. Law, and R. Maeda. Updated Process Flowsheets for Manganese Nodule Processing. BuMines IC 8924, 1983, 100 pp.

3. Haynes, B. W., and S. L. Law. Predicted Characteristics of Waste Materials From the Processing of Manganese Nodules. BuMines IC 8904, 1982, 10 pp.

4. Haynes, B. W., D. C. Barron, G. W. Kramer, and S. L. Law. Methods for Characterizing Manganese Nodules and Processing Wastes. BuMines IC 8953, 1983, 10 pp.

5. Haynes, B. W., D. C. Barron, G. W. Kramer, R. Maeda, and M. J. Magyar. Laboratory Processing and Characterization of Waste Materials From Manganese Nodules. BuMines RI 8938, 1985, 16 pp.

6. Dames and Moore, and E.I.C. Corporation. Description of Manganese Nodule Processing Activities for Environmental Studies, Vol. III. Processing Systems Technical Analysis. U.S. Dep. Commerce–NOAA, Office of Marine Minerals, Rockville, MD, 1977, 540 pp.; NTIS PB 274912 (set).

7. Haynes, B. W., S. L. Law, and W. J. Campbell. Metals in the Combustible Fraction of Municipal Solid Waste. BuMines RI 8244, 1977, 16 pp.

8. Haynes, B. W., G. W. Kramer, and J. A. Jolly. Fluorine and Uranium in Phosphate Rock Processing and Waste Materials. BuMines RI 8576, 1981, 17 pp.

9. Haynes, B. W., and G. W. Kramer. Characterization of U.S. Cement Kiln Dust. BuMines IC 8885, 1982, 19 pp.

10. American Society for Testing and Materials. Annual Book of Standards Part 19: Natural Building Stones; Soil and Rock; Peats, Mosses, and Humus. Philadelphia, PA, 1977, 494 pp.

11. Kramer, G. W., and B. W. Haynes. Anion Characterization of Florida Phosphate Rock Mining Materials and U.S. Cement Kiln Dust by Ion Chromatography. BuMines RI 8661, 1982, 8 pp.

12. Federal Register. Parts II-IX, Environmental Protection Agency; Hazardous Waste and Consolidated Permit Regulations. V. 115, No. 98, May 19, 1980, Book 2, pp. 33063-33285; 110-CFR, Parts 260-265.

13. American Society for Testing and Materials. Standard Test Method for Shake Extraction of Solid Waste With Water. D 3987 in 1982 Annual Book of ASTM Standards: Part 31, Water. Philadelphia, PA, 1982, pp. 1423-1427.

14. U.S. Environmental Protection Agency/Corps of Engineers. Ecological Evaluation of Proposed Discharge of Dredged Material Into Ocean Waters. Environmental Effects Laboratory, Waterways Experiment Station, U.S. Army Corps of Engineers, Vicksburg, MS, July 1977, 103 pp.

15. Murray, J., and A. F. Renard. Deep-Sea Deposits. Rep. on the Scientific Results of the Voyage of HMS Challenger During the Years 1873-1876. Longmans and Co., London, England, 1891, 525 pp.

16. Glasby, G. P. (ed.). Marine Manganese Deposits. Elsevier Oceanography Series, v. 15, 1977, 523 pp.

17. Sorem, R. K., and R. H. Fewkes. Manganese Nodules. IFI/Plenum Data Co., New York, 1979, 723 pp.

18. Aumento, F., D. E. Lawrence, and A. G. Plant. The Ferromanganese Pavement on San Pablo Seamount. Geol. Survey Canada, Paper 68-32, 1968, 30 pp.

19. Cronan, D. S. Underwater Minerals. Academic Press, Inc., Ltd., London, England, 1980, 362 pp.

20. Bischoff, J. L., and D. Z. Piper. Marine Geology and Oceanography of the Pacific Manganese Nodule Province. Plenum Press, New York, 1979, 842 pp.

21. Turner, S., and P. R. Buseck. Manganese Oxide Tunnel Structures and Their Intergrowths. Sci., v. 203, 1979, pp. 456-458.

22. _____. Todorokite: A New Family of Naturally Occurring Manganese Oxides. Sci., v. 212, 1981, pp. 1024-1027.

23. Turner, S., M. Siegel, and P. R. Buseck. Structural Features of Todorokite Intergrowths in Manganese Nodules. Nature, v. 296, 1982, pp. 841-842.

24. Siegel, M. Studies of the Mineralogy, Chemical Composition, Textures, and Distribution of Manganese Nodules at a Site in the North Equatorial Pacific Ocean. Ph.D. Thesis, Harvard Univ., Cambridge, MA, June 1981, 274 pp.

25. Chukhrov, F. V., A. I. Gorshkov, A. V. Sivtsov, and V. V. Berezovskaya. (New Mineral Phases of Oceanic Manganese Microconcretions.) Izvest. Akad. Nauk SSSR Ser. Geol., No. 1, 1979, pp. 83-90.

26. Chukhrov, F. V., A. I. Gorshkov, B. B. Zvyagin, and L. P. Ermilova. Iron Oxides as Minerals of Sedimentary Environments and Chemogenic Eluvium. Paper in Geology and Geochemistry of Manganese Volume I: General Problems: Mineralogy, Geochemistry, Methods (Proc. 2d Int. Symp. Geol. and Geochemistry of Manganese, Sydney, Australia, Aug. 17-24, 1976), ed. by I. Varentsov, and G. Grasselly. Schweizerbart, Stuttgart, Fed. Rep. Germany, 1980, pp. 231-257.

27. Chukhrov, F. V., B. B. Zvyagin, A. I. Gorshkov, L. P. Ermilova, V. V. Korovushkin, E. S. Rudnitskaya, and N. Yu. Yakubovskava. (Feroxyhyte, a New Modification of FeOOH.) Internat. Geol. Rev., v. 19, 1976, pp. 873-890.

28. Burns, R. G. Uptake of Cobalt Into Ferromanganese Nodules, Soils, and Synthetic Manganese (IV) Oxides. Geochim. Cosmochim. Acta, v. 40(1), 1976, pp. 95-102.

29. Murray, J. W., and J. G. Dillard. The Oxidation of Cobalt (II) Adsorbed on Manganese Dioxide. Geochim. Cosmochim. Acta, v. 43, 1979, pp. 781-787.

30. Hey, M. H., and P. G. Embrey. Twenty-eighth List of New Mineral Names. Miner. Mag., v. 39, 1974, pp. 903-932.

31. Burns, R. G., V. M. Burns, and H. W. Stockman. A Review of the Todorokite-Buserite Problem: Implications to the Mineralogy of Marine Manganese Nodules. Am. Mineral., v. 68, 1983, pp. 972-980.

32. Fleischer, M. Glossary of Mineral Species 1980. Mineralogical Record, Tucson, AZ, 1980, 192 pp.

33. Burns, R. G., and V. M. Burns. Manganese Oxides. Ch. in Marine Minerals, ed. by R. G. Burns. Litho Crafters, Inc., Chelsea, MI, v. 6, 1979, pp. 1-46.

34. Chukhrov, F. V., A. I Gorshkov, and A. V. Sivtsov. (New Structural Variety of Todorokite.) Izvest. Akad. Nauk SSSR Ser. Geol., No. 5, 1981, pp. 88-91.

35. Chukhrov, F. V., A. I. Gorshkov, A. V. Sivtsov, and V. V. Berezovskaya. (Structural Varieties of Todorokite.) Isvest. Akad. Nauk SSSR Ser. Geol., No. 12, 1978, pp. 86-95.

36. _____. New Data of Natural Todorokite. Nature, v. 278, 1979, pp. 631-632.

37. Burns, R. G., and V. M. Burns. The Mineralogy and Crystal Chemistry of Deep-Sea Manganese Nodules. A Polymetallic Resource of the Twenty-first Century. Phil. Trans. Royal Soc. (London), v. A286, 1977, pp. 283-301.

38. Murray, J. W. Iron Oxides. Ch. in Marine Minerals, ed. by R. G. Burns. Litho Crafters, Inc., Chelsea, MI, v. 6, 1979, pp. 47-98.

39. Burns, V. M., and R. G., Burns. Diagenetic Features Observed Inside Deep-Sea Manganese Nodules From the North Equatorial Pacific. Scanning Electron Microscopy, v. 1, 1978, pp. 245-252.

40. _____. Post-Depositional Metal Enrichment Processes Inside Manganese Nodules From the North Equatorial Pacific. Earth and Planetary Sci. Letters, v. 39, 1978, pp. 341-348.

41. Frazer, J. Z., and M. B. Fisk. Availability of Copper, Nickel, Cobalt, and Manganese From Ocean Ferromanganese Nodules (III) (grant G0264024, Scripps Inst. Oceanography). BuMines OFR 140(2)-80, 1980, 112 pp; NTIS PB 81-145971.

42. Fisk., M. B., J. Z. Frazer, J. S. Elliott, and L. L. Wilson. Availability of Copper, Nickel, Cobalt, and Manganese From Ocean Ferromanganese Nodules (II) (grant G0264024, Scripps Inst. Oceanography). BuMines OFR 140(1)-80, 1979, 63 pp.; NTIS PB 81-145963.

43. Frazer, J. Z., and M. B. Fisk. Geological Factors Related to Characteristics of Seafloor Manganese Nodule Deposits (grant G0264024, Scripps Inst. Oceanography). BuMines OFR 142-80, 1980, 41 pp.; NTIS PB 81-145831.

44. Frazer, J. Z., M. B. Fisk, J. Elliott, M. White, and L. Wilson. Availability of Copper, Nickel, Cobalt, and Manganese From Ocean Ferromanganese Nodules (grant G0264024, Scripps Inst. Oceanography). BuMines OFR 121-79, 1978, 141 pp.; NTIS PB 300 356.

45. Sorem, R. K., R. H. Fewkes, W. D. McFarland, and W. R. Reinhart. Physical Aspects of the Growth Environment of Manganese Nodules in the "Horn Region," East Equatorial Pacific Ocean. Proc. La Genese des Nodules de Manganese, Paper 289, Colloques Internationaux du Centre National de la Recherche Scientifique, Paris, France, Sept. 25-30, 1978, pp. 61-76.

46. Fewkes, R. H., W. D. McFarland, W. R. Reinhart, and R. K. Sorem. Development of a Reliable Method for Evaluation of Deep Sea Manganese Nodule Deposits (grant G0274013, WA State Univ.). BuMines OFR 64-80, 1979, 94 pp.; NTIS PB 80-182116.

47. _____. Evaluation of Metal Resources at and Near Proposed Deep Sea Mine Sites (grant G0284008, WA State Univ.). BuMines OFR 108-80, 1980, 239 pp.; NTIS PB 80-228992.

48. Monget, J. M., J. W. Murray, and J. Mascle. A World-Wide Compilation of Published Multicomponent/Analyses of Ferromanganese Concretions. Int. Decade of Ocean Exploration (IDOE), Manganese Nodule Project Tech. Rep. No. 12, Aug. 1976, 130 pp.; NTIS PB 263 389.

49. Toth, J. R. Deposition of Submarine Crusts Rich in Manganese and Iron. Geol. Soc. of America Bull., pt. 1, v. 91, 1980, pp. 44-54.

50. Harris, R. C. Mercury Content of Deep-Sea Manganese Nodules. Nature, v. 219, 1968, pp. 54-55.

51. Glasby, G. P., R. R. Keays, and P. C. Rankin. The Distribution of Rare Earth, Precious Metal and Other Trace Elements in Recent and Fossil Deepsea Manganese Nodules. Geochem. J., v. 12, 1978, pp. 229-243.

52. Piper, D. Z., and M. Williamson. Composition of Pacific Ocean Ferromanganese Nodules. Marine Geol., v. 23, 1977, pp. 285-303.

53. Volkov, I. I., and L. S. Fomina. New Data on the Geochemistry of the Rare Earths in the Ocean Sediments. Geochemistry Int., v. 10, 1973, pp. 1178-1187.

54. Agiorgitis, G., and H. Gundlach. Platin-Gehalte in Tiefsee-Mangenkrollen. Naturwissenschaften, v. 65, 1978, p. 534.

55. Flanagan, F. J., and D. Gottfried. USGS Rock Standards, III. Manganese-Nodule Reference Samples USGS Nod-A-1 and USGS-Nod-P-1. U.S. Geol. Surv. Prof. Paper 1155, 1980, 39 pp.

56. Shilo, N. A., L. V. Razin, G. A. Khomenko, and G. I. Agal'tov. The Mode of Occurrence of Gold and Platinum in Ferromanganese Nodules From the Ocean Floor. Doklady Akad. Nauk SSSR, v. 232(2), 1977, pp. 466-469.

57. Busch, R. A., R. R. Backer, L. A. Atkins, and C. D. Kealy. Physical Property Data on Fine Coal Refuse. BuMine RI 8062, 1975, 40 pp.

58. Allen, T. Particle Size Measurement. Chapman & Hall, 1975, pp. 301-312.

59. Potter, R. M., and G. R. Rossman. The Tetravalent Manganese Oxides: Identification, Hydration, and Structural Relationships by Infrared Spectroscopy. Am. Mineral., v. 64, 1979, pp. 1199-1218.

60. _____. Mineralogy of Manganese Dendrites and Coatings. Am. Mineral., v. 64, 1979, pp. 1219-1226.

61. Price, W. J. Analytical Atomic Absorption Spectrometry. Heyden, 1974, p. 80.

62. U.S. Environmental Protection Agency. Methods for Chemical Analysis of Water and Wastes. Environmental Monitoring and Support Laboratory, Cincinnati, OH, EPA-600/4-79-020, Mar. 1979, 460 pp.

63. Haynes, B. W. Electrothermal Atomic Absorption Determination of Arsenic and Antimony in Combustible Municipal Solid Waste. At. Absorp. Newsl., v. 17, No. 3, 1978, pp. 49-52.

64. Manning, D. C. Spectral Interferences in Graphic Furnace Atomic Absorption Spectroscopy I. The Determination of Selenium in an Iron Matrix. At. Absorp. Newsl., v. 17, No. 5, 1978, pp. 107-108.

65. Koizuma, H., and K. Yasuda. New Zeeman Method for Atomic Absorption Spectrophotometry. Anal. Chem., v. 47, 1975, pp. 1679-1682.

66. Sighinolfi, G. P., and C. Gorgoni. AA Spectrochemical Analysis for Ultra Trace Elements in Geological Materials by Hydride-Forming Techniques: Selenium. Talanta, v. 28, 1981, pp. 169-172.

67. Koch, R. C. Activation and Analysis Handbook. Academic, 1960, 219 pp.

68. Ricci, E., and F. F. Dyer. Second Order Interference in Activation Analysis. Nucleonics, v. 22, No. 6, 1964, pp. 45-50.

69. Brunfelt, A. O., and E. Steinnes. A Neutron-Activation Scheme Developed for the Determination of 42 Elements in Lunar Material. Talanta, v. 18, 1971, pp. 1197-1208.

70. Bertin, E. P. Principles and Practice of X-Ray Spectrometric Analysis. Plenum, 1970, 679 pp.

71. Small, H., T. S. Stevens, and W. C. Bauman. Novel Ion Exchange Chromatographic Methods Using Conductimetric Detection. Anal. Chem., v. 47, 1975, pp. 1801-1809.

72. Sawicki, E., J. D. Mulik, and E. Wittgenstein. Analysis of Industrial Wastestreams. Dionex Corp. (Sunnyvale, CA) Applications Note No. 11, Aug. 1978, 2 pp.

73. _____. Ion Chromatographic Analysis of Environmental Pollutants. Ann Arbor Sci., v. 1-2, 1978, 645 pp.

74. U.S. Congress. Resource Conservation and Recovery Act. Public Law 94-580, Oct. 21, 1976.

75. Caron, M. H. Process of Recovering Values From Nickel and Cobalt-Nickel Ores. U.S. Pat. 1,487,145, Mar. 18, 1924.

76. Alonso, A., and J. Daubenspek. Modifications in Nicaro Metallurgy. Trans. Met. Soc. of AIME, v. 217, 1960, pp. 253-257.

77. Reid, J. G. Operations at the Greenvale Nickel Project Mine and Refinery. Proc. Int. Laterite Symp., ed. by D. J. I. Evans, R. S. Shoemaker, and H. Veltman, Soc. Min. Eng. AIME, New York, 1979, pp. 368-381.

78. Richardson, J. M., L. G. Stevens, and M. C. Kuhn. The Recovery of Metal Values From Nickel-Bearing Laterite Ores by Reductive Roast/Ammonia Leach Technology. Ch. 4 in Process and Fundamental Consideration of Selected Hydrometallurgical Systems, ed. by M. C. Kuhn. Soc. Min. Eng. AIME, New York, 1981, pp. 38-62.

79. Graaf, J. E. The Treatment of Lateritic Nickel Ores – A Further Study of the Caron Process and Other Possible Improvements – Part I. Effect of Reduction Conditions. Hydrometall., v. 5, 1979, pp. 47-65.

80. _____. The Treatment of Lateritic Nickel Ores – A Further Study of the Caron Process and Other Possible Improvements – Part II. Leaching Studies. Hydrometall., v. 5, 1980, pp. 255-271.

81. Szabo, L. J. Recovery of Metal Values From Manganese Deep Sea Nodules Using Ammoniacal Cuprous Leach Solutions. U.S. Pat. 3,983,017, Sept. 28, 1976.

82. Agarwal, J. C., H. E. Barner, N. Beecher, D. S. Davies, and R. N. Kust. Kennecott Process for Recovery of Copper, Nickel, Cobalt, and Molybdenum From Ocean Nodules. Min. Eng., v. 31, No. 12, 1979, pp. 1704-1709.

83. Agarwal, J. C., N. Beecher, D. S. Davies, G. L. Hubred, V. K. Kakaria, and H. J. Moslen. Comparative Economics of Recovery of Metals From Ocean Nodules. Marine Min., v. 2(1-2), 1979, pp, 119-149.

84. Carlson, E. T., and C. S. Simons. Pressure Leaching of Nickeliferous Laterites With Sulfuric Acid. Paper in Extractive Metallurgy of Copper, Nickel, and Cobalt, ed. by P. Queneau. Interscience Publ., Inc., New York, 1961, pp. 363-397.

85. Duyvesteyn, W. P. C., G. W. Wicker, and R. E. Doane. An Omnivorous Process for Laterite Deposits. Paper in Proc. Int. Laterite Symp., New Orleans, LA, Feb. 19-21, 1979, Soc. Min. Eng. AIME, New York, 1979, pp. 553-570.

86. Neuschutz, D., V. Scheffler, and H. JunghanB. Verfahren Zur Aufarbeitung von Manganknollen Durch Schwefelsaure Drucklaugung. (Method for the Processing of Manganese Nodules by Sulfuric Acid Pressure Leaching.) Erzmetall, v. 30(2), 1977, pp. 61-67.

87. Halbach, P., K. Koch, H-J. Renner, and K-H. Ujma. Pyrometallurgical Processing of Manganese Nodules and Lateritic Nickel Ores Using Waste Materials as Reducing Agents. Erzmetall, v. 30, 1977, pp. 458-464.

88. Montanteme, J., A. Greffe, and F. Grandjacques. Selective Reduction of Nickel Ore With a Low Nickel Content. U.S. Pat. 4,073,641, Feb. 14, 1978.

89. Septier, L., F. Dubrous, and M. Demango. Process for the Treatment of Complex Metal Ores Containing, in particular, Manganese and Copper, Such as Oceanic Nodules. U.S. Pat. 4,162,916, July 31, 1979.

90. Sridhar, R., J. S. Warner, and M. C. E. Bell. Non-Ferrous Metal Recovery From Deep Sea Nodules. U.S. Pat. 4,049,438, Sept. 20, 1977.

91. Wilder, T. C., J. J. Andreola, and W. E. Galin. Reduction Processes for Manganese Nodules Using Fuel Oil. J. Met., v. 33, Mar. 1981, pp. 64-69.